

INVESTIGATION OF THE TEMPORAL DEVELOPMENT OF TAU PATHOLOGY IN TAU58/2 TRANSGENIC MICE

By

Bahar Kavyani

(Pharm.D.)

A THESIS SUBMITTED IN FULFILMENT OF THE REQUIREMENT FOR THE
DEGREE OF
MASTER OF RESEARCH
MACQUARIE UNIVERSITY
FACULTY OF MEDICINE AND HEALTH SCIENCES
DEPARTMENT OF BIOMEDICAL SCIENCES
JUNE 2020



MACQUARIE
University

Declaration

The following is a thesis submitted to Macquarie University in fulfilment of the requirement for the Degree of Master of Research.

The work presented in this thesis is my own and to the best of my knowledge and belief, original. References and sources of information have been acknowledged in the text and references list. I hereby declare that I have not submitted this material, either in full or in part, for a degree at this or any other institution

This thesis used tissue from TAU58/2 mice that were collected as part of a larger project led by the primary supervisor A/Prof Bingyang Shi. The animal tissue was collected by Prof Tim Karl (Western Sydney University) under approved ethics (A12910). The tissue was used at Macquarie University in the FMHHS PC2 laboratories, with institutional biosafety approval (# 5974 -52019597412350). All procedures were performed in accordance with this protocol.

Bahar Kavyani 45062927

Acknowledgement

Foremost, I would like to thank Professor Roger Chung, as my supervisor and mentor throughout this research, for the encouragement and guidance he has given me to keep working to the best of my abilities. Also, my principle supervisor, Dr Bingyang Shi, for offering me the great opportunity of working on this project.

My sincerest thanks to Dr Stephanie Rayner for training me in the lab, and helping me with troubleshooting, and more importantly for her patience and wonderful companionship.

Thank you, Rowan Radford, for introducing IHC method and amazing world of microscopy to me, and largely for pushing me out of my comfort zone and teaching me to be a more independent researcher.

My appreciation is extended to other Chung's group members who have contributed to this work, Dr Amanda Wright for her insights into design of this study, and her valuable feedback on my thesis. Dr Jia Li, for advising me in presenting the results and writing my thesis, and Dr Rose Chesworth for providing the brain tissue.

I would like to express my gratitude to my fellow researchers in the lab: Flora, Luan, Jennilee, Andres, Hannah, Katherine, Maxinne. Lab would have been a lonely place without you.

To my family, especially my husband, thank you for your constant support.

Finally, thank you to Dr Jen Rowland and Dr Dane Turner for your priceless advice and support during this 10-month long MRes project.

Abstract

Alzheimer's disease (AD) is a progressive neurodegenerative disease, which is a major public health burden in the world. Despite recent progress has been made in understanding the pathology of AD, the exact causes of AD are still unclear. Two of the hallmark pathologies of AD are the formation of β -amyloid plaques and neurofibrillary tangles (NFTs). NFTs are composed of hyperphosphorylated Tau protein which aggregates and forms insoluble Tau. Several transgenic mouse models for AD have been developed to identify the underlying molecular mechanisms by demonstrating tauopathy such as TAU58/2, a P301S mutant Tau transgenic mouse line. Current study has investigated the expression profile of Tau regarding different phosphorylation sites, and isoforms in TAU58/2 mouse model in hippocampus during different stages of disease progression by Western blot, and in comparison with their wild type littermates. Also, abnormal Tau distribution, morphology, and its correlation with neuronal loss as well as neuroinflammation in TAU58/2 mouse model has been studied by immunohistochemistry. Data provided by this MRes project will define the time points for future experiments that will seek to downregulate these proteins. Tau phosphorylation at Ser202/Thr205 and Thr231 sites as well as total Tau levels were increased in hippocampus both in three and twelve months old, whereas insoluble Tau formation only occurred in 12 months and at Ser202/Thr205 phosphorylation site. Results obtained from Western blot were confirmed by IHC; in addition, it uncovered the distribution and morphology of Phospho-Tau, as well as Astrogliosis. These results provide important insights into Tauopathy in TAU58/2 mouse model at two timepoints. Given the fact that reported changes begin as soon as 3 months of age, additional studies to assess neuronal loss and neuroinflammation are needed to gain a comprehensive understanding of the best timepoint to apply nanoparticle-based therapies in the future.

Contents

1	INTRODUCTION	1
1.1.	Alzheimer's DISEASE (AD)	1
1.1.1	Major Biological Hallmarks of AD	1
1.1.2	Neuroinflammation in AD.....	6
1.1.3	Mouse model of AD.....	6
1.2	Previous studies designed to rectify pathological changes in AD.....	7
1.2.1	Targeting Tau.....	7
1.2.2	Targeting A β	8
1.3	Strategy of developing therapeutics for AD	11
1.4	TAU58/2 mouse model.....	11
1.5	Aims of this MRes project.....	12
1.5.1	Aim 1	12
1.5.2	Aim 2	13
2	METHODOLOGY	15
2.1	Mice.....	15
2.2	Tissue collection	15
2.3	Protein extraction (RAB-RIPA-Formic Acid (FA) extraction)	16
2.4	Protein quantification (DC Protein assay)	17
2.5	Western blot	17
2.5.1	Gel Electrophoresis.....	17
2.5.2	Transferring	17
2.6	Immunohistochemistry.....	18
2.6.1	Microscopy analysis	18
3	RESULTS	21
3.1	Optimising protein extraction of soluble and insoluble Tau in brain lysates	21
3.2	Protein extraction and quantification from experimental mice.....	22
3.3	Western blot optimisation.....	23
3.3.1	Optimisation of Tau antibody concentrations for Immunoblotting.....	23
3.3.2	Optimising housekeeping gene for immunoblotting	24
3.4	Immunoblotting measurement of Tau	24
3.4.1	Transgenic TAU58/2 mice revealed a significant raise in total and phosphorylated Tau at 3 months of age. 25	
3.4.2	Transgenic TAU58/2 mice have a significant increase in total and hyperphosphorylated Tau at 12 months of age.	32
3.4.3	Comparison between levels of Tau protein expression in 3 months and 12 months and across all fractions, showed elevated tauopathy.....	38
3.5	Immunohistochemistry (IHC)	39
3.5.1	Optimisation of IHC conditions	39
3.5.2	Tau Pathology and neuroinflammation investigation	40
3.5.3	Nissl staining and counter staining.....	51
3.5.4	IHC overview	52
4	DISCUSSION	54
4.1	Study background.....	54
4.2	Results summary	54
4.3	Limitations	55

4.4	Future directions	55
4.5	Conclusion	56
APPENDIX		57
A.1	Method	57
A.1.1	<i>Mice tissue</i>	57
A.1.2	<i>Protein extraction</i>	57
A.2	Results	58
A.2.1	<i>Western blot</i>	58
A.2.2	<i>Total protein</i>	58
REFERENCES		59

List of Figures

Figure 1. β -amyloid plaques	2
Figure 2. Tau phosphorylation and NFT formation	3
Figure 3. Tau gene, longest , and phosphorylation sites	5
Figure 4. Illustration of experimental procedure for main project plan.....	14
Figure 5. Detection of soluble and insoluble Tau from mouse brain samples	22
Figure 6. Antibody testing	23
Figure 7. Comparison between β -actin and GAPDH as housekeeping genes	24
Figure 8. Western blot analysis in 3-month-old TAU58/2 mice and WT mice in soluble fractions (RAB, RIPA) and insoluble fraction (FA).....	26
Figure 9. AT8 protein expression in 3-month-old WT and TAU58/2 samples in all fractions	28
Figure 10. AT180 protein expression in 3-month-old WT and TAU58/2 samples in all fractions	29
Figure 11. HT7 protein expression in 3-month-old WT and TAU58/2 samples in all fractions	30
Figure 12. rD4 protein expression in 3-month-old WT and TAU58/2 samples in all fractions.....	31
Figure 13. Western blot analysis in 12-month-old TAU58/2 mice and WT mice in soluble fractions (RAB, RIPA) and insoluble fraction (FA)	32
Figure 14. AT8 protein expression in WT and TAU58/2 samples in all fractions	34
Figure 15. AT180 protein expression in 12-month-old WT and TAU58/2 samples in all fractions	35
Figure 16. HT7 protein expression in 12-month-old WT and TAU58/2 samples in all fractions	36
Figure 17. rD4 protein expression in 12-month-old WT and TAU58/2 samples in all fractions.....	37
Figure 18. Blocking endogenous mice IgG optimisation.....	39
Figure 19. Total Tau staining by HT7 antibody in 3-month-old TAU58/2 and WT mice	42
Figure 20. Tau phosphorylation at Ser202/Thr205 phosphorylation site marked by AT8 in 3-month-old TAU58/2 and WT mice.	43
Figure 21. Tau phosphorylation at Thr231 phosphorylation site in 3-month-old TAU58/2 and WT mice	44
Figure 22. Astroglisis detected by GFAP antibody in 3-month-old TAU58/2 and WT mice	45
Figure 23. Total Tau staining by HT7 antibody in 12-month-old TAU58/2 and WT mice	47
Figure 24. Tau phosphorylation at Ser202/Thr205 phosphorylation site marked by AT8 in 12-month-old TAU58/2 and WT mice.....	48
Figure 25. Tau isoforms rD3 and rD4 in 12-month-old TAU58/2 and WT mice	49
Figure 26. Astroglisis detected by GFAP antibody in 12-month-old TAU58/2 and WT mice	50
Figure 27. Nissl staining and counter staining in addition to Tau protein expression in TAU58/2	52
Figure 28. Staining with DAPI and Neurotrace in both TAU58/2 and WT mice at 12 months	52

List of Tables

Table 1. First AD transgenic mouse models.....	7
Table 2. Tau modification agents.....	8
Table 3. Modifying treatments targeting Ab and Tau protein report at different clinical trial phases.....	9
Table 4. Western blot antibodies.....	13
Table 5. Immunohistochemistry and immunofluorescence antibodies.....	13
Table 6. Mouse cohort.....	15
Table 7. Extraction buffer.....	17
Table 8. Primary antibodies, their concentrations and applications.....	19
Table 9. Secondary antibodies, their concentrations and applications.....	20
Table 10. 12-month samples protein concentration.....	22
Table 11. 3-month samples protein concentration.....	22
Table 12. Bands densities for five antibodies in 3-month-old TAU58/2 and WT littermates.....	26
Table 13. AT8 Normalization results for all fractions in 3-month-old WT and TAU58/2 mice.....	28
Table 14. AT180 Normalization results for all fractions in 3-month-old WT and TAU58/2 mice.....	29
Table 15. HT7 Normalization results for all fractions in 3-month-old WT and TAU58/2 mice.....	30
Table 16. Normalization results for all fractions in 3-month-old WT and TAU58/2 mice.....	31
Table 17. Bands densities for five antibodies in 12-month-old TAU58/2 and WT littermates.....	33
Table 18. AT8 Normalization results for all fractions in 12-month-old WT and TAU58/2 mice.....	34
Table 19. AT180 Normalization results for all fractions in 12-month-old WT and TAU58/2 mice.....	35
Table 20. HT7 Normalization results for all fractions in 12-month-old WT and TAU58/2 mice.....	36
Table 21. rD4 Normalization results for all fractions in 12-month-old WT and TAU58/2 mice.....	37
Table 22. Mean signals reported for Tau protein expression.....	38
Table 23. Antibodies' concentrations examined and chosen.....	40

Abbreviations

Aβ	Amyloid- β
AD	Alzheimer's disease
APP	Amyloid precursor protein
BBB	Blood-brain barrier
BSA	Bovine serum albumin
cDNA	coding DNA
DNA	deoxyribonucleic acid
FA	Formic acid
FTD	frontotemporal dementia
GFAP	Glial Fibrillary Acidic Protein
IHC	immunohistochemistry
NFT	Neurofibrillary tangles
MAPT	Microtubule-associated protein tau
mRNA	messenger RNA
PAGE	polyacrylamide gel electrophoresis
PBS	Phosphate buffered saline
PFA	Paraformaldehyde
PTM	Post translational modification
RAB	reassembly buffer
ER	endoplasmic reticulum
rD3	3-repeat Tau isoform
rD4	4-repeat Tau isoform
RIPA	radioimmunoprecipitation assay
RNA	ribonucleic acid
RT	room temperature
SDS	sodium dodecyl sulfate
TBS	tris-buffered saline
WB	Western blot
WT	wild type

Introduction

1.1. Alzheimer's disease (AD)

Alzheimer's disease (AD) is a progressive neurodegenerative disease that has become a global public health burden. For example, the global burden of the disease was USD \$818 billion in 2015 [1] and 82% of the costs or \$670 billion comes from countries with high incomes such as Australia [2]. AD is the most common form of dementia, with other forms of dementia including vascular dementia, Lewy body dementia, frontotemporal dementia (FTD), progressive supranuclear palsy (PSP), and Parkinson's disease (PD) [3]. Diagnosis of the disease for early interventions is not easy for AD due to its complicated nature as there are various risk factors involved in pathology of the disease, including genetic factors, increasing average age of the population, cerebrovascular disease, traumatic brain injury, depression, hormonal disturbance, inflammation, hyperlipidaemia, and hyperglycaemia [4]. Several medications are available to treat and slow the progress of AD symptoms, including cholinesterase (ChE) inhibitors, such as rivastigmine, donepezil and galantamine, and antagonism of the N-methyl-D-aspartate-receptor (NMDA-receptor) like Memantine [5]. However, these medications can only enhance the quality of life for the patient and cannot slow the rate of decline, thus unfortunately there is currently no cure for AD. Therefore, gaining a further understanding of disease progression, and developing new drugs that can assist in regulating pathological proteins may be of clinical benefit to AD patients.

1.1.1 Major Biological Hallmarks of AD

Alzheimer's disease is characterised classically primarily by two pathological hallmarks; the formation of β -amyloid plaques and neurofibrillary tangles (NFTs) [6-8].

1.1.1.1 β -amyloid plaques

β -amyloid is a naturally occurring peptide, produced through several biochemical pathways. Both cleavage of Amyloid Precursor Protein (APP) with BACE-1 (β -secretase) (Fig. 1A) [9], and mutations to the APP gene (that occurs in some humans, which can enhance this process of abnormal cleavage of APP) leads to production of $A\beta$. Another gene involved in formation of $A\beta$ is PSEN [10]. PSEN1 and PSEN2 encode the presenilin 1 (PS1) and presenilin 2 (PS2) proteins respectively, a catalytic subunit of γ secretase (an intramembranous protease involved in cleavage of APP). In disease, $A\beta$ has the tendency to misfold and subsequently aggregates and finally forms the $A\beta$ plaques extracellularly [11](Figure .1B).

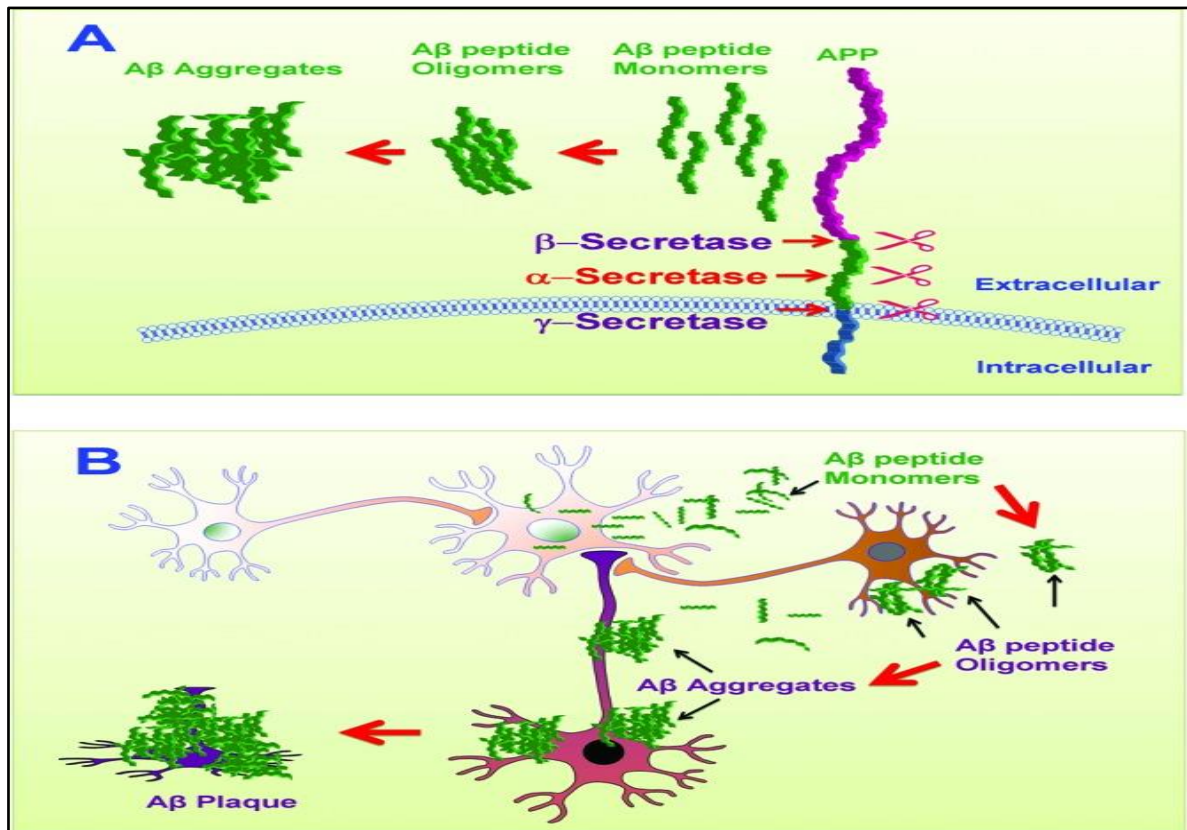


Figure 1. *β*-amyloid plaques. A) A β production, B) formation of A β plaques. Sourced from DOI: 10.1021/ml300058m

Decreasing extracellular A β levels, and/or preventing A β aggregation, has been considered as a primary treatment strategy for AD. Strategies that have been investigated include immunotherapies, aggregation inhibitors and secretase inhibitors, have been tested in several animal models and clinical trials [12]. Unfortunately, many of these agents have failed in clinical trials. In addition, several studies have demonstrated that β -amyloidosis cannot lead to the disease solely and it is commonly accompanied by neurofibrillary degeneration in AD patients [13]. Consequently, the focus of recent studies has been shifted to Tau protein alterations and NFT formations in AD patients.

1.1.1.2 NFTs

NFTs occur within neurons, and are composed of hyperphosphorylated Tau protein [6-8], a microtubule-associated protein that regulates the bundling and stabilization of axonal microtubules [6, 14, 15]. In the normal brain, Tau is involved in functions including cell signalling, synaptic plasticity and regulation of genomic stability [16]. The MAPT gene located on human chromosome 17 (17q21.31) and comprising 16 exons, encodes the microtubule-associated protein Tau. This gene has been demonstrated in Figure 3. In the adult human brain, six Tau isoforms have been identified, differing by the presence of zero (0N), one (1N) or two inserts in N-terminal (2N) and existence of three (3R), or four (4R) C-terminal microtubule binding repeats [17]. Accumulation of different isoforms differs in various tauopathies [18, 19]. The relatively most effective isoform in promoting microtubule assembly is 2N4R, while the least effective one is 0N3R [20, 21]. Interestingly, increase in 4R expression promotes Tau aggregation and NFT formation.

Post-translational modification of Tau (PTM), such as phosphorylation, acetylation, nitration, glycation, glycosylation, ubiquitination, and truncation, changes its function and localization [22], and promotes aggregation and tangles formation [23]. Hyperphosphorylation of Tau has been hypothesised as the most compelling cause of dysfunctional Tau in AD and related tauopathies [14, 24, 25]. This abnormality in Tau modification, contributes to drop in normal neuronal activity and consequently chronic progressive neurodegeneration in AD and related tauopathies [25]. So far, more than 80

phosphorylation sites have been found in the Tau protein, and depending upon the site the binding affinity of Tau to microtubules (MT) can be altered [26]. These changes result in the formation of oligomers and misfolded Tau that form Tau deposits and, eventually, neurofibrillary tangles [16], potentially initiating downstream pathological signalling. NFT formation is depicted in Figure 2.

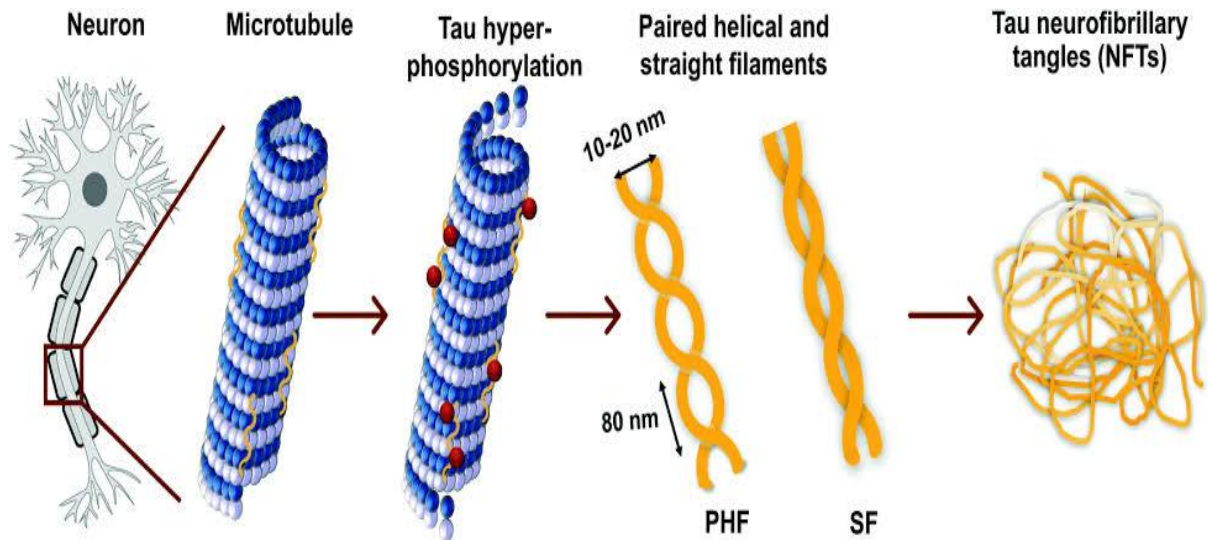


Figure 2. Tau hyperphosphorylation and NFT formation. Image sourced from DOI: 10.1039/C7CS00706J

Tau hyperphosphorylation is proven to occur in AD at different phosphorylation sites and was reported for the first time by Yasuo Ihara's group [27]. Some of these alterations in phosphorylated Tau in AD have been examined by mimicking Tau phosphorylation through replacing different residues with negatively charged glutamate or aspartate in cell culture [28]. As a result, hyperphosphorylation at sites in proline-rich region have been introduced that contribute to the dissociation of Tau from microtubules. This detached Tau undergoes self-aggregation and oligomers formation [29, 30]. These phosphorylation sites have been illustrated in Figure 3. Hyperphosphorylated and non-phosphorylated Tau have been quantified and increase in total Tau for several fold in AD patients has been reported, as an attempt of affected neurons to maintain their function through synthesising more Tau [31]. Another reason contributing to the elevated levels of total Tau in AD, is slower turnover of hyperphosphorylated Tau in several fold [32], due to the fact that the abnormal hyperphosphorylated Tau is less likely to be proteolyzed by the calcium activated neutral protease [33, 34]. Thus, in addition to phosphorylated Tau, Total Tau alterations are necessary to measure in AD studies, and reducing total Tau may provide some benefit to AD patients.

Tau propagation refers to the proposed pattern of Tau spreading from one neuron to another [35]. Some studies show that Tau aggregation is taken up by postsynaptic neurons and act as a seed of increasing Tau aggregation [36], leading to formation of NFT in the recipient neurons. [37]. This form of Tau progression has been confirmed in several transgenic Tau mouse models, providing strong evidence for inter-neuronal Tau propagation in the rodent brain [7, 38, 39]. Similar findings were reported from cell culture model [40], and postmortem AD patients in humans [41]. The activity-dependent release of Tau via exosomes has also been reported, leading to uptake by adjacent cells in brain [42, 43]. Interestingly, the propagation of NFTs is highly correlated with cognitive disease progression. According to Classic Braak staging in AD, NFTs appear sequentially in the transentorhinal/peripheral cortex (Braak stage I), the CA1 region of the hippocampus (Braak stage II), limbic structures (Braak stage III), amygdala, thalamus and claustrum (Braak Stage IV), isocortical areas (Braak stage V), and finally, primary sensory, motor and visual regions (Braak stage VI). This

classification prioritise brain regions for more investigation [44]. Overall, it can be concluded that Tau proteins exist in many forms and different locations including both inside and outside of neurons, which in addition to disruption of microtubules, leads to neuron functional disturbance and finally neuron death presenting as dementia.

Although normal Tau is usually soluble and can be isolated from the cytosol, Tau protein obtained from AD patients brain tissue has been found in three main states; soluble, oligomeric, and fibrillated [24, 25, 45]. All these states have been considered in causing tauopathy related conditions. In addition to fibrillated Tau, for instance, in 3×Tg mice that demonstrates both plaque and tangle pathology, reduction in soluble hyperphosphorylated Tau accompanied with soluble A β has improved cognitive impairment [46]. Thus, studying all forms of Tau in AD patients and AD mouse models in addition to its aggregation and NFT formation would be beneficial to our understanding of tauopathies.

In this study two phosphorylation sites in proline-rich region and total Tau have been targeted for quantification and future investigations. Significant increases in phosphorylation at serine and threonine (such as Thr231 and Ser202/Thr205) has previously been shown in AD [47], and as such antibodies (Abs) directed against these phospho-serine-proline or phospho-threonine-proline motifs have been established as diagnostic marker for the postmortem AD [48]. Among these Abs, AT180 labels phosphorylated threonine 231 and AT8, which is the most prominent of the AT-series of monoclonal Abs [49], recognizes a doubly phosphorylated epitope including S199, S202 and T250 [50, 51]. In addition to these two, HT7 antibody which detect total Tau has been applied given the importance of detecting changes in total Tau expression level, which occurs normally as a result of alteration in Tau phosphorylation in tauopathies. Phosphorylation sites targeted by our exploited Abs have been signed by arrows in Figure 3.

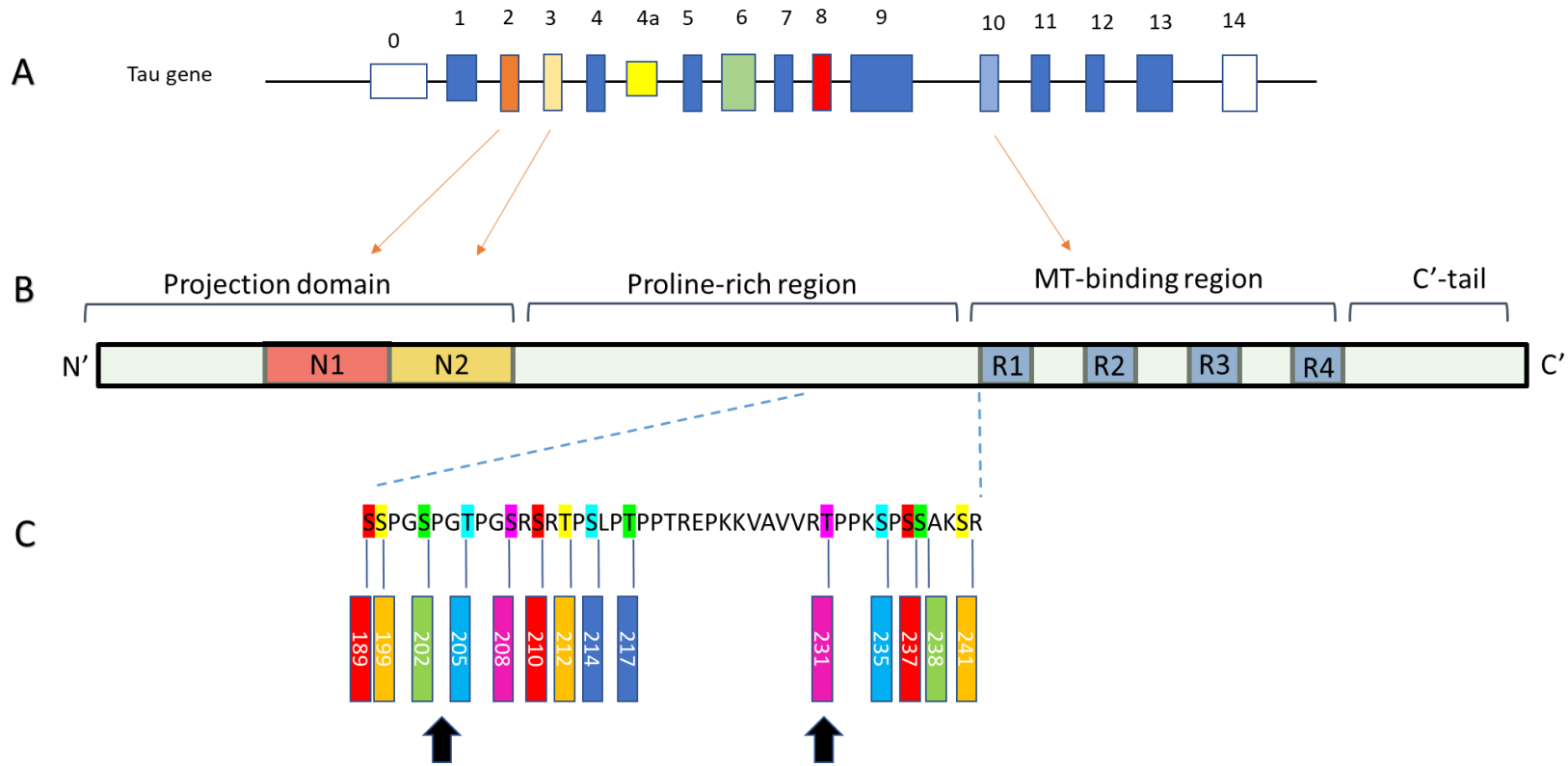


Figure 3. Tau gene, longest transcript, and phosphorylation sites. A) The MAPT gene. B) Tau protein (isoform4). C) Phosphorylation sites in proline-rich region and our targeted phosphorylation sites identified by arrows.

In addition to different phosphorylation sites targeted by Tau antibodies, these antibodies differ in staining NFTs at their different morphological stages. According to Kimura et al. (1996), NFTs are divided into Pre-NFT, intra-neuronal NFT (iNFT) and extra-neuronal NFT (eNFT), that are formed during sequential stages in AD and as the disease progresses from mild to severe [52]. AT8, AT180 and HT7 detect all forms of NFT from early stages [53], however the percentage relative to each one of p-NFT, iNFT and eNFT varies between antibodies [47, 54]. These characteristics are exploited to study stages of the disease as well as neuronal morphology alteration and neuropil threats (REF). These antibodies combined by DNA-banding stains demonstrate a comprehensive picture of NFT formation and neuronal loss at different stages of the disease.

In addition to the role of NFT formation in tauopathies, the non-fibrillized hyperphosphorylated Tau has demonstrated the inhibitory activity in yeast, drosophila, and in mouse models that express human brain Tau. The expression of the longest human brain Tau (2N4RTau) in yeast generates pathological phosphoepitopes responsible for formation of Tau aggregates at later stages [55]. The same accumulation of abnormally phosphorylated Tau with no sign of Tau fibrillization leading to neurodegeneration has been reported in wild type human Tau- and mutated human Tau-transgenic drosophila [56]. Similar conclusion has been drawn in another study conducted in a P301L Tau transgenic mouse model, based on the experiment in which cognitive impairments improved after suppression of hyperphosphorylated human despite formation of neurofibrillary tangles [57]. These studies highlight the importance of the cytosolic hyperphosphorylated Tau in tauopathies independently from insoluble Tau formation.

The abnormal hyperphosphorylation of Tau leads to morphological alterations of the endoplasmic reticulum (ER) and the Golgi apparatus [58-60], which in addition to forming neurofibrillary tangles, is known to be responsible in AD pathology. Moreover, the abnormal N-glycosylation of Tau in AD as a result of Phospho-Tau gathering in the somato-dendritic compartment might lead to the morphological alterations of the ER and the Golgi apparatus. This has been examined both in neuronal cultures and in neurons in JNPL3 P301L Tau transgenic mice [61]. For instance, this drop in mitochondria and RER in P301S Tau transgenic mice illustrating abnormal Phospho-Tau accumulation has been reported previously [62]. In addition, chronic accumulation of this abnormally phosphorylated Tau could contribute to neurodegeneration due to protracted ER stress originating from existence of misfolded protein in the ER [63]. This Hyperphosphorylation of Tau might also alter ER and Golgi which leads to neurodegeneration. These changes can be further studied to shed light on effects of hyperphosphorylation of Tau rather than its aggregation.

1.1.2 Neuroinflammation in AD

In addition to cell death and endoplasmic reticulum stress, neuroinflammation has been observed in areas of plaque deposition in postmortem AD patient brains by an increase in the number of Astrocytes and Microglia [64]. Although neuroinflammation in healthy brain acts as a defence mechanism in phagocytosis of debris material, in AD this neuroinflammation and innate immune response lead to disease progression. In this mechanism, Astrocytes and Microglia are activated by pathologic misfolded or aggregated proteins attached to their pattern recognition receptors and release cytokines and chemokines creating a chronic inflammatory status. Targeting neuroinflammation and its immune response has been considered as new approach to propose new therapeutic interventions [65]. Thus, neuroinflammation as well as neural death and synaptic dysfunction are considered as essential issues that need to be investigated more closely.

1.1.3 Mouse model of AD

Animal models used in AD studies can be divided into transgenic or non-transgenic models and animal models for aging [66]. Several transgenic mouse models for AD have been developed to identify underlying molecular mechanisms and develop therapeutics for AD. The first transgenic mouse model was published in 1995, by the Games' group. Since then, a large number of transgenic mouse models

of AD has been developed by mutating AD-linked genes including APP, PSEN1, PSEN2, and MAPT [67, 68]. Various transgenic mice types developed for AD, containing genes for either beta-amyloid or Tau protein, have been demonstrated in Table 1.

Table 1. First AD transgenic mouse models. Sourced from <https://doi.org/10.1002/msj.20159>.

Mutant	First transgenic model	Year
APP	PDAPP	1995
BACE1	hBACE	1996
PSEN1/2	APP/PS1	1998
MAPT	TAPP	2001

There are several missense Tau mutations associated with frontotemporal dementia [69-71]. Among these, four of them have been studied vigorously: G272V, P301L, V337M, and R406W. As such, Santacruz and colleagues [57] devised an experimental transgenic mouse model, in which human four-repeat Tau with the P301L mutation was induced; and correlation between cognitive deficiencies and emerging hyperphosphorylated Tau was reported.

Mouse model used in this project is TAU58/2. TAU58/2 is a P301S mutant Tau transgenic mouse line. This model presents an age-dependent motor and memory deficit Tau hyperphosphorylation and consequently NFT formation that resembles the Tau pathology in AD is reported in this mouse model [72]. In this study, we evaluated Tau hyperphosphorylation, total Tau level and Tau aggregation and insoluble formation in this mice model.

1.2 Previous studies designed to rectify pathological changes in AD

1.2.1 Targeting Tau

In AD, hyperphosphorylated Tau aggregates to form NFT and is a potential leading cause of neurodegeneration in the disorder [26]. Tau can be targeted at the expression level or by targeting deregulated post-translational modifications. At the expression level, RNA targeted therapies utilise Watson Crick base pairing-focused antisense mechanisms which aims to degenerate or inactivate targeted mRNA [73]. These therapies are designed based on exploiting either siRNA or ASOs. ASOs are chemically modified, single stranded oligonucleotides which reduce targeted mRNA levels via two mechanisms. First, they activate RNase H enzyme in the nucleus and increase the degradation of binding mRNA to them. Secondly, they alter mRNA splicing and inhibit mRNA translation in the cytoplasm [74]. To induce total Tau reduction, ASOs against Tau were injected intracerebroventricularly (ICV) to old PS19 transgenic mice with P301S mutation, resulting in reduction of Tau phosphorylation and deposition. In addition, it prevented neuronal death and prolonged neuronal survival [75]. On the downside, ASO therapies have a short half-life and are notoriously unstable and there are concerns about safety including tolerability and side effects.

Application of siRNA contributes to inhibition of a particular mRNA and its cleavage. This change is conducted through activation of the same pathway by which RNAi regulates mRNA. In this pathway, mRNA will be regulated at the level of post transcriptional processing in the cytoplasm and via the RNA-induced silencing complex [76, 77]. In one study, siRNA against MAPT was injected stereotactically into the brains of P301S mice to suppress Tau expression which could effectively reduce Tau levels with no signs of neurotoxicity or neuroinflammation as well as apoptosis [78]. Therefore, improving drug delivery mechanisms to deliver siRNAs against Tau may be of benefit for AD patients.

Other several therapies targeting Tau have been investigated, such as disrupting Tau misfolding [79], targeting Tau acetylation [80], inhibiting Tau-induced proteasome impairment [81], and Tau immunotherapy [82-85]. For example, one noteworthy substance is Methylthioninium chloride (Methylene blue dye) based on its capability to disaggregate PHF *in vitro*. This agent has been reported to reduce the number of Tau aggregates in Tau transgenic mice, and it has contributed to significant inhibition of cognitive impairment in a PHASE II double-blind clinical trial in AD patients [86, 87]. However, efficacy of these approaches is not yet confirmed. Drugs targeting post-translational modifications which prevent Tau–microtubule binding and reduce Tau misfolding are listed in Table 2.

Table 2. Tau modification agents sourced from <https://doi.org/10.1038/s41582-018-0013-z>

Mode of action	Example drugs
Phosphate modifiers	Memantine
Kinase inhibitors	Flavopiridol, Roscovitine (CDK5 inhibitor) Tideglusib (GSK3 β inhibitor)
Tau acetylation inhibitors	Salsalate
Tau deglycosylation	MK-7819
Tau truncation inhibitors	Caspase inhibitors
Tau aggregation inhibitors	Methylene blue and curcumin as promising candidates
Microtubule stabilizer	TPI287(ongoing clinical trial)

1.2.2 Targeting A β

Given the fact that elevated A β levels have been reported in both familial AD (FAD) and sporadic AD (SAD), reducing A β can be advantageous for treating disease. Therefore, immunotherapies targeting different forms of A β , BACE1 inhibitors or γ secretase inhibitors have been vastly exploited [88-90]. However, immunotherapies face a few limitations such as their cohort design, optimum time for intervention, and low efficacy due to low blood-brain barrier (BBB) passage of antibodies. An alternative would be siRNA-mediated downregulation of APP. Various studies have been conducted to deliver such therapies [91, 92]. However, as APP has other biological functions, this potentially could cause side effects [93, 94]. Complete deletion of BACE1 also caused serious adverse effects [95]. An alternative way to target BACE1 is to deliver exosomes loaded with BACE siRNA [96]. In addition ASOs have been exploited as another therapeutic approach, and in one study 39% decrease in A β levels was observed after a series of 4 weekly ICV injection of ASO targeting the mutated site [97]. To summarize, strategies to reduce A β levels including immunotherapy, applying ASOs or siRNA, have not been completely successful, and further investigation exploring other approaches are pivotal.

The PSEN1/2 genes have also been shown to contribute to the formation of A β [10]. In order to develop treatment targeting PSEN, several studies have been conducted in A β PP/PSEN [98]. A wide array of miRNAs targeting proteins involved in AD pathogenesis have been identified such as miR-9 targeting BACE1 and PSEN1. Furthermore, a few therapies targeting misfold proteins have been tested. Unfortunately, most of the new agents have failed in clinical trials. Late stage disease modifying treatments targeting A β and Tau protein are listed in Table 3.

Table 3. Modifying treatments targeting A β and Tau protein report at different clinical trial phases. Sourced from DOI: 10.3233/JAD-190507 and <https://clinicaltrials.gov>

Drug	mechanism of action	Clinical Trial Phase	Results
Atabecestat	BACE inhibitor	Phase II/III	Liver toxicity
CNP520	BACE inhibitor	Terminated	Due to worsening of cognitive function
Elenbecestat	BACE inhibitor	Two Phase III trials	Ongoing
Lanabecestat	BACE inhibitor	Phase III	Lack of efficacy
Etazolate	A-secretase	Phase II	In the first three months of treatment no significant differences between treatment groups reported
LY3202626	BACE inhibitor	Terminated	Lack of efficacy
Verubecestat	BACE inhibitor	Terminated	worsening cognition and daily function in patients
Scyllo-inositol (ELND005)	A β aggregation	Phase II	Serious side events
Avagacestat	γ -secretase inhibitor	Phase II	Serious adverse effects
r-flurbiprofen (Flurizan)	γ -secretase inhibitor	Phase III	Lack of efficacy; Poor bioavailability
Semagacestat	γ -secretase inhibitor	Terminated	Lack of efficacy
Aducanumab	Aggregated A β	Terminated	lack of efficacy
BAN2401	A β clearance	Phase III	Did achieve primary endpoint at 18 months, however there are concerns regarding <i>APOE</i> genotype difference between placebo and drug groups
Bapineuzumab	A β clearance	Terminated	Lack of efficacy

Crenezumab	Aggregated A β	Terminated	lack of efficacy
IVIg (Gammagard)	A β clearance	Phase III	Ongoing
Gantenerumab	A β clearance	Phase II/III Phase II/III	Lack of efficacy Higher dose Phase III trial in mild AD and prevention trial are ongoing
LY3002813	Aggregated A β	Phase II	Ongoing
Solanezumab	Soluble A β	Terminated	Lack of efficacy
CAD106	A β	Phase III	Ongoing
ACI-24	A β	Phase I/II	Ongoing
BIIB092	Tau	Phase II	Ongoing
C2N 8E12	Tau	Phase II	Ongoing
AADvac-1	Tau	Phase II	Ongoing
LY3303560	Tau	Phase II	Ongoing
RO7105705	Tau	Phase II	Ongoing

1.3 Strategy of developing therapeutics for AD

Small interfering RNAs (siRNAs) are able to degrade target mRNA and suppress its expression with high specificity [99]. Both viral and non-viral (synthetic) carriers have been investigated for delivery of siRNAs into brain [100, 101]. Several carriers like nanoparticles can be used to transport these siRNAs to their desirable targets. However, one of the major hurdles to develop pharmaceutical interventions for AD is existence of the blood-brain barrier (BBB), which guards against unwanted neurotoxic blood-borne substances and cells into brain parenchyma [102].

Viral vectors can efficiently penetrate the BBB and are capable of high cell transfection rates. However, carcinogenesis, immunogenicity and broad tropism are among their limitations [103, 104]. Although non-viral carriers have the potential to address many of these limitations of viral carriers [105], they are not efficient to cross BBB. Many nanoparticle (NPs) drug delivery systems such as polymeric NPs, liposomes, metal-based NPs and others are designed and applied accordingly. Given the fact that brain capillary endothelial cells (BCECs) are at the first line to hinder the transport of nanoparticles from the vasculature into the brain parenchyma [106, 107], ligand-targeted delivery systems are introduced to integrate with their corresponding receptors overexpressed in BCECs in order to increase the chance of brain accumulation of ligand-bound nanoparticles.

Recently, a novel nanoparticle GLU-NPs, which binds to the glucose transporter 1 (GLUT1) in BCECs, has been investigated. A mild hypoglycaemia caused by fasting leads to GLUT1 migration from abluminal to luminal plasma membrane in BCECs [108]. Following glucose injection and GLU-NPs administration, maximised luminal GLU-NPs binds to the GLUT1 receptor and then the NP complex is recycled back to the abluminal BCEC side. This not only enhances the accumulation of GLU-NPs in the brain remarkably, but also decreases toxicity and side effects.

In previous studies, BACE1 expression silencing by GLU-NPs loaded with BACE1 siRNA was investigated (unpublished lab studies). A reduction of 30 % in BACE1 mRNA was observed in whole mice brain after 8 hours of fasting with subsequent glucose treatment compared to control mice which were treated with non-glucosylated NPs containing scrambled siRNA. Thus, effective in-vivo BACE-1 silencing ability by GLU-BACE-NPs was reported in wild type mice. These results suggested siRNAs could be delivered with GLU-NPs to cross BBB to AD lesion.

This MRes project will investigate expression of phosphorylated Tau in TAU58/2 mice. This will lay the foundation to develop siRNA-based treatment for AD in TAU58/2 mice model in the future.

1.4 TAU58/2 mouse model

In 2015, Ittner and his group characterized a novel P301S mutant transgenic mouse line, TAU58/2, which demonstrates early-onset motor defects, Tau hyperphosphorylation, NFT formation, exited microglia and axonal pathology at 3 and 10 months of age. All these features made it an instrumental mouse model in future studies in both FTLD and AD. This mouse model expresses the human ON4R Tau isoform with the P301S mutation under the control of the mouse Thy1.2 promoter. The corresponding cDNA For pronuclear injection (C57Bl/6xBALB/c background) was inserted into vector pTSC21, linearized and vector sequences removed [109]. The expression of P301S mutant human Tau has been measured in several brain regions of TAU58/2 mice including the hippocampus, cortex and brainstem [110]. At 1 month of age reduced body weights can be observed. At 3 months of age, Gallyas-positive NFTs in the cortex and the brainstem appears. At this age, phosphorylated Tau can be detected by anti Ser214 (pS214) antibody with IHC method [111]. Phosphorylation of Tau increased remarkably by 10 months of age. Similarly, two other anti-Tau phosphorylated at Ser422 (pS422) and Thr231 (pT231) demonstrated raise in staining intensity; however, the amounts of staining for Tau phosphorylated at S214 in the cerebral cortex, hippocampus and cerebellum is greater than S422 or T231. Although the overall amount of phosphorylated Tau increased with age, the amount of pS214-specific staining decreased in comparison with 3-month-old

mice in the subiculum of TAU58/2 mice. Regardless of these differences the greatest amount of Tau-specific staining (per μm^2) was reported in the midbrain, cerebellum and brainstem [111].

Several studies have been conducted to evaluate the pathological changes and memory dissociation in TAU58/2. Ittner et al (2019) studied gene expression and localization of proteins involved in cellular processes contributing to neuropathy such as glutamatergic signalling, protein scaffolding and genes excitatory. MAPT Gene dysregulation as the origin of Tau accumulation were reported when comparing TAU58/2 with wild type littermates in both young and old age groups [112]. A separate study was conducted in 2017 as an attempt to understand the underlying mechanisms for motor deficits related to tauopathies [113]. Hyperphosphorylated Tau was detected in the cell bodies and axons of motor neurons. Moreover, axonal degradation and the denervation of neuromuscular junctions as well as myelin abnormalities were hypothesised as mechanisms responsible for deterioration of motor function [113]. Behavioural changes including disinhibition-like behaviour were investigated in another study. This research introduced amygdala as primary and early site of pathological Tau deposition in these mice, also confirmed the resemblance between TAU58/2 and human FTD regarding neuropathological and behavioural changes [114]. Jeugd and his group in 2016 studied behavioural changes in three age cohorts in TAU58/2 mice and prominent Tau pathology in brain regions underlying these behaviours was reported which confirmed its application as a suitable model to test therapeutic investigations [115]. This in-depth understanding and robust phenotype of the TAU58/2 mice makes them a great model for investigating therapeutics for AD. Therefore, this model has been studied in this project at two ages: 3 months and 12 months of age. These timepoints have been chosen regarding previous studies in which changes in Tau expression started as soon as 3 months and behavioural changes were observed after 10 months.

1.5 Aims of this MRes project

Overall project hypothesis is that nanoparticle-mediated delivery of siRNA against Tau in neurons delays disease onset in AD mice. In this MRes study, I will measure the expression pattern of various forms of Tau in TAU58/2 mice at different ages. This will be used to determine the treatment window for future studies that evaluate the effectiveness of nanotechnology-based siRNA therapeutics for AD treatment. While previous studies of this mouse strain have reported agepoints both pre- and post-disease onset, it is well-described that housing conditions and other variables can affect these parameters and therefore there is variance in the same mouse line if held in different animal facilities. Therefore, it is important to define these parameters for the colony that will be utilised for therapeutic treatment. Moreover, I will study the expression of a range of phosphorylated Tau at various phosphorylation sites in addition to previously studied sites, which will provide valuable basic data needed for the main project.

This study focuses on the evaluation of Tau protein levels in a transgenic mouse model for AD (TAU58/2). This project will determine the expression profile of this target in disease-affected areas of the brain (hippocampus, midbrain and cortex) during different stages of disease progression. This data will define the timepoints for future experiments that will seek to downregulate related protein and evaluate whether this will alter disease trajectory or not. Notably, as the future treatments include application of nanoparticles, investigation through intact BBB in mice is preferable when compared to in vitro cell experiments. The research plan of this MRes project is divided into two parts as follows:

1.5.1 Aim 1

To determine protein expression levels of Tau and phosphorylation status in TAU58/2 mice models over the disease time course.

Mice will be anaesthetised then transcardially perfused with ice-cold 0.9% sodium chloride (NaCl) solution, so that the brain could be harvested. The brain will be hemisected and from half of the brain

the hippocampus, midbrain, cortex will be isolated for Tau protein measurement. Different antibodies listed in Table 4 will be utilized to detect total Tau and Phospho-Tau at two different phosphorylation sites and Tau isoforms. These measurements will provide us with the Tau protein expression levels in both total and phosphorylated form in TAU58/2 mice at two agepoints, in our newly established colony.

Table 4. Western blot antibodies

Antibodies Catalogue number	Company	Description
05-803	Merck	Detects Tau (3-repeat isoform RD3)
05-804	Merck	Detects Tau (3-repeat isoform RD3)
AT8(# MN1020)	Thermo fisher	Targets PHF-Tau (Ser202/Thr205)
HT7(# MN1000)	Thermo fisher	Detects all forms of Tau
AT180(#MN1040)	Thermo fisher	Detects Phospho-Tau (Thr231)

1.5.2 Aim 2

To correlate changes in Tau protein levels with neuronal loss and neuroinflammation in this mice model over the disease time course.

The other half of the brain will be exploited for immunostaining. List of antibodies that will be utilized in this project is shown in Table 5. Briefly the brain tissue will be fixed in 4% Paraformaldehyde then will be sectioned by vibratome. Afterwards, sections will be incubated with primary Ab followed by labelling with DRAQ5 and Neurotrace for counterstaining and Nissl staining, and finally with fluorescently conjugated secondary antibodies (Alexa Fluor 488 (green), Alexa Fluor 594 (red)). Iba1 and GFAP antibodies will be used to measure gliosis and indirectly neuroinflammation as during gliosis, GFAP (in astrocytes) and Iba1 (in microglia) are upregulated compared to normal condition. Three different brain regions will be stained including hippocampus, cortex, and midbrain. This part of the study will assist to confirm, and complete data obtained in aim 1 and establish the baseline data required to determine when treatment should begin to target various pathologies.

Table 5. Immunohistochemistry and immunofluorescence antibodies

Description	Host	Company	Catalogue No.	Dilution	
				IHC	WB
Anti-Glial Fibrillary Acidic Protein	Rabbit	Dako	z0334	1:1000	NA
Anti Iba1	Rabbit	Wako	019-19741	1:500	NA
Anti-Tau (3-repeat isoform RD3)	Mouse	Merck	05-803	1:500	1:1000
Anti-Tau (3-repeat isoform RD4)			05-804	1:500	1:1000
Anti-Total Tau			MN1000	1:1000	1:1000
PHF-Tau (Ser202/Thr205)		Thermo fisher	MN1020 (AT8)	1:1000	1:1000
Phospho-Tau (Thr231)			MN1040 (AT180)	1:1000	1:1000

An overall study design has been demonstrated in Figure 4.

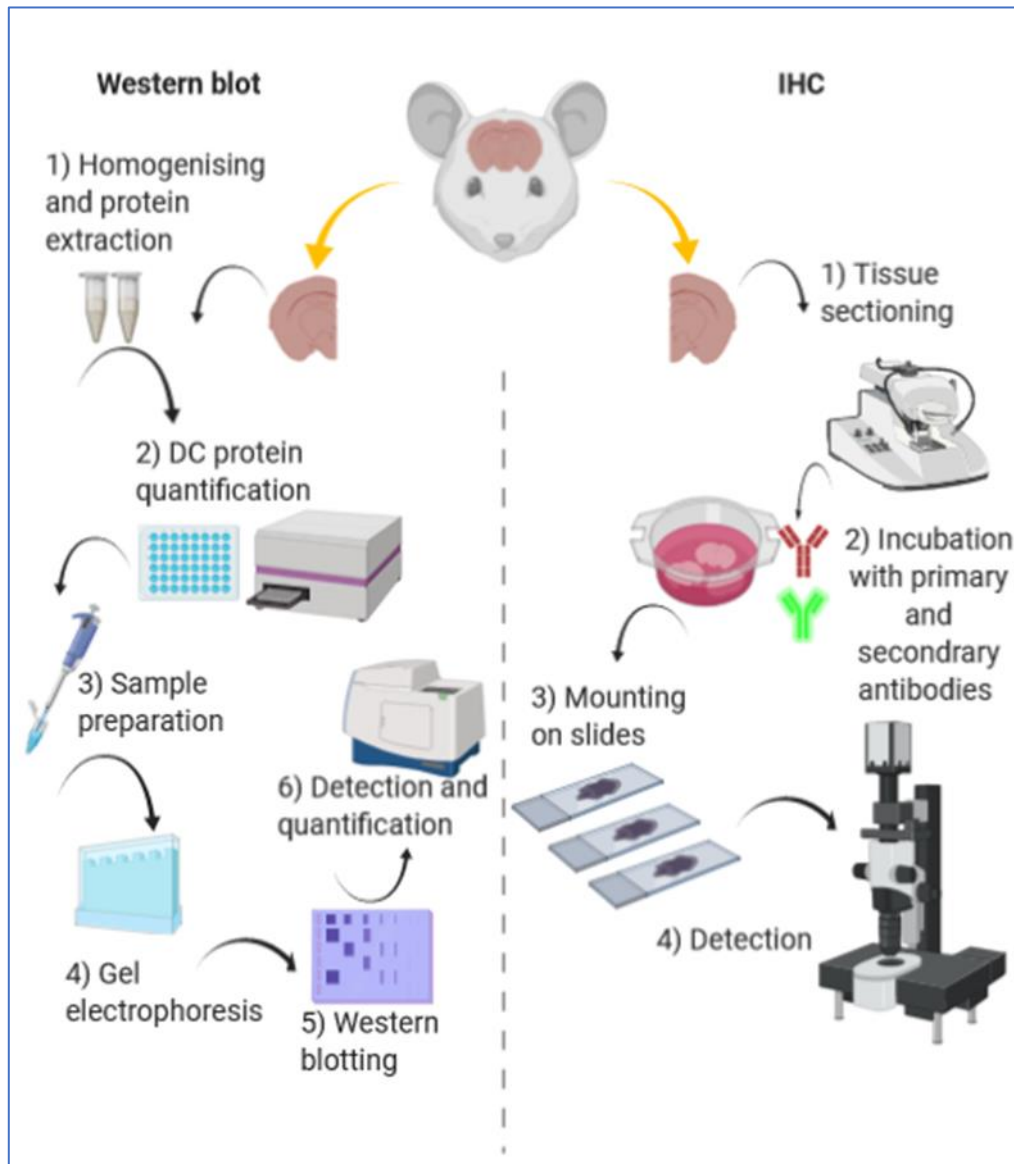


Figure 4. Illustration of experimental procedure for main project plan. Created with Biorender.com

Methodology

2.1 Mice

This thesis used tissue from TAU58/2 mice that was collected as part of a larger project led by the primary supervisor A/Prof Bingyang Shi. The animal tissue was collected by Prof Tim Karl (Western Sydney University) under approved ethics (A12910). The tissue was used at Macquarie University in the FMHHS PC2 laboratories, with institutional biosafety approval (# 5974 -52019597412350). All procedures were performed in accordance with this protocol. Female transgenic TAU58/2 mice which express the human ON4R Tau isoform with the P301S mutation [116] (under the control of the mouse Thy1.2 promoter), were utilized in this project. All animals were obtained from Western Sydney University where they were held by Prof Karl and euthanized by his staff, and I received the tissue for analysis. Cages were changed on a weekly basis; ambient temperature maintained at 23°C, and all cages were kept on automatic 12-hour light/dark cycle.

Mice at the 3 and 12 months used for tissue collections. As Table 6 shows, a total of 14 mice, including 8 twelve-month-old mice and 6 three-month-old mice were used in this project. In twelve-month-old mice group, there were four WT littermates (C57Bl/6xBALB/c background) and four transgenic TAU58/2 mice and in three-month-old mice group there were three mice for each WT and TAU58/2. As previous studies on TAU58/2 had reported no significant difference between two genders and we had Female Mice available, investigation was conducted only on Female mice.

Table 6. Mouse cohort

Wild type	TAU58/2
# 4 (F) 12-month-old	# 4 (F) 12-month-old
#3 (F) 3-month-old	#3 (F) 3-month-old

F: female

2.2 Tissue collection

Prior to collecting tissues, mice were anaesthetised with a cocktail of ketamine (8,7 mg/mL) and xylazine (2mg/mL), and underwent transcardial perfusion with ice-cold 0.9% sodium chloride (NaCl) solution at a pump rate of 10mL/min. The brain was hemisected and the hippocampus from one hemisphere was dissected, and frozen at -80°C for protein biochemistry. This was performed by Dr Rose Chesworth (Western Sydney University). The remaining brain hemispheres were fixed by 4% Paraformaldehyde (PFA; Sigma-Aldrich; St Louis, MO) Phosphate-buffered saline (PBS; pH 7.4) for 24 hrs, followed by immersion in 30% sucrose in 1x PBS for 2-3 days or until the tissue sinks. Fixed mouse hemispheres were then embedded in 2% (w/v) Low-Melting Temperature Agarose (Sigma Aldrich, A9414) in 1xPBS

and coronally sectioned at 30 μm using a Leica VT1200s vibratome and stored in 1xPBS containing 0.02% (w/v) sodium azide until processed for immunohistochemistry. This was performed by Bahar Kavyani, with guidance from Dr Amanda Wright.

2.3 Protein extraction (RAB-RIPA-Formic acid (FA) extraction)

Prior extracting protein, hippocampus of four transgenic and WT mice for 12-month timepoint, three transgenic and WT mice for 3-month timepoint were defrosted. Prior to protein extraction, hippocampus was weighed for each mouse, which has been reported in Appendix. Protein extraction was then performed according to solubility. Soluble and insoluble Tau protein were sequentially extracted with “reassembly buffer” (RAB), “radioimmunoprecipitation assay buffer” (RIPA) and 70% Formic Acid (FA) extraction (RAB-RIPA-FA extraction) as described previously; RAB buffer is used for the extraction of soluble proteins and it does not extract detergent extractable insoluble proteins, while RIPA buffer contains detergents. Therefore, RIPA has been used as a complementary buffer in addition to RAB to extract proteins in Sequential Extraction RAB/RIPA/Formic Acid protocol [117]. RAB, RIPA and FA formula is indicated in Table 7. In brief, hippocampus tissue was homogenized in ice-cold 10 $\mu\text{L}/\text{mg}$ Reassembly Buffer (RAB) [0.1 M MES, 1 mM EGTA, 0.5 mM MgSO₄, 0.75 M NaCl, 0.02 M NaF, 1 mM PMSF, for hippocampus and protease inhibitors (Complete Mini, Roche Applied Science, Mannheim, Germany), pH 7.0], 1 to 9 ratio, by stamping with a douncer 30 times and passing through a 29 gauge syringe 10 times. Then, samples were centrifuged at 50,000 x g for 20 min at 4 °C in The Beckman TL-100 ultracentrifuge. Supernatant, composing RAB fraction, was collected and snap-frozen. After washing with RAB, pellets were resuspended in prechilled 7.5 $\mu\text{L}/\text{mg}$ radioimmunoprecipitation assay (RIPA) buffer [1% (v/v) Triton-X-100, 150mM NaCl, 1% (w/v) sodium deoxycholate, 1% SDS, 50mM Tris-HCl, pH 8 and protease inhibitor cocktail (Roche)] and, processed then centrifuged as above. Supernatant was collected as RIPA fraction and snap-frozen. Finally, the remaining pellets were extracted with 70% Formic Acid (FA), 7.5 μL CH₂O₂ per 1mg of tissue, followed by adding neutralizing buffer (1M Tris, 0.5 M Na₂HPO₄). Insoluble fraction will be referred to FA extracted fraction because at this stage Formic Acid dissolves insoluble pellet, and soluble fractions are RAB and RIPA extracted fractions. All extractions were performed by Bahar Kavyani, with guidance from Stephanie Rayner.

7. Table Extraction buffers

Buffer	Content	Concentration	Stock solution	10mL total
RAB	MES (pH 7.4)	100mM	0.5M	2mL
	EGTA	1mM	100Mm	100uL
	MgSO4	0.5mM	1M	5uL
	NaCl	750mM	3M	2.5mL
	NaF	20mM	1M	200uL
	Na3VO4	1mM	100mM	100uL
	Protease inhibitor	1 Tablet per 10mL		
	dH2O		100%	5.095mL
RIPA	Tris (pH 8.0)	50mM	1M	500uL
	NaCl	150mM	3M	500uL
	NP40	1%	100%	100uL
	EDTA	5mM	100mM	500uL
	Na deoxycholate	0.5%	6%	833.33uL
	SDS	0.1%	10%	100uL
		dH2O		100%
FA	Formic Acid	70%	100%	7mL
	dH2O		100%	3mL

2.4 Protein quantification (DC Protein assay)

The DCTM (Bio-Rad Laboratories) as a detergent compatible method was chosen as a colorimetric assay to determine protein concentration following detergent solubilization. Proteins concentration for both soluble and insoluble Tau were measured using this kit and read at 750 nm with PHERAstar FS microplate reader (BMG Labtech, Australia) according to the product manual. Briefly, 5 µL of the protein lysate samples from TAU58/2 and WT mice brains, were diluted with Milli-Q® H₂O to 1:20 and 1:10, and 5 dilutions of a protein standard containing from 0.2 mg/ml to about 1.5 mg/ml protein were loaded in duplicate into a 96-well optical reaction plate. A 50:1 dilution of solution A to solution S was prepared and 25µL of this working solution was added to each well. Finally, 200 µL of reagent B was added and the plate was incubated for 15 minutes at room temperature. Serial dilutions of DC were used for standard preparations and protein was calculated based on the DC standard curve.

2.5 Western blot

2.5.1 Gel Electrophoresis

For soluble: 20 µg of each total protein lysate combined with 4 µL 4X Laemmli sample buffer, 2 µL 10X NuPAGE® reducing agent, and Milli-Q® H₂O to a total volume of 20 µL. For insoluble: 8 µg of each total protein lysate combined with 10 µL 4X Laemmli sample buffer, 4 µL 10X NuPAGE® reducing agent, and Milli-Q® H₂O to a total volume of 40 µL. Preparations were denatured (95°C for 5 min), loaded into a mini BLOT 12% Bis-Tris SDS-PAGE gel (NuPAGE®, Life Technologies) . Precision plus proteinTM dual colour standard (4 µL) was used as ladder. Gel was run (180 V for 40 min) in 1X MES SDS running buffer (C₆H₁₃NO₄S, Biorad). When the dye reaches half of the gel, the filter papers and membrane were incubated in 1x transfer buffer at room temperature (RT).

2.5.2 Transferring

Proteins were transferred electrophoretically onto the nitrocellulose membrane (BioRad, 1620115) using a semi-dry transfer method using the Trans-blot® TurboTM transfer system (BioRad). Membrane was blocked in blocking buffer (3% BSA in TBST) for up to one hour, then incubated with primary antibodies (1:1000) at 4°C overnight on a shaker. Primary antibodies used are demonstrated in Table 3. After incubation with primary antibodies, membranes were washed with TBS-T for 5 minutes and

with TBS for 5 minutes three times. Next, membranes were incubated with secondary antibodies (LiCor, ms680 and ms800 dilution: 1/10000) for one hour on the shaker at RT. After this, washing steps were performed then rinsed with Milli-Q® H₂O before imaging.

To confirm complete protein transfer from the gel to NC membrane, Coomassie staining was used for gels (for 30 minutes wash, followed by de-staining in 25% CH₃OH (overnight, 4°C)). Also, Ponceau S solution was used to stain membranes and after imaging them using Li-Cor Odyssey CLx system, the membranes were washed multiple times with Milli-Q® H₂O and 1X TBST (5 min) until the stain is removed completely. Dried membranes were stored at RT to be reused if needed.

Detection of signals was performed by Li-Cor Odyssey CLx system. New LICOR detection system (Odyssey CLx) exploits infrared (IR) fluorescent technology. To quantify the proteins of interest, LiCor Image Studio software was used to draw a rectangle around each protein band to obtain the signal intensity output provided by the software. The signal intensity was then normalised to the constitutively expressed housekeeping protein, β -actin, and one-way ANOVA with multiple comparisons ($P < 0.05$) performed on the data using GraphPad Prism (version 7).

2.6 Immunohistochemistry

Free-floating sections were transferred to 24-well plates and washed 3 times in 1x TBS for 10 min where all following incubations are performed on an orbital shaker. Sections were subsequently incubated with 10% Normal Goat Serum (NGS) + 0.3M Glycine + 50 μ g/mL Goat F(ab) anti-mouse IgG (Abcam ab6668) in 1X TBS for 2 hrs at RT to block non-specific binding, reduce fixation induced autofluorescence and block endogenous mouse IgG [118, 119]. Following blocking, sections were further washed before being incubated with primary antibodies (Table 8) diluted in 1% NGS in 1XTBS for 48 hrs at 4°C. Sections were then washed before being incubated with secondary antibodies (Table 9) diluted in 1% NGS in TBS over night at 4°C in the dark. After additional washes sections were counterstained with 1:100 Neurotrace Blue or Red (Invitrogen, N21479 and N21482) and 2.5 μ M DRAQ5 (Abcam, ab108410) or 2.5 μ M DAPI (Invitrogen, D1306) in PBS for 90 min at RT. Finally, sections were washed before being mounted on microscope slides with mounting media (Dako, S303) and coverslipped.

2.6.1 Microscopy analysis

Mouse brain sections which had been processed for fluorescence immunohistochemistry as described above were subsequently imaged on a Leica DMI8 widefield microscope. A 10x 0.3 numerical aperture objective was used to image coronal, hemi-sections in their entirety in order to assess the anatomical distribution of antigens. Images were stitched using ImarisStitcher (9.3) and Imaris (9.3.1) was used to export images. All images were captured by Bahar Kavyani, with assistance from Rowan Radford.

Table 8. Primary antibodies, their concentrations, and applications

Description			Host	Company	Catalogue No.	Dilution	
						IHC	WB
Anti-Glial Protein	Fibrillary	Acidic	Rabbit	Dako	Z0334	1:1000	NA
Anti Iba1			Rabbit	Wako	019-19741	1:500	NA
NeuN			Mouse	Merck	MAB377	1:500	NA
Anti-Tau (3-repeat isoform RD3)			Mouse		05-803	1:500	1:1000
Anti-Tau (3-repeat isoform RD4)				Merck	05-804	1:500	1:1000
Anti-Total Tau					MN1000	1:1000	1:1000
PHF-Tau (Ser202/Thr205)				Thermo fisher	MN1020 (AT8)	1:1000	1:1000
Phospho-Tau (Thr231)					MN1040 (AT180)	1:1000	1:1000

Table 9. Secondary antibodies, their concentrations, and applications

Antibody	Species	Dilution(application)	Catalogue No.	Brand
AlexaFluor488 mouse	anti- Goat	1:250(IHC)	A11001	Invitrogen
AlexaFluor568anti- rabbit	Goat	1:250(IHC)	A11008	Invitrogen
IRDye 680LT Donkey anti- Mouse IgG	Donkey	1:10000(WB)	LCR-926-68022	LiCor/ Millenium Science
IRDye 800CW Donkey anti- Mouse IgG	Donkey	1:10000(WB)	LCR-926-32212	LiCor/ Millenium Science

3

Results

The following chapter details the outcomes of each experimental strategy performed, including Western blot and immunofluorescence staining.

3.1 Optimising protein extraction of soluble and insoluble Tau in brain lysates

In AD mice, there are soluble and insoluble Tau in the brain. Soluble Tau can be extracted by RAB and RIPA buffers. Stronger buffer, like FA, is used to isolate the insoluble form. To establish the protocol to extract both forms of Tau in experimental mice (wild type and TAU58/2 transgenic mice), we first optimised the extraction conditions for Tau, including soluble and insoluble forms, from mouse brain. Brain tissues from a wild type and a TAU58/2 transgenic mouse at 12 months of age were used for optimisation. Phospho-Tau antibody (AT8) was used to probe Tau (Figure 5A), soluble Tau (RAB, RIPA fraction, lane 2-5) was detected in TAU58/2 mouse brain samples at 50 kDa, but not in the samples from WT mice, suggesting a successful extraction as previously reported [37]. However, FA fraction shows no bands at 50 kDa in lanes 7-8 (bands in Lane 5, TAU58/2, are leaked ladder from the left well), indicating extraction for insoluble Tau did not work. To address this issue, sonication was performed on the insoluble pellets in FA for 10 minutes. As shown in Figure 5B, Tau was detected at the correct size (50 kDa) in the sample from TAU58/2 (lane 9), but not in WT sample (lane 10). This indicates that sonication facilitated extraction for insoluble form of Tau. This protocol has been attached in the Appendix A.1.2. Collectively, these results indicate that by sequential extraction with RAB, RIPA and FA (with sonication), both soluble and insoluble Tau can be successfully extracted from experimental mice used in this thesis.

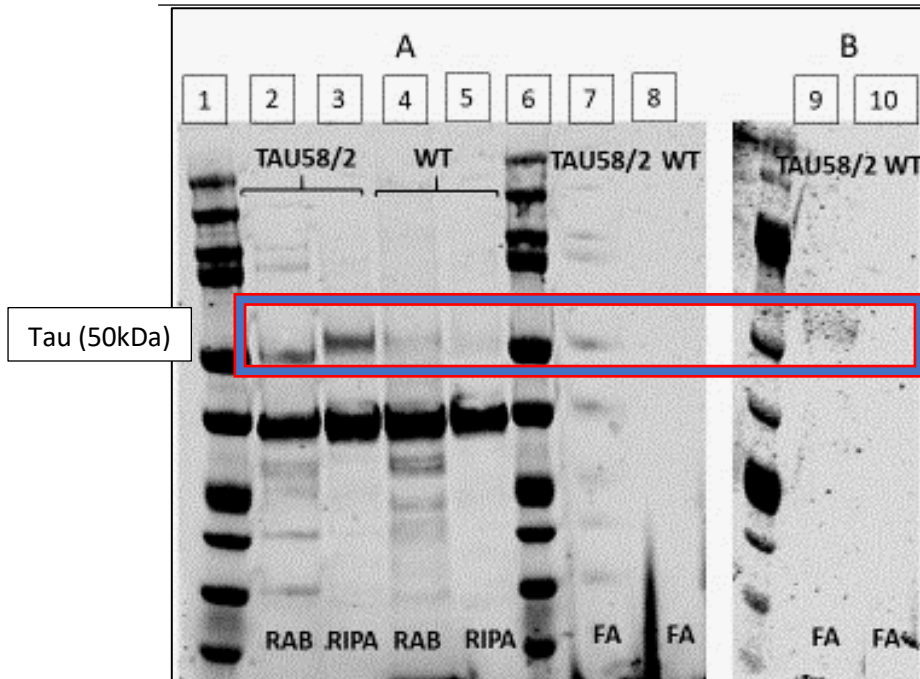


Figure 5. Detection of soluble and insoluble Tau from mouse brain samples (WT and TAU58/2 mice). Both at 12-month agepoint. RIPA and RAB were used for soluble Tau extraction. FA was used for extraction of the insoluble form. Anti-Phospho-Tau MN1020 or AT8 (50 kDa) was used to probe Phospho-Tau, and β -actin (42kDa) was employed as loading control. Precision plus proteinTM dual colour standard (4 μ L) has been loaded as a ladder in lanes 1,6,9. A) Soluble Tau fractions (RIPA, RAB) in TAU58/2 mouse and in wild type littermate, as well as insoluble Tau (FA fraction) in TAU58/2 and WT mice, respectively. As depicted only soluble fractions in TAU58/2 can be observed before optimization. B) Insoluble Tau band has emerged after optimization (lane 9). GAPDH has been utilized as positive control in Figure 5A.

3.2 Protein extraction and quantification from experimental mice.

I then used the established protocol shown above to extract Tau from experimental TAU58/2 and WT mice at 3 months and 12 months of age. Concentration of each fraction was determined by DC protein assay (Table 10, 11).

Table 10. 12-month samples protein concentration

Sample No.	RAB (μ g/ μ l)	RIPA (μ g/ μ l)	FA (μ g/ μ l)
TAU58/2 (#414)	0.733	0.768	0.345
WT (#415)	0.629	0.804	0.333
TAU58/2 (#420)	0.811	0.973	0.305
WT (#421)	0.586	0.942	0.301
WT (#425)	0.746	0.735	0.327
TAU58/2 (#426)	0.730	0.803	0.395
WT (#432)	0.955	0.480	0.256
TAU58/2 (#433)	0.939	0.582	0.301

Table 11. 3-month samples protein concentration

Sample No.	RAB (μ g/ μ l)	RIPA (μ g/ μ l)	FA (μ g/ μ l)
TAU58/2 (#570)	0.536	0.824	0.336
TAU58/2 (#564)	0.564	0.738	0.391
WT (#571)	0.74	0.722	0.336
WT (#576)	0.877	0.809	0.421
WT (#577)	0.661	0.445	0.319
TAU58/2 (#578)	0.669	0.535	0.364

3.3 Western blot optimisation

3.3.1 Testing Tau antibody concentrations for Immunoblotting

To systematically investigate Tau expression in WT and TAU58/2 transgenic mice, I tested several Tau antibodies targeting different isoforms of Tau and phosphorylated site. Aliquots from the same protein sample (RAB fraction from TAU58/2) was used for testing. The antibodies I tested are: total Tau (catalogue number: MN1000, 1:1000, ThermoFisher), Phospho-Tau at Thr231 (catalogue number: MN1040, 1:1000, ThermoFisher), Phospho-Tau at Ser202/Thr205 (catalogue number: MN1020, 1:1000, ThermoFisher), anti-Tau Isoform rD3 (catalogue number: 05-803, 1:1000, Merck), anti-Tau Isoform rD4 (catalogue number: 05-804, 1:1000, Merck), Phospho-Tau at Ser199 (catalogue number: 44-777, 1:1000, ThermoFisher), Phospho-Tau at Ser396 (catalogue number: ab109390, 1:1000, Abcam), Phospho-Tau at Ser199 phosphorylation site (catalogue number: ab92676, 1:1000, Abcam) as shown in Figure 6, MN1040, MN1020 and MAB361 showed a single specific band for Tau at around 50 kDa. MN1000 and MAB361, label total Tau (phosphorylated and non-phosphorylated Tau), while MN1040 targets phosphorylated Tau at specific phosphorylation site (Thr231). 05-803 and 05-804 which mark Tau isoform rD3 and Tau isoform rD4 respectively, demonstrate two bands for Tau, as they are not specific to human Tau and detect both mice and human Tau (both expressed in TAU58/2 mice). Other anti-Phospho-Tau antibodies (44-777, ab109390, ab92676) showed multiple nonspecific bands which led to their elimination from the current study. Both MN1000 and MAB 361 show strong and specific detection of total Tau. Therefore, MN1000 was chosen for the following experiment. Collectively, antibodies labelling total Tau (MN1000), Phospho-Tau at Thr231 (MN1040), Phospho-Tau at Ser202/Thr205 (MN1020), Tau Isoform rD3 (05-803) and Tau Isoform rD4 (05-804), were finalized to be used in Immunoblotting assay. Notably, MN1020 has not been shown in Figure 6 as it was tested for

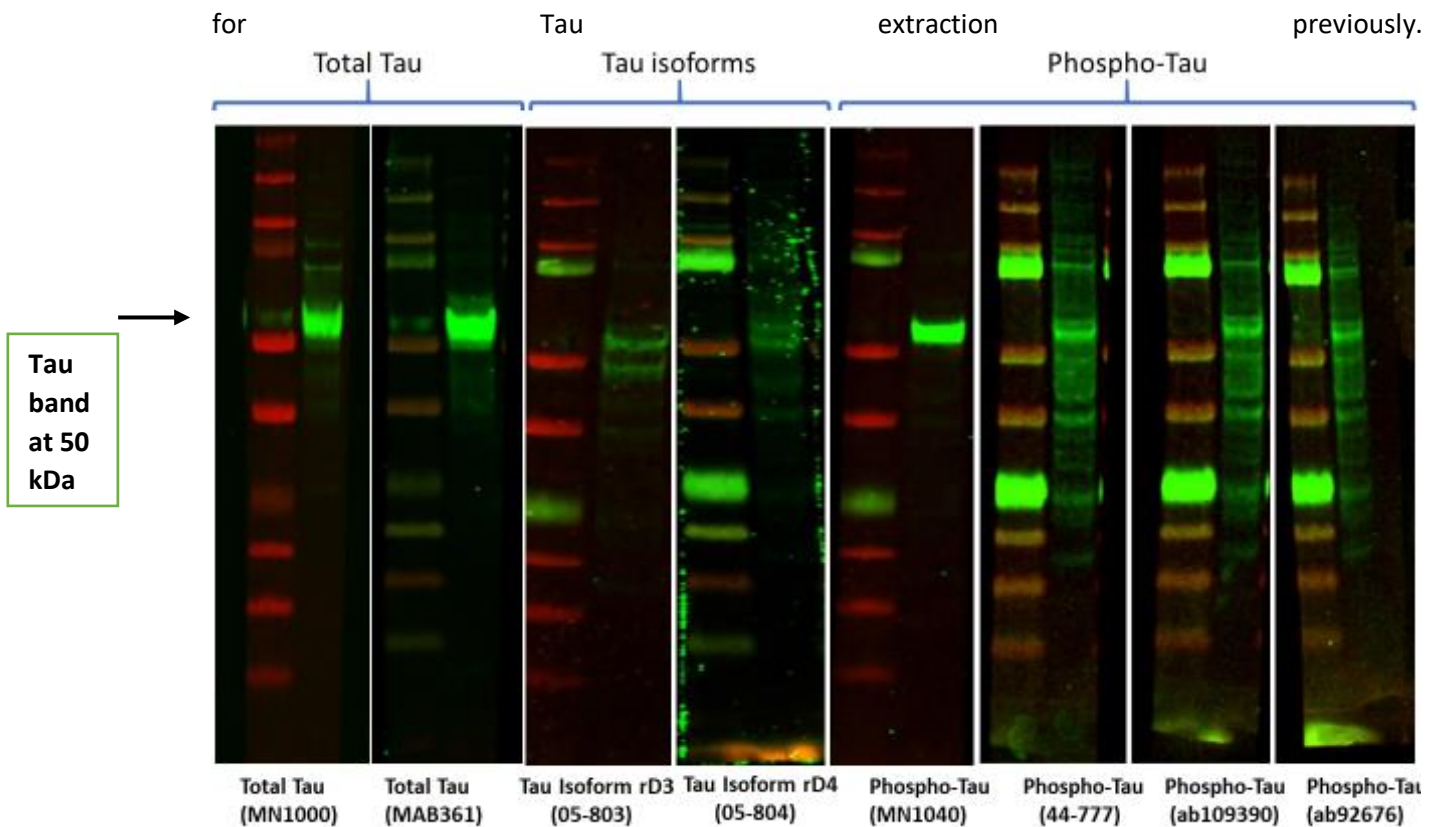


Figure 6. Antibody testing. 8 Tau antibodies were tested and MN1040, MN1020, 05-803, 05-804 have shown less nonspecific bands. MN1040: Detects Phospho-Tau (Thr231), MN1000: Detects total Tau, MAB 361: Detects total Tau, 05-803: Detects Tau (3-repeat isoform rD3), 05-804: Detects Tau (4-repeat isoform rD4), 44-777: Detects Phospho-Tau (Ser199), ab109390: Detects Phospho-Tau (Ser396), ab92676: Detects Phospho-Tau (Ser199).

3.3.2 Optimising housekeeping gene for immunoblotting

To choose proper housekeeping gene for our experiment, both GAPDH and β -actin antibodies were utilised (1:500, Merck) across soluble and insoluble fractions in transgenic mice and wild type littermate. Both antibodies showed bands for insoluble Tau (FA) and soluble Tau (RAB, RIPA) fractions in TAU58/2 and WT mice. As expected, based on insoluble fraction lower protein concentration, their related bands were less detectable than soluble bands. Given the fact that β -actin illustrated stronger bands than GAPDH for FA fraction in both groups, it was chosen as optimal positive control (Figure 7). Ladder has been loaded in the left well prior to each mouse various fractions. Sample used for optimisation was 12-month-old TAU58/2 and wild type dissected hippocampus tissue.

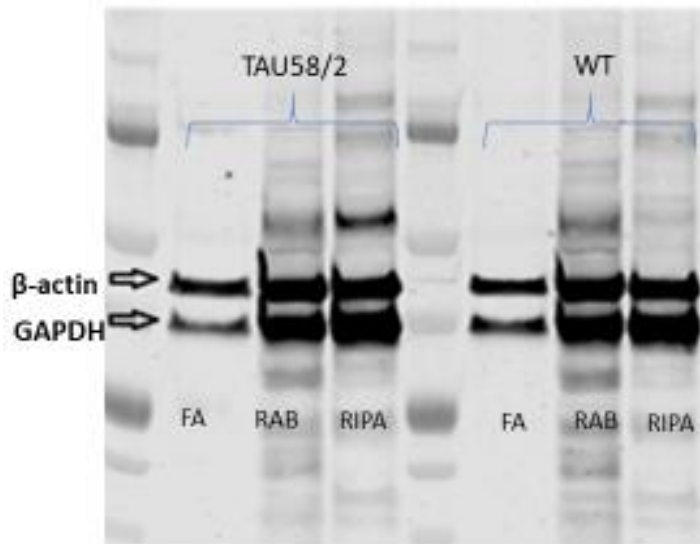


Figure 7. Comparison between β -actin and GAPDH as housekeeping genes. As band for β -actin was stronger for insoluble fraction (FA) in comparison with GAPDH, β -actin was chosen as a housekeeping gene.

3.4 Immunoblotting measurement of Tau

Following optimisation, I aimed to quantify total Tau and Phospho-Tau in TAU58/2 mice at early and late stages of AD. To probe and quantify Tau phosphorylation and aggregation in TAU58/2 mice in hippocampus, Western blot experiments for five chosen antibodies (MN1020 or AT8, MN1040 or rAT180, MN1000 or HT7, 05-803 or rD3, 05-804 or rD4) from optimisation step, were performed. First two antibodies detect phosphorylated Tau at two distinct phosphorylation sites (Ser202/Thr205 and Thr231), HT7 detects total Tau and two other antibodies detect rD3 and rD4 Tau isoforms, respectively. These experiments were done for two timepoints (three months and twelve months) to monitor these changes as disease progresses.

3.4.1 Transgenic TAU58/2 mice revealed a significant raise in total and phosphorylated Tau at 3 months of age.

Western blot for three 3-month-old TAU58/2 mice were performed to measure Tau protein expression at early stages of the disease. These transgenic mice were compared to three wild type mice regarding total Tau levels and phosphorylation in two sites including Ser202/Thr205 and Thr231. Moreover, the expression of two Tau isoforms (rD3 and rD4) also were investigated. The gels were shown in Figure 8 with quantification in Table 13 and Figure 9.

Alterations in both total Tau and phosphorylated Tau levels, were recorded as soon as 3 months of age in TAU58/2 mice in this study. Total Tau as well as phosphorylated Tau at Ser202/Thr205 (probed by AT8) and Thr231 phosphorylation sites (probed by AT180), were overexpressed in young TAU58/2 mice when compared to age-matched wild type mice in both soluble fractions (RAB, RIPA). Given the fact that Tau solubility drops from RAB to FA fraction, intensity of bands from RAB to FA decreases. Consequently, nonsignificant bands for insoluble fraction (FA) in total Tau and Phospho-Tau were detected. In FA fraction we noticed bands in TAU58/2 mice when HT7, AT8, AT180 antibodies were used, although some variables presented. However, after quantification (Table 13-15 and Figure 9-11), these bands were not significantly different.

Between two isoforms of Tau examined in this assay, only rD4 which is a 4-repeat Tau isoform (labelled by 05-804) was expressed significantly in TAU58/2 in RAB and RIPA fractions and not in FA fraction. On the other hand, it should be noted that although all antibodies showed increase in soluble hippocampal Tau protein level (both total and phosphorylated) at this time, protein level quantities differ from one to another. Total Tau detected by HT7 demonstrated the most increase in band intensity, then Tau rD4 isoform (marked by 05-804), followed by Phospho-Tau at Ser202/Thr205 site (marked by AT8) and finally phosphorylated Tau at Thr231 site (labelled by AT180), versus wild type Tau protein expression.

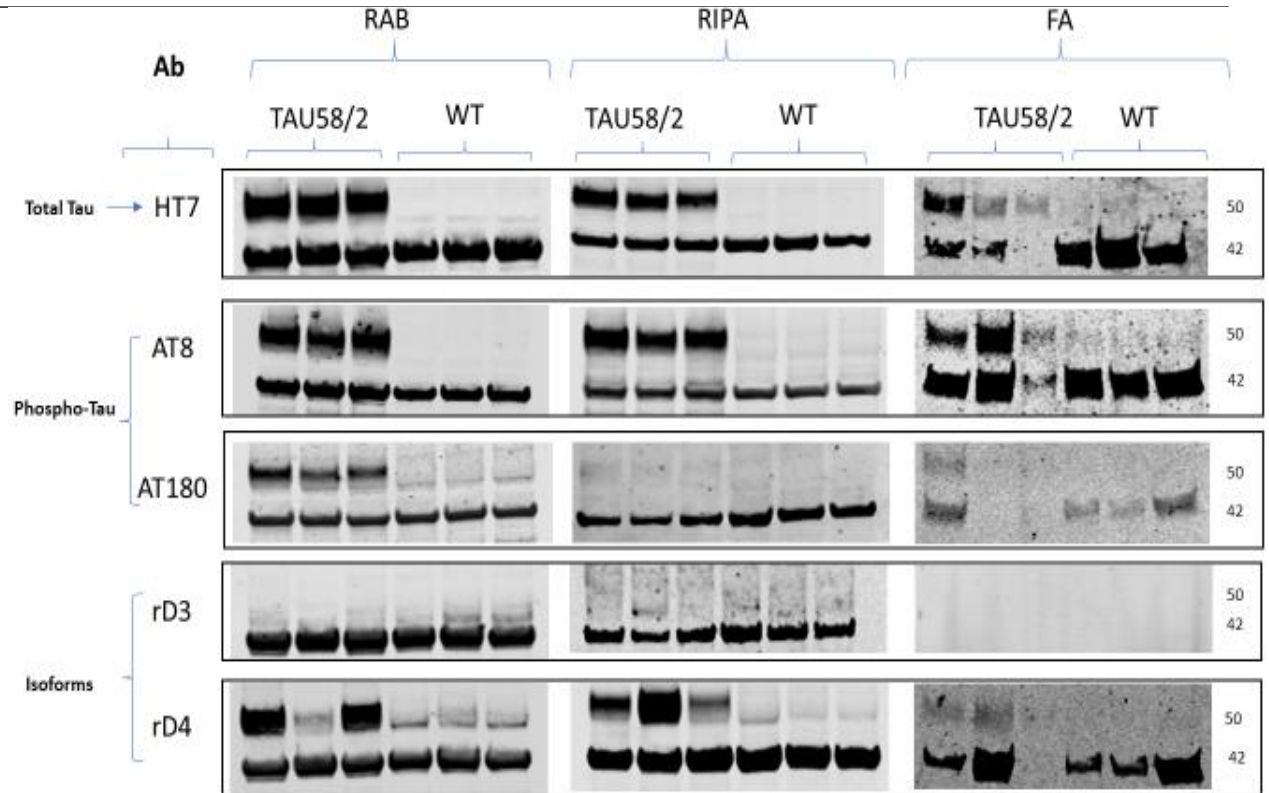


Figure 8. Western blot analysis in 3-month-old TAU58/2 and WT mice in soluble fractions (RAB, RIPA) and insoluble fraction (FA). Total Tau (HT7) was increased in soluble fraction ($p < 0.0001$ for RAB and $p < 0.05$ for RIPA versus nonspecific for FA). Phosphorylated Tau at Ser202/Thr205 phosphorylation site, labelled with AT8 showed strong bands in both soluble fractions (RAB and RIPA : $p < 0.01$). Significant bands were detected for phosphorylate Tau labelled by AT180 at Thr231 site in RAB ($p < 0.01$) and RIPA ($p < 0.05$) fractions. Tau 4-repeat isoform (rD4) protein expression level in RAB and RIPA fractions were significantly more than WT samples with P value of $p < 0.001$ and $p < 0.05$, respectively. Tau soluble and insoluble protein fractions were extracted from the hippocampus of 3-month-old female TAU58/2 mice ($n=3$) compared with wild type (WT) littermates ($n=3$). β -actin is used as loading control which illustrates band at 42 kDa. Tau can be detected by bands at 50 kDa. Non-specific bands were also evident in all blots.

For quantification, band intensities were extracted from LiCor Image Studio software (Table 12) and were used for normalization.

Table 12. Bands densities for five antibodies in 3-month-old TAU58/2 and WT littermates

3 months results		AT8			AT180			HT7			rD3			rD4		
Sample	Channel	RAB	RIPA	FA	RAB	RIPA	FA	RAB	RIPA	FA	RAB	RIPA	FA	RAB	RIPA	FA
TAU58/2 Mouse1	800	3730	2150	8.52	1030	63.6	20.2	35900	7730	283	244	12.7	2.07	7890	1140	15.4
TAU58/2 Mouse2	800	2110	1280	21.8	523	16.8	2.54	29600	5720	77.3	135	17.2	1.39	1390	6840	17.2
TAU58/2 Mouse3	800	3150	1640	2.42	556	18.6	0.189	27800	4720	48.1	222	13.9	0.63	7330	600	5.32
WT Mouse1	800	34	47.1	0.448	28.2	20.2	1.11	143	68.5	11.2	167	2.56	2.17	1240	26.8	5.01
WT Mouse2	800	32.1	46.9	0.729	73.8	13.5	2.25	79.1	41.5	28	376	2.26	2.97	1280	34.1	5.88
WT Mouse3	800	73.2	38.8	0.571	50.9	13.1	1.9	82	70.1	9.57	343	2.11	1.21	1160	26	6.48

Relative protein expression for RAB, RIPA, FA fractions for each TAU58/2 mouse has been normalized to β -actin based on LiCor handbook and the following formula:

$$\text{Normalized Signal} = \frac{\text{Target Band Signal}}{\text{Lane Normalization Factor}}$$

$$\text{Lane Normalization Factor} = \frac{\text{HKP Signal for Each Lane}}{\text{HKP Signal from Lane with Highest HKP Signal}}$$

Results have been reported in Tables 13-16. In addition, to investigate whether these differences between WT and TAU58/2 are significant, student t-test ($p < 0.05$) was performed on the data using GraphPad Prism (version 8) and results have been reported in Figures 9-12 in the mean \pm standard error of the mean (SEM).

Table 13. AT8 Normalization results for all fractions in 3-month-old WT and TAU58/2 mice.

Target protein (not normalized)	Sample treatment	Replicate	RAB				RIPA				FA			
			Normalization		Normalized to HKP		Normalization		Normalized to HKP		Normalization		Normalized to HKP	
			Target (800 nm)	LNF (HKP)	Apply LNF	Norm. Target	Target (800 nm)	LNF (HKP)	Apply LNF	Norm. Target	Target (800 nm)	LNF (HKP)	Apply LNF	Norm. Target
Lane														
1	WT	1	34	0.7607	44.693	44	47.1	1	47.1	47	0.448	1	0.448	0
2		2	32.1	0.8195	39.171	39	46.9	0.98104	47.806	48	0.729	0.981	0.74309	0
3		3	73.2	0.808	90.5915	90	38.8	0.91588	42.364	42	0.571	0.9159	0.62345	0
5	TAU58/2	1	3730	0.9456	3944.76	3945	2150	0.89929	2390.8	2391	8.52	0.8993	9.47415	9
6		2	2110	1	2110	2110	1280	0.85071	1504.6	1505	21.8	0.8507	25.6256	26
7		3	3150	0.937	3361.93	3361	1640	0.93602	1752.1	1752	2.42	0.936	2.58542	3

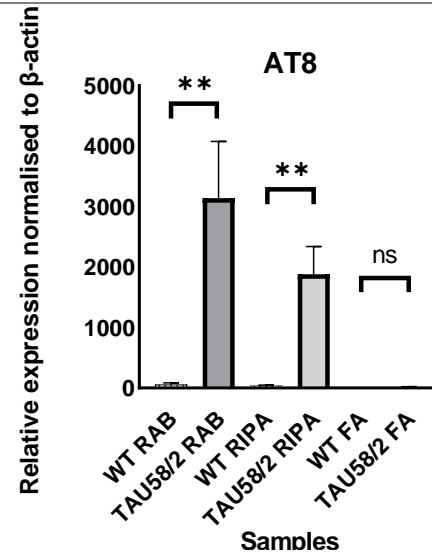


Figure 9. AT8 protein expression in 3-month-old WT and TAU58/2 samples in all fractions. (student's *t*-test; *n*=3/group). Each value presents the mean \pm standard error of the mean (SEM). ***p*<0.01, ns: nonsignificant.

Table 14. AT180 Normalization results for all fractions in 3-month-old WT and TAU58/2 mice.

Target protein (not normalized)	Sample treatment	Replicate	RAB				RIPA				FA			
			Normalization		Normalized to HKP		Normalization		Normalized to HKP		Normalization		Normalized to HKP	
Lane			Target (800 nm)	LNF (HKP)	Apply LNF	Norm. Target	Target (800 nm)	LNF (HKP)	Apply LNF	Norm. Target	Target (800 nm)	LNF (HKP)	Apply LNF	Norm. Target
1	WT	1	28.2	0.9021	31.2594	31	20.2	0.83776	24.112	24	1.11	0.8378	1.32496	1
2		2	73.8	0.9149	80.6651	81	13.5	1	13.5	13	2.25	1	2.25	2
3		3	50.9	0.9021	56.4222	56	13.1	0.80531	16.267	16	1.9	0.8053	2.35934	2
5	TAU58/2	1	1030	1	1030	1030	63.6	0.73451	86.588	86	20.2	0.7345	27.5012	27
6		2	523	0.9149	571.651	572	16.8	0.2885	58.233	58	2.54	0.2885	8.80429	9
7		3	556	0.8511	653.3	653	18.6	0.51327	36.238	36	0.189	0.5133	0.36822	0

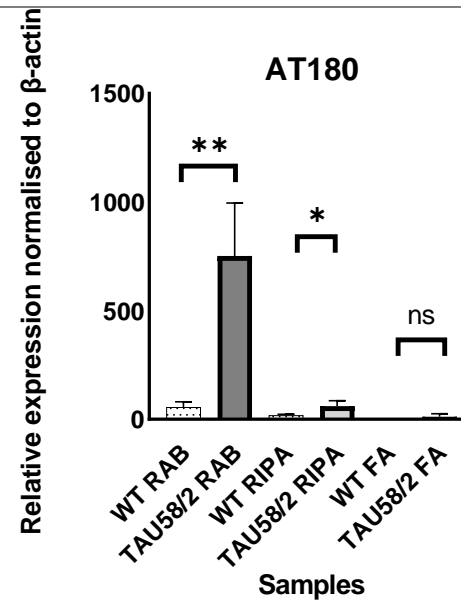


Figure 10. AT180 protein expression in 3-month-old WT and TAU58/2 samples in all fractions. (student's t-test; n=3/group). Each value presents the mean \pm standard error of the mean (SEM). *p<0.05, **p<0.01, ns: nonsignificant.

Table 15. HT7 Normalization results for all fractions in 3-month-old WT and TAU58/2 mice.

Target protein (not normalized)	Sample treatment	Replicate	RAB				RIPA				FA			
			Normalization		Normalized to HKP		Normalization		Normalized to HKP		Normalization		Normalized to HKP	
			Target (800 nm)	LNF (HKP)	Apply LNF	Norm. Target	Target (800 nm)	LNF (HKP)	Apply LNF	Norm. Target	Target (800 nm)	LNF (HKP)	Apply LNF	Norm. Target
Lane														
1	WT	1	143	0.7761	184.25	184	68.5	0.97859	69.999	70	11.2	0.9786	11.4451	11
2		2	79.1	0.8507	92.9772	93	41.5	1	41.5	42	28	1	28	28
3		3	82	1	82	82	70.1	0.76231	91.957	92	9.57	0.7623	12.5539	12
5	TAU58/2	1	35900	0.8856	40538.8	40539	7730	0.45824	16869	16869	283	0.4582	617.575	617
6		2	29600	0.8657	34193.1	34193	5720	0.80086	7142.4	7142	77.3	0.8009	96.5217	96
7		3	27800	0.6716	41391.1	41391	4720	0.803	5878	5878	48.1	0.803	59.9005	59

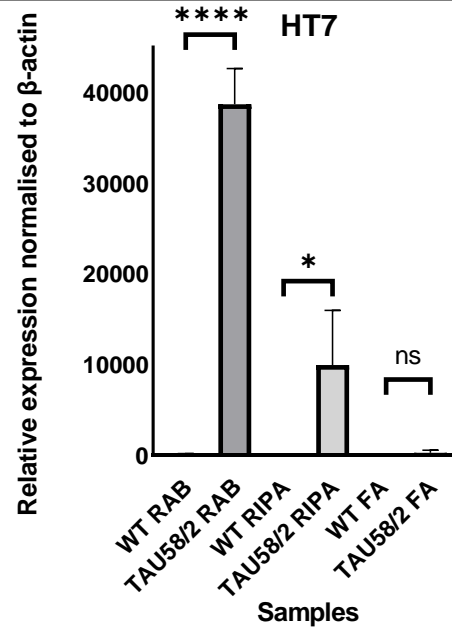


Figure 11. HT7 protein expression in 3-month-old WT and TAU58/2 samples in all fractions. (student's t-test; n=3/group). Each value presents the mean \pm standard error of the mean (SEM). * $p < 0.05$. *** $p < 0.0001$, ns= nonsignificant.

Table 16. rD4 Normalization results for all fractions in 3-month-old WT and TAU58/2 mice.

Target protein (not normalized)	Sample treatment	Replicate	RAB				RIPA				FA			
			Normalization		Normalized to HKP		Normalization		Normalized to HKP		Normalization		Normalized to HKP	
			Target (800 nm)	LNF (HKP)	Apply LNF	Norm. Target	Target (800 nm)	LNF (HKP)	Apply LNF	Norm. Target	Target (800 nm)	LNF (HKP)	Apply LNF	Norm. Target
Lane														
1	WT	1	1240	0.9181	1350.54	1350	26.8	1	26.8	27	5.01	1	5.01	5
2		2	1280	1	1280	1280	34.1	0.92199	36.985	36	5.88	0.922	6.37754	6
3		3	1160	0.9146	1268.33	1268	26	0.86525	30.049	30	6.48	0.8652	7.48918	7
5	TAU58/2	1	7890	0.7722	10217	10217	1140	0.78723	1448.1	1448	17.2	0.7872	21.8486	22
6		2	1390	0.669	2077.61	2078	6840	0.80851	8460	68460	30.4	0.8085	37.6	38
7		3	7330	0.8114	9033.9	9034	600	0.98582	608.63	609	5.32	0.9858	5.39655	5

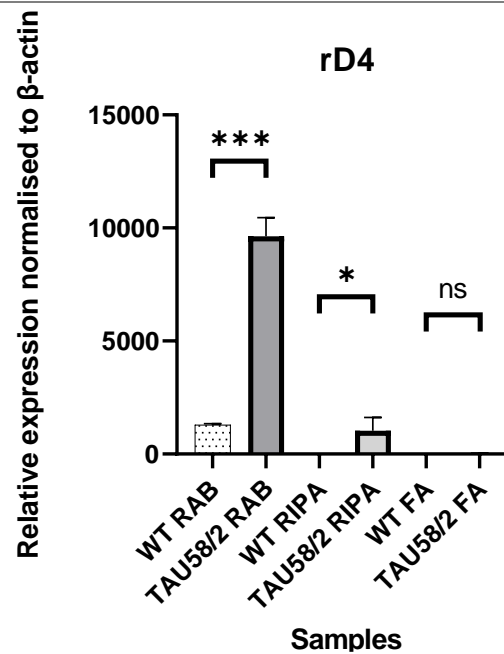


Figure 12. rD4 protein expression in 3-month-old WT and TAU58/2 samples in all fractions. (student's t-test; n=3/group). Each value presents the mean± standard error of the mean (SEM). *p<0.05. ***p<0.001, ns= nonsignificant.

3.4.2 Transgenic TAU58/2 mice have a significant increase in total and hyperphosphorylated Tau at 12 months of age.

To gain insight into overexpression of total Tau and phosphorylation of Tau at the 12-month time point, Western blot for four transgenic mice for different phosphorylation sites (Ser202/Thr205 and Thr231) and different Tau isoforms (3-repeat isoform rD3, 4-repeat isoform rD4) was performed. Western blot gel is shown Figure 13 and quantification for all antibodies is shown in Table 17-21 and Figure 14-17.

As expected, total Tau was overexpressed across all transgenic mice as compared to WT mice (Figure 13) in both soluble and insoluble forms. On the other hand, Tau phosphorylation was observed in both phosphorylation sites in TAU58/2 mice at 12 months in soluble fractions. However, AT8 bands which marks doubly phosphorylation site (S202/S205) are stronger when comparing to AT180 labelling Phospho-Tau at Thr231. In addition, differences between bands for AT180 in FA fraction were not significant after quantification. Therefore, unlike AT8, another distinctive result for AT180 is the lack of insoluble Tau formation at this phosphorylation site (Table 19, Figure 15). Lastly, Tau isoform rD4 (probed by 05-804 Ab) has been detected in TAU58/2 mice model in the absence of Tau isoform3 labelled by 05-803 antibody. This detection of Tau isoform rD4 is due to design of TAU58/2 mice line and under control of Thy1.2 promotor. Bands in isoform rD4 were stronger than bands detected for Phospho-Tau, as rD4 antibody (05-804) labels total 4-repeat isoform Tau (rD4). Moreover, significant formation of insoluble Tau was observed and quantified for this isoform (Table 21, Figure 17). All samples were normalized with β -actin as the positive control.

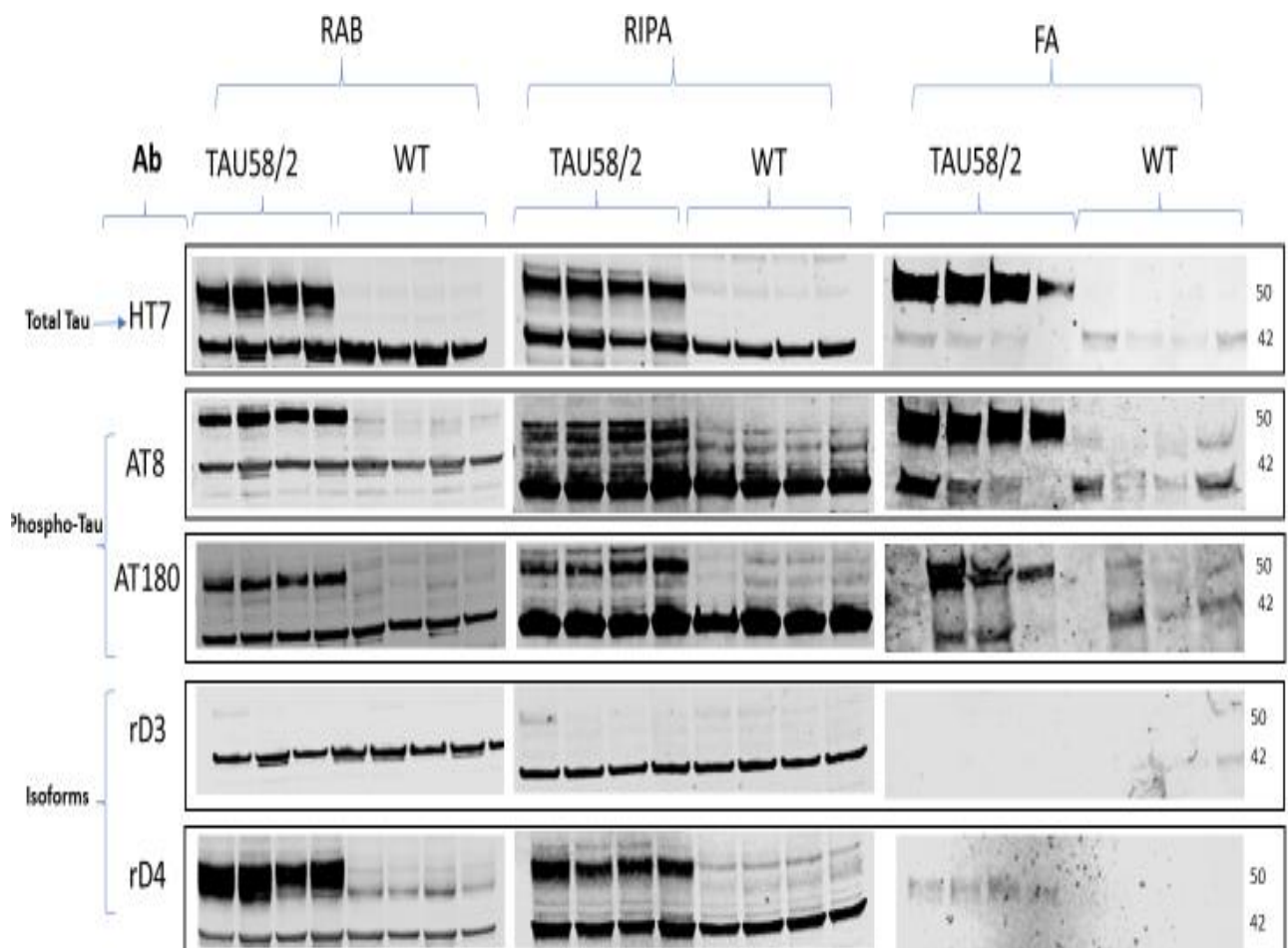


Figure 13. Western blot analysis in 12-month-old TAU58/2 mice and WT mice in soluble fractions (RAB, RIPA) and insoluble fraction (FA). Total Tau, analysed with the HT7 antibody, revealed a significant increase in the RAB ($p < 0.0001$), RIPA ($p < 0.001$) and FA fractions ($p < 0.05$) in transgenic mice compared to WT mice. AT8 antibody labelling Phospho-Tau at Ser202/Thr205 site showed bands in 12-month-old TAU58/2 mice as compared to age matched WT littermates in all three of the RAB ($p < 0.01$), RIPA ($p < 0.001$) and FA ($p < 0.05$) fractions. AT180 which marks Phospho-Tau at Thr231 site, demonstrated increased levels of protein in RAB ($p < 0.0001$) and RIPA ($p < 0.001$) fraction but not in FA fraction. Tau soluble and insoluble protein fractions were

extracted from the hippocampus of 12-month-old female TAU58/2 mice (n=4) compared with wild type (WT) littermates (n=4). β -actin is used as loading control which illustrate band at 42 kDa. Tau can be detected by bands at 50 kDa.

To quantify bands intensity, LiCor Image Studio software was used, and intensities are reported in pixels for Tau bands at different phosphorylation sites and for two isoforms (Table 17).

Table 17. Bands densities for five antibodies in 12-month-old TAU58/2 and WT littermates

12 months results		AT8			AT180			HT7			rD3			rD4		
Sample	Channel	RAB	RIPA	FA	RAB	RIPA	FA	RAB	RIPA	FA	RAB	RIPA	FA	RAB	RIPA	FA
TAU58/2 Mouse1	800	4840	228	889	1220	823	0.536	48700	48700	1640	1060	48.9	1.67	13500	314	18700
TAU58/2 Mouse2	800	9900	292	756	1070	842	242	45500	45500	1310	175	10.8	0	10400	198	14100
TAU58/2 Mouse3	800	10900	425	629	1020	1130	198	33900	33900	1350	189	6.99	1.05	6040	190	20100
TAU58/2 Mouse4	800	15500	339	283	1410	1100	110	40100	40100	314	156	12.7	0.749	11200	241	10800
WT Mouse1	800	174	37.3	11.9	25.1	26.2	14.2	8.14	8.14	9.65	349	16.6	0.00488	56.6	25.8	2860
WT Mouse2	800	99	25.8	1.42	34.3	34	57.4	37.6	37.6	3.45	114	17.1	2.17	66.6	27.8	3880
WT Mouse3	800	170	39.4	2.12	14.6	47.4	18.5	23.3	23.3	2.15	191	8.69	2.38	94.7	29.7	3440
WT Mouse4	800	130	47.2	12.9	9.47	90	26.4	41.6	41.6	4.06	76.9	7.22	0	36.2	14	587

Relative protein expression for RAB, RIPA, FA fractions for each TAU58/2 mice has been normalized to β -actin based on LiCor handbook and the following formula:

$$\text{Normalized Signal} = \frac{\text{Target Band Signal}}{\text{Lane Normalization Factor}}$$

$$\text{Lane Normalization Factor} = \frac{\text{HKP Signal for Each Lane}}{\text{HKP Signal from Lane with Highest HKP Signal}}$$

Quantities of protein expression after normalization to the housekeeping gene, have been reported in Tables 18-21. Furthermore, to determine whether these differences between WT and TAU58/2 are significant, student t-test ($p < 0.05$) was performed on the data using GraphPad Prism (version 8) and each value presents the mean \pm standard error of the mean (SEM) for each mice cohort. These results have been reported in Figure 14-17.

Table 18. AT8 Normalization results for all fractions in 12-month-old WT and TAU58/2 mice.

Target protein (not normalized)			RAB				RIPA				FA			
			Normalization		Normalized to HKP		Normalization		Normalized to HKP		Normalization		Normalized to HKP	
Lane	Sample treatment	Replicate	Target (800 nm)	LNF (HKP)	Apply LNF	Norm. Target	Target (800 nm)	LNF (HKP)	Apply LNF	Norm. Target	Target (800 nm)	LNF (HKP)	Apply LNF	Norm. Target
1	WT	1	174	1	174	174	37.3	1	37.3	37	11.9	1	11.9	12
2		2	99	0.6808	145.421	145	25.8	0.68078	37.898	37	1.42	0.8863	1.60212	1.6
3		3	170	0.7427	228.904	229	39.4	0.74267	53.052	53	2.12	0.794	2.67016	2.7
4		4	130	0.684	190.048	190	47.2	0.68404	69.002	69	12.9	0.9272	13.9132	14
5	TAU58/2	1	4840	0.886	5462.79	5463	228	0.88599	257.34	258	889	0.833	1067.18	1067
6		2	9900	0.9218	10739.6	10739	292	0.92182	316.76	317	756	0.8615	877.584	878
7		3	10900	0.8599	12675.4	12675	425	0.85993	494.22	495	629	0.8384	750.269	750
8		4	15500	0.9414	16465.4	16465	339	0.94137	360.11	360	283	1	283	283

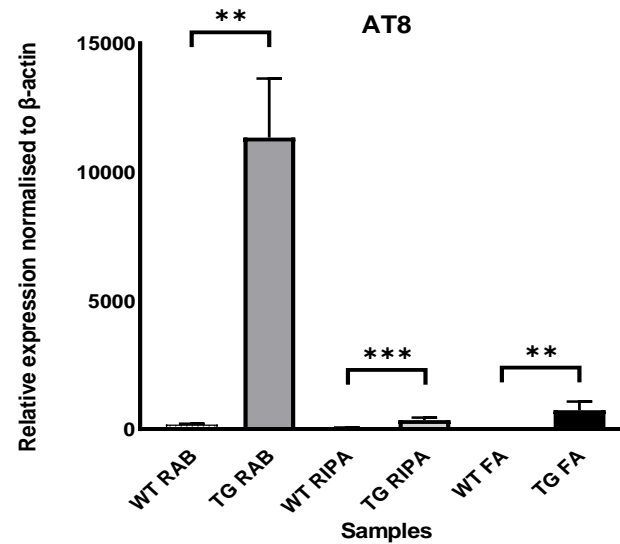


Figure 14. AT8 protein expression in WT and TAU58/2 samples in all fractions. (student's *t*-test; $n=4/\text{group}$). Each value presents the mean \pm standard error of the mean (SEM). ** $p < 0.01$, *** $p < 0.001$

Table 19. AT180 Normalization results for all fractions in 12-month-old WT and TAU58/2 mice.

Target protein (not normalized) Lane	Sample treatment	Replicate	RAB				RIPA				FA			
			Normalization		Normalized to HKP		Normalization		Normalized to HKP		Normalization		Normalized to HKP	
			Target (800 nm)	LNF (HKP)	Apply LNF	Norm. Target	Target (800 nm)	LNF (HKP)	Apply LNF	Norm. Target	Target (800 nm)	LNF (HKP)	Apply LNF	Norm. Target
1	WT	1	25.1	0.8974	27.9708	28	26.2	0.88272	29.681	29	14.2	0.8827	16.0867	16
2		2	34.3	0.939	36.5292	36	34	0.84568	40.204	40	57.4	0.8457	67.8745	67
3		3	14.6	0.8322	17.5443	17	47.4	0.77778	60.943	61	18.5	0.7778	23.7857	24
4		4	9.47	0.767	12.347	12	90	0.83951	107.21	107	26.4	0.8395	31.4471	31
5	TAU58/2	1	1220	0.8779	1389.61	1390	823	1	823	823	0.536	1	0.536	0
6		2	1070	0.8308	1287.93	1288	842	0.95062	885.74	886	242	0.9506	254.571	255
7		3	1020	0.9334	1092.75	1093	1130	0.8642	1307.6	1308	198	0.8642	229.114	229
8		4	1410	1	1410	1410	1100	0.98148	1120.8	1121	110	0.9815	112.075	112

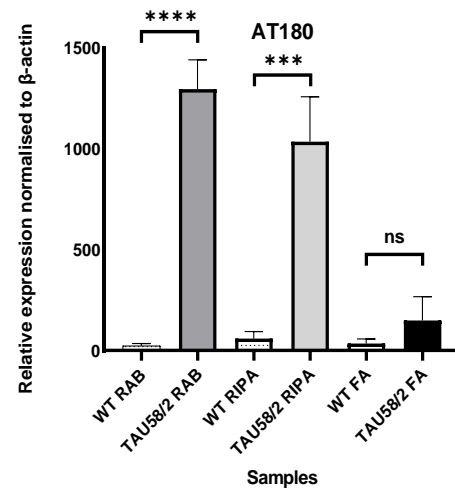


Figure 15. AT180 protein expression in 12-month-old WT and TAU58/2 samples in all fractions. (student's t-test; n=4/group). Each value presents the mean \pm standard error of the mean (SEM). *** p <0.001. **** p <0.0001. ns: nonsignificant

Table 20. HT7 Normalization results for all fractions in 12-month-old WT and TAU58/2 mice.

Target protein (not normalized)	Sample treatment	Replicate	RAB				RIPA				FA			
			Normalization		Normalized to HKP		Normalization		Normalized to HKP		Normalization		Normalized to HKP	
			Target (800 nm)	LNF (HKP)	Apply LNF	Norm. Target	Target (800 nm)	LNF (HKP)	Apply LNF	Norm. Target	Target (800 nm)	LNF (HKP)	Apply LNF	Norm. Target
Lane														
1	WT	1	8.14	1	8.14	8	35.9	0.71861	49.957	50	9.65	0.7186	13.4286	13
2		2	37.6	0.731	51.434	51	18.9	0.75758	24.948	25	3.45	0.7576	4.554	4
3		3	23.3	0.7448	31.2824	31	0.338	0.7619	0.4436	0	2.15	0.7619	2.82188	3
4		4	41.6	0.7011	59.3311	59	6.66	1	6.66	6	4.06	1	4.06	4
5	TAU58/2	1	48700	0.6322	77034.5	77034	990	0.84416	1089.8	1090	1640	0.8442	1942.77	1943
6		2	45500	0.6414	70940.9	70941	920	0.77056	939.57	940	1310	0.7706	1700.06	1700
7		3	33900	0.646	52478.6	52479	724	0.63203	1558.5	1558	1350	0.632	2135.96	2136
8		4	40100	0.6529	61420.8	61421	985	0.70996	1387.4	1387	314	0.71	442.28	443

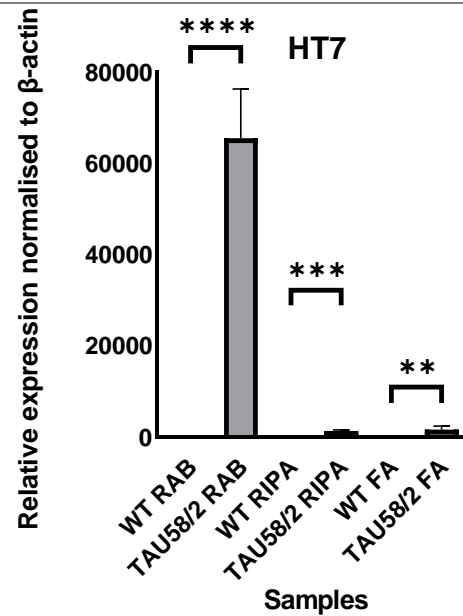


Figure 16. HT7 protein expression in 12-month-old WT and TAU58/2 samples in all fractions. (student's t-test; n=4/group). Each value presents the mean ± standard error of the mean (SEM). **p<0.01, ***p<0.001. ****p<0.0001

Table 21. rD4 Normalization results for all fractions in 12-month-old WT and TAU58/2 mice.

Target protein (not normalized)	Sample treatment	Replicate	RAB				RIPA				FA			
			Normalization		Normalized to HKP		Normalization		Normalized to HKP		Normalization		Normalized to HKP	
			Target (800 nm)	LNF (HKP)	Apply LNF	Norm. Target	Target (800 nm)	LNF (HKP)	Apply LNF	Norm. Target	Target (800 nm)	LNF (HKP)	Apply LNF	Norm. Target
Lane														
1	WT	1	56.6	0.9149	61.868	62	25.8	0.99886	25.83	26	2860	0.9989	2863.27	2863
2		2	66.6	0.6881	96.7856	97	27.8	0.96114	28.924	29	3880	0.9611	4036.86	4037
3		3	94.7	0.7693	123.098	123	29.7	0.89257	33.275	33	3440	0.8926	3854.03	3854
4		4	36.2	0.6416	56.4228	56	14	0.968	14.463	14	587	0.968	606.405	606
5	TAU58/2	1	13500	1	13500	13500	314	0.98971	317.26	317	18700	0.9897	18894.3	18894
6		2	10400	1	10400	10400	198	0.928	213.36	213	14100	0.928	15194	15194
7		3	6040	0.6663	9064.49	9065	190	0.90171	210.71	211	20100	0.9017	22290.9	22291
8		4	11200	0.8822	12695.8	12695	241	1	241	241	10800	1	10800	10800

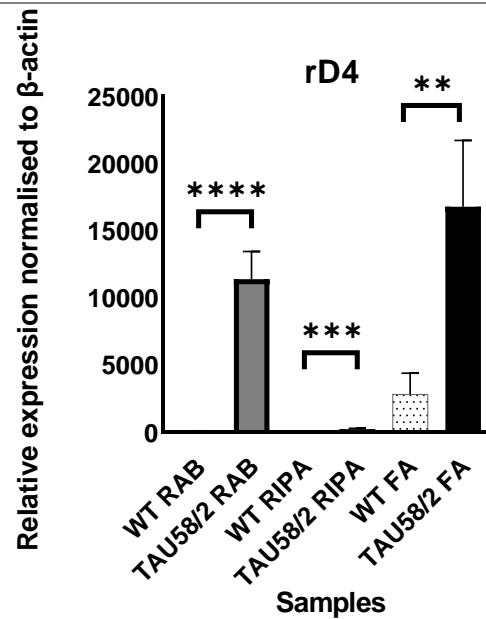


Figure 17. rD4 protein expression in 12-month-old WT and TAU58/2 samples in all fractions. (student's t-test; n=4/group). Each value presents the mean± standard error of the mean (SEM). **p<0.01, ***p<0.001. ****p<0.0001

3.4.3 Comparison between levels of Tau protein expression in 3 months and 12 months and across all fractions, showed elevated tauopathy

To draw a comparison between two agepoints, the mean quantified signals detected by Odyssey CLx machine for each antibody and in both age cohorts, have been reported in Table 14, after being normalized to β -actin as positive control. It should be noted that quantification has not been performed for 3-repeat Tau isoform as there was no band detected in both age groups. In addition, all nonsignificant differences have been coloured red in the Table 22.

In 3-month-old mice, there were significantly greater amounts of total Tau, phosphorylated Tau and rD4 isoform in TAU58/2 mice versus wild type in the soluble fraction. In the FA fraction, there was not any significant level of insoluble Tau in the TAU58/2 mice.

In 12-month-old mice, there was also significantly greater amounts of each Tau in the TAU58/2 mice versus wild type mice in the soluble fraction. In the insoluble fraction, there was a significant accumulation of insoluble Tau in only the TAU58/2 mice except for Tau phosphorylation at Thr231 phosphorylation site. As expected, protein expression (both soluble and insoluble) has elevated more in older mice. Notably, dramatic increase in insoluble Tau protein expression has been reported in 4-repeat Tau isoform quantifications for FA fraction in old TAU58/2 mice.

Table 22. Mean signals reported for Tau protein expression. Total Tau, phosphorylated Tau, rD4 isoform for RAB, RIPA and FA fractions in 3-month-old and 12-month-old TAU58/2 and wild type mice are included.

Ab	3-month-old						12-month-old					
	TAU58/2			WT			TAU58/2			WT		
	RAB	RIPA	FA	RAB	RIPA	FA	RAB	RIPA	FA	RAB	RIPA	FA
HT7	38707.67	4910.46	254.7	119.66	68	17	65468.75	1243.75	1555.5	37.25	20.25	6
AT8	3138.66	1882.66	12.66	57.66	45.6	0	11335.5	357.5	744.5	184.5	49	7.575
AT180	751.66	60	12	56	17.66	1.6	1295.25	1034.5	149	23.25	59.25	34.5
RD4	7109.66	23505.67	21.66	1299.33	31	6	11415	245.5	16794.75	84.5	25.5	2840

3.5 Immunohistochemistry (IHC)

3.5.1 Optimisation of IHC conditions

Tau, including soluble and insoluble forms, was measured by Western blot using a range of antibodies targeting at total and different phosphorylation sites. Both total and Phospho-Tau were upregulated in brain lysate from 3 and 12-month-old TAU58/2 mice. For further studies in distribution and morphology of the Tau expression in the brain, I then probed for Tau in brain and across various regions in young and old experimental mice by IHC. In addition, we investigate neuroinflammation and neuron loss, both of which are important pathological features of AD.

3.5.1.1 Endogenous mice IgG blocking optimisation

In order to detect Tau in brain section, I first optimised IHC conditions including blocking step and antibody concentrations. First, a free-floating IHC paradigm was optimized, by labelling brain sections from one wild type sample with the total Tau Ab (HT7). Initial investigations showed background fluorescence, presumed to be endogenous mice IgG. To examine blocking efficiency, the primary antibody was eliminated from the protocol and hemi-sections were incubated with labelled secondary antibody after blocking. As off-target signals were detected again, application of unconjugated Fab antibody to block endogenous mice IgG was investigated. Different concentrations of Goat F(ab) anti-mouse IgG (Abcam ab6668) were applied (20, 40, 50 μ g/ml) to find optimum concentration. Figure 18 shows elimination of background staining after optimizing blocking step and adding 50 μ g/ml Goat F(ab) anti-mouse IgG to 10% Normal Goat Serum (NGS) + 0.3M Glycine blocking solution.

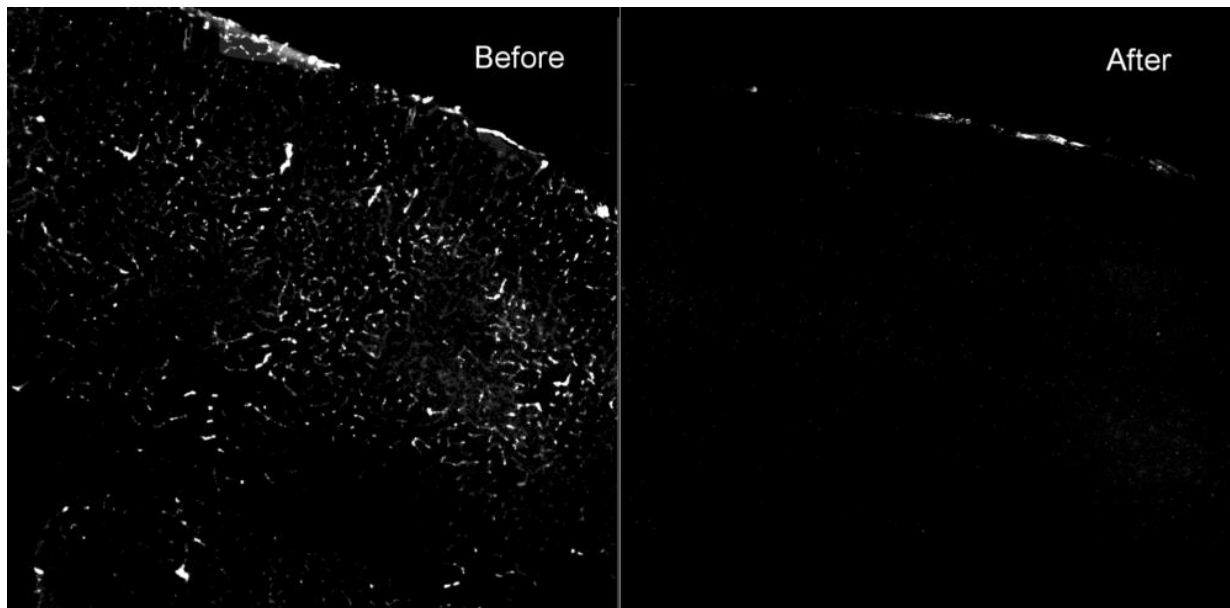


Figure 18. Blocking endogenous mice IgG optimisation. On the left is the magnified 12-month-old wild type brain hemisection before blocking, which demonstrates background staining of endogenous mice IgG in white. On the right magnified 12-month-old wild type brain hemisection after blocking with 50 μ g_mL goat anti mouse Fab secondary antibody in which white nonspecific dots have been eliminated.

3.5.1.2 Optimisation of antibodies for labelling Tau, Astrocytes and Microglia

Five Tau antibodies were tested here as they demonstrated Tau alterations in brain lysate TAU58/2 by Western blot. In addition, to study neuroinflammation, an anti-Glial Fibrillary Acidic Protein (GFAP, Dako) and an anti Iba1 (Iba1, Wako) antibodies were administered to label Astrocytes and Microglia, respectively.

These Abs were tested with the concentrations proposed in the product sheet to obtain the best staining results. Optimum chosen concentrations have been demonstrated in Table 23.

Table 23. Antibodies' concentrations examined and chosen.

Antibody	Tested Concentrations	Optimum concentration
AT8	1:1000	1:1000
AT180	1:1000	1:1000
GFAP	1:1000	1:500
Iba1	1:1000, 1:500	1:500
HT7	1:1000	1:1000
rD4	1:1000, 1:500	1:500
rD3	1:1000, 1:500	1:500

3.5.2 Tau Pathology and neuroinflammation investigation

Tau phosphorylation and aggregation have previously been histologically investigated in the brains of TAU58/2 mice [116]. Here, to determine whether these changes exhibit age-dependant accumulation, Tau modifications and aggregation leading to formation of insoluble Tau, have been studied in both age groups of 3 months and 12 months. This was performed using immunohistochemistry staining and widefield microscopy with five Tau antibodies recognising phosphorylated Tau, total Tau, and insoluble Tau. For this purpose, entire hemisected brain sections were stained to gain an understanding of the distribution, and the morphology of the Tau protein. In addition, neuroinflammation across various brain regions in both age groups was investigated.

3.5.2.1 3-month-old TAU58/2 and WT mice results

Overexpression of Phospho-Tau, total Tau and formation of insoluble Tau across different regions in young mice have been reported here. These sections were stained for HT7, GFAP, AT8 and AT180 (Figure 10-22).

Total Tau detected by HT7 antibody, was overexpressed in various regions of the brain in TAU58/2 mice in comparison with the wild type mice. Regarding its distribution, regions in which these changes have occurred are magnified in the Figure 19, as well as brain hemisection in TAU58/2 and WT mice. Both soluble and insoluble Tau can be observed, and insoluble formations of total Tau has been indicated by formation of dense white dots (puncta). Regarding Tau morphology both neuritic and puncta forms were reported in the image.

AT8 antibody was exploited to detect Tau phosphorylation at Ser202/Thr205 phosphorylation site. As Figure 20 shows expression of Phospho-Tau was reported at different locations in the brain including hippocampus, amygdala, cortex, and midbrain. Insoluble Tau can be detected across these regions as well. However, no change in phosphorylation or insoluble formation have been found in investigating wild type brain section shown on the right.

Another Phospho-Tau antibody, staining phosphorylated Tau at Thr231 site (AT180), has confirmed Tau phosphorylation in 3-month-old TAU58/2 mice in multiple regions (Figure 21). Although when comparing to total Tau and phosphorylated Tau at Ser202/Thr205 site, it seems to be less robustly stained. In addition, limited number of dense white dots can be seen in the stained regions.

In addition to Tau phosphorylation and aggregation, neuroinflammation is a well-described feature of AD. Gliosis is a major neuroinflammatory event, a process whereby astrocytes are activated resulting in morphological changes, including shortening and thickening of their processes as well as increased proliferation and release of pro-inflammatory factors [120]. To determine if the number of astrocytes elevated at Tau pathology presented in TAU58/2 mice, coronal sections of the brain taken from TAU58/2 at three months of age, were immunohistochemically stained for intermediate filament protein, glial fibrillary acidic protein (GFAP). Also, to monitor these possible alterations during disease progression, both age group were examined. Figure 22 demonstrates these changes in Astrocytes regarding their population in affected regions of the brain. As magnified in this image, astrocytes are more populated in regions where Tau alterations have been marked by Tau antibodies.

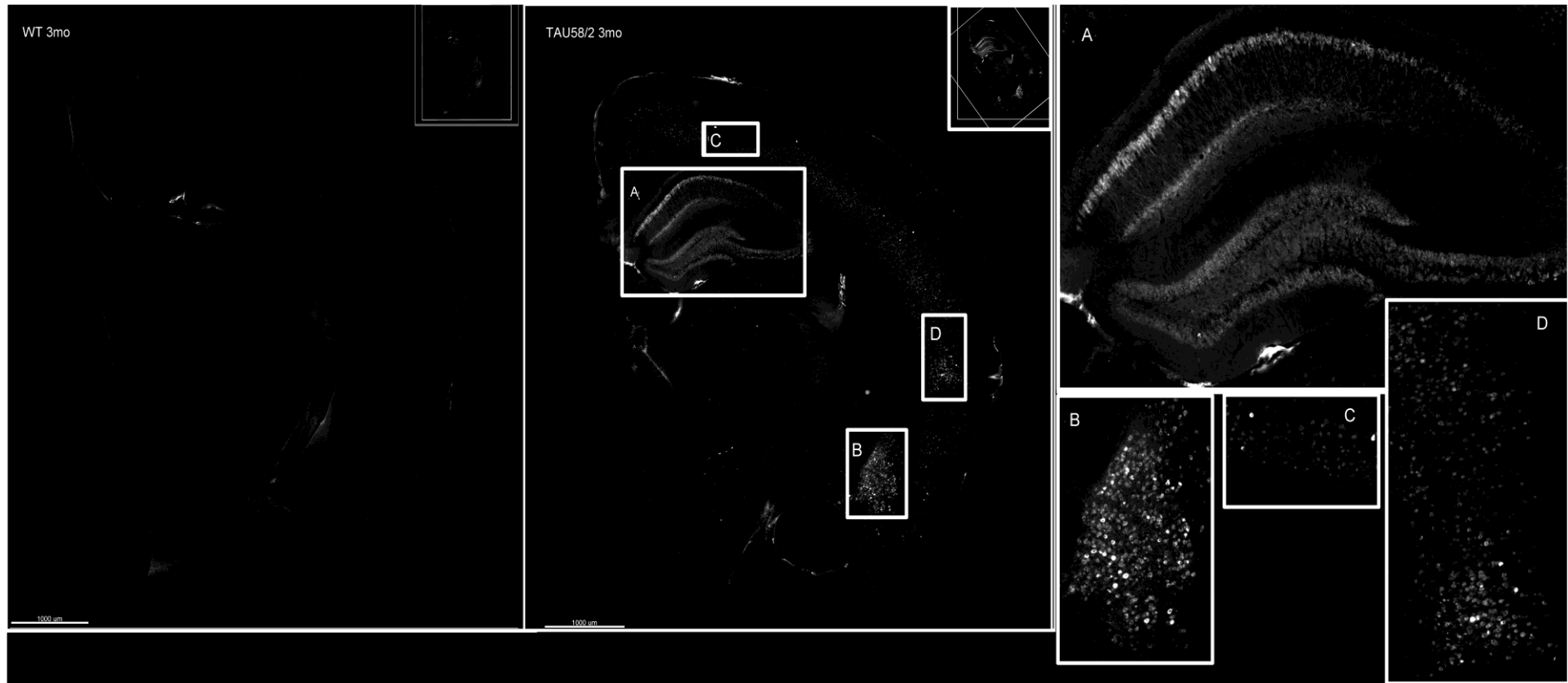


Figure 19. Total Tau staining by HT7 antibody in 3-month-old TAU58/2 and WT mice. Both young transgenic and wild type brain sections have been demonstrated and selected areas (A, B, C, D) have been magnified to show Tau alterations in TAU58/2 mice while there is no change in WT. A, B sections illustrate hippocampus, amygdala, respectively while C and D show two sections of the cortex. Dense white dots (puncta) represent formation of insoluble Tau. These selected areas have been magnified three times and scale bar for brain section=1000um.

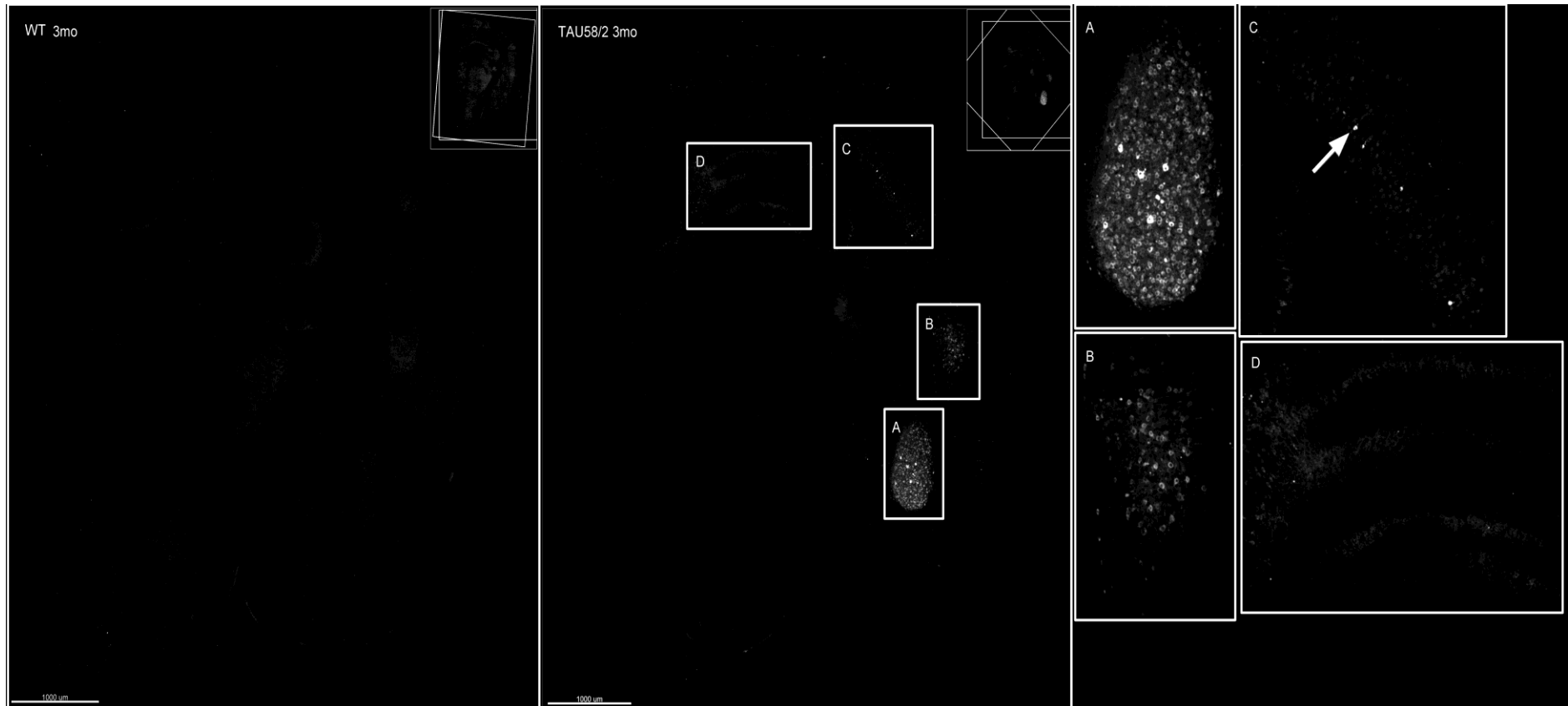


Figure 20. Tau phosphorylation at Ser202/Thr205 phosphorylation site marked by AT8 in 3-month-old TAU58/2 AND WT mice. Tau phosphorylation is shown in TAU58/2 mice in comparison with wild type where no changes are detected. A, B, C and D selections are demonstrating these changes in TAU58/2 in amygdala, two cortex areas and hippocampus, respectively. Dense dot arrowed in C section has been shown as a sample of insoluble Tau formation in cortex which can be detected across all other regions as well. These selected areas have been magnified three times and scale bar for brain section=1000um.

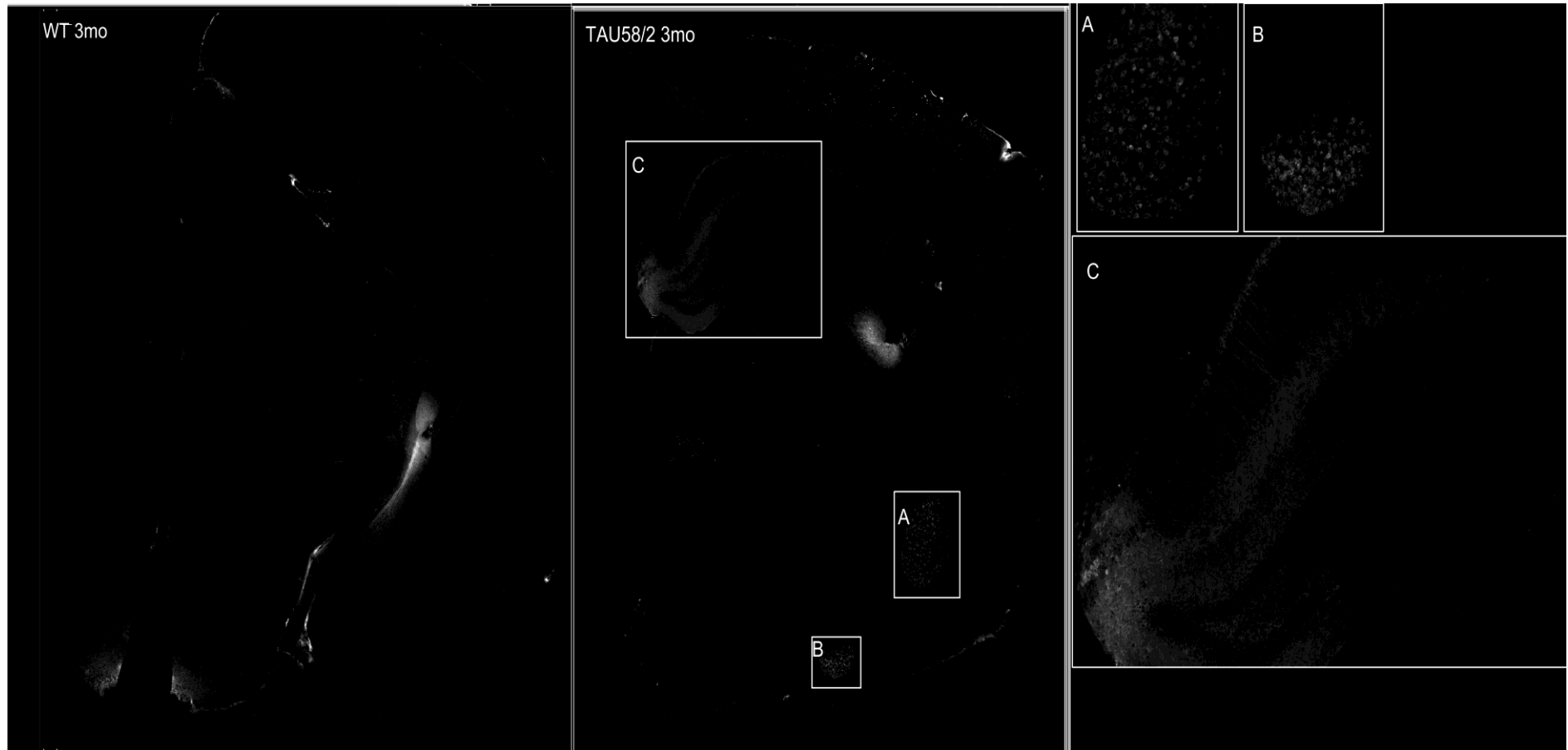


Figure 21. Tau phosphorylation at Thr231 phosphorylation site in 3-month-old TAU58/2 and WT mice. Amygdala basal and lateral as well as hippocampus have been shown in A, B and C selections, respectively. These selected areas have been magnified three times and scale bar for brain section=1000um.

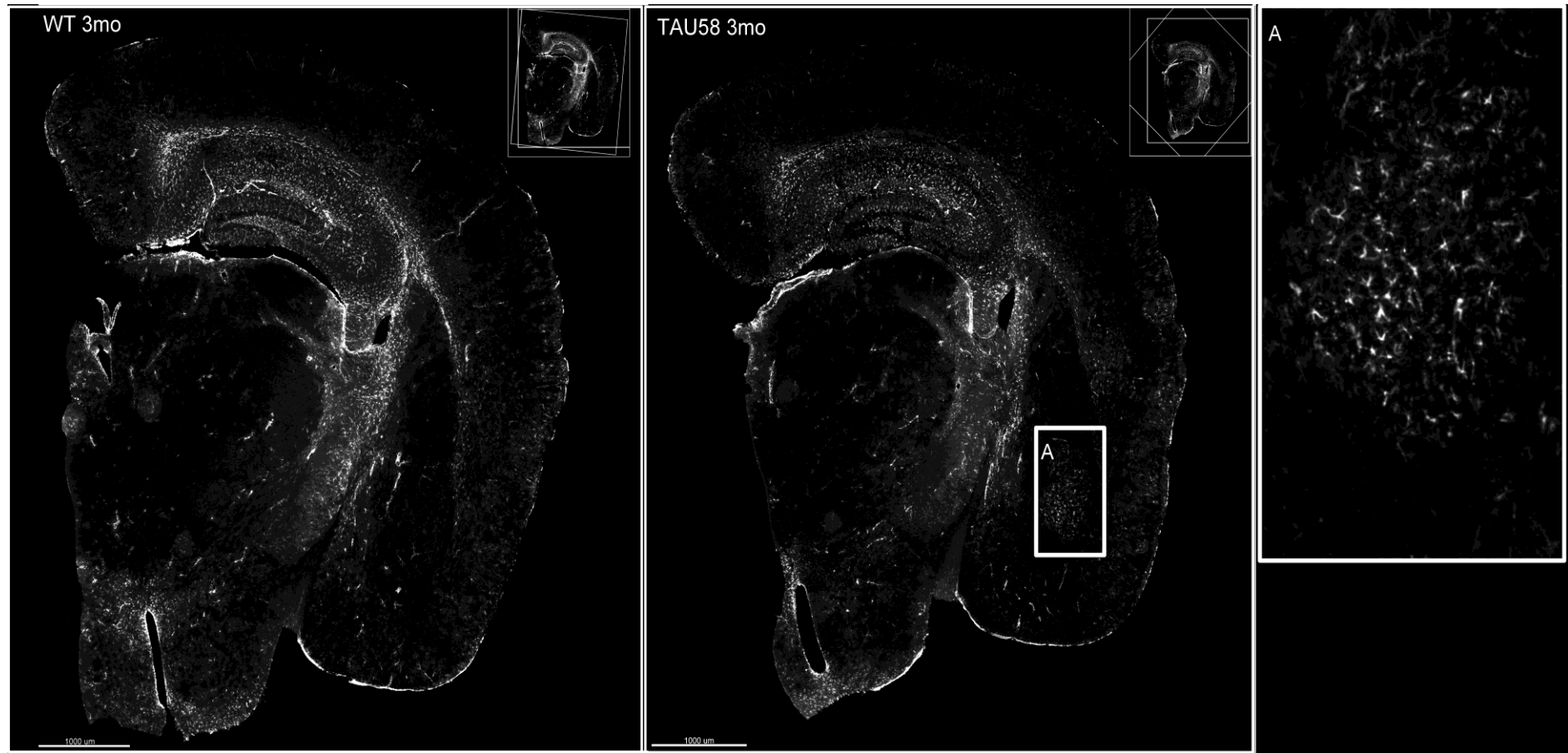


Figure 22. Astrogliosis detected by GFAP antibody in 3-month-old TAU58/2 and WT mice. Astrocytes labelled in TAU58/2 and WT brain sections have been demonstrated. Increased number of Astrocytes in amygdala in TAU58/2 brain section has been magnified in selection A. This selected area has been magnified three times and scale bar for brain section

3.5.2.2 12-month-old TAU58/2 and WT

Phospho-Tau at both sites and total Tau, both soluble and insoluble, were overexpressed in hippocampus, cortex, amygdala nuclei and midbrain significantly in old TAU58/2 mice, which indicate that these changes are progressive with age. Insoluble Tau formation, which is regarded as confirmation of NFT formation in other AD mice models, was observed across these regions as well. Images obtained with five antibodies, have been shown in Figure 23-26.

Total Tau levels, identified by HT7 antibody, were elevated in TAU58/2 old mice. This was expected based on the observation of the similar results for the same antibody in 3 months. However, the relative staining intensity of Total Tau, in both soluble and insoluble form, have escalated through aging in this mice model. Same regions of the brain demonstrated Tau expression compared to the wild type mice (Figure 23).

To determine the locational expression of Tau phosphorylation at Ser202/Thr205 tissue was stained with AT8 antibody. By looking at Figure 24, increase in Tau phosphorylation can be observed remarkably in this stage across various brain regions. Insoluble Tau were reported in all these regions. Notably, no change was evident in the wild type samples as depicted.

Tau isoforms have been studied in addition to Tau phosphorylation and insoluble formation in 12-month-old mice to identify Tau isoform expressed in TAU58/2 mouse model. rD4 isoform expression in cortex, amygdala and hippocampus shown in Figure 25, when compared to the wild type, is evident. In addition, several dense white dots (puncta) indicating the presence of insoluble Tau, can be observed. In contrast, no protein expression has been displayed for isoform rD3 which is similar to the stained wild type section, confirming the observations we saw in the Western blot.

Last set of images depicted in Figure 26, is associated with GFAP antibody, which labels Anti-Glial Fibrillary Acidic Protein as a classic marker for Astrocytes activation and population. Increase in number and activation of Astrocytes have been demonstrated in locations near neurons harbouring phosphorylated Tau in different regions such as amygdala and midbrain. These changes are more distinguished if being compared to nonpathological condition in wild type mice.

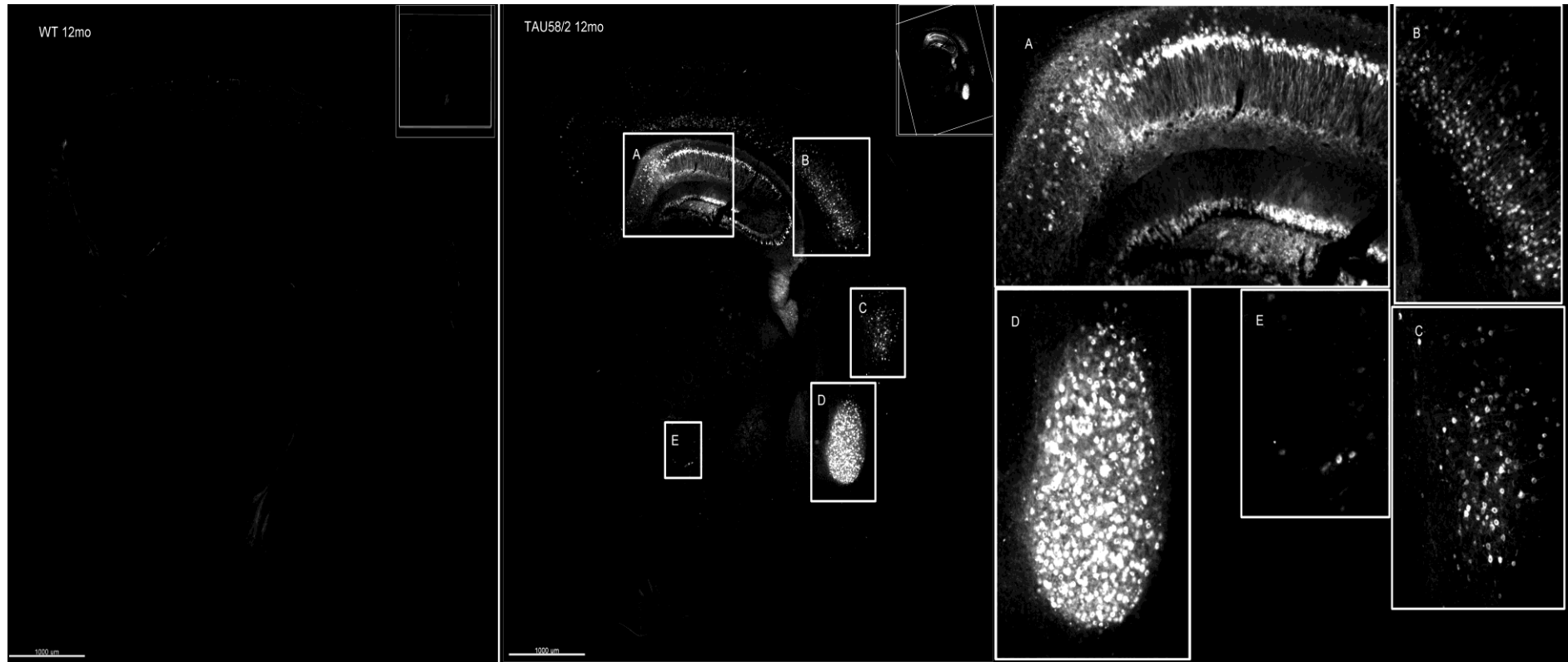


Figure 23. Total Tau staining by HT7 antibody in 12-month-old TAU58/2 and WT mice. Both young transgenic and wild type brain sections have been demonstrated and selected areas (A, B, C, D, E) have been magnified to show Tau alterations in TAU58/2 mice while there is no change in WT. Total Tau expression in hippocampus, cortex (two sites), amygdala and midbrain have been magnified in sections A-E, respectively. Insoluble Tau is indicated with dense white dots (puncta). These selected areas have been magnified three times and scale bar for brain section=1000µm.

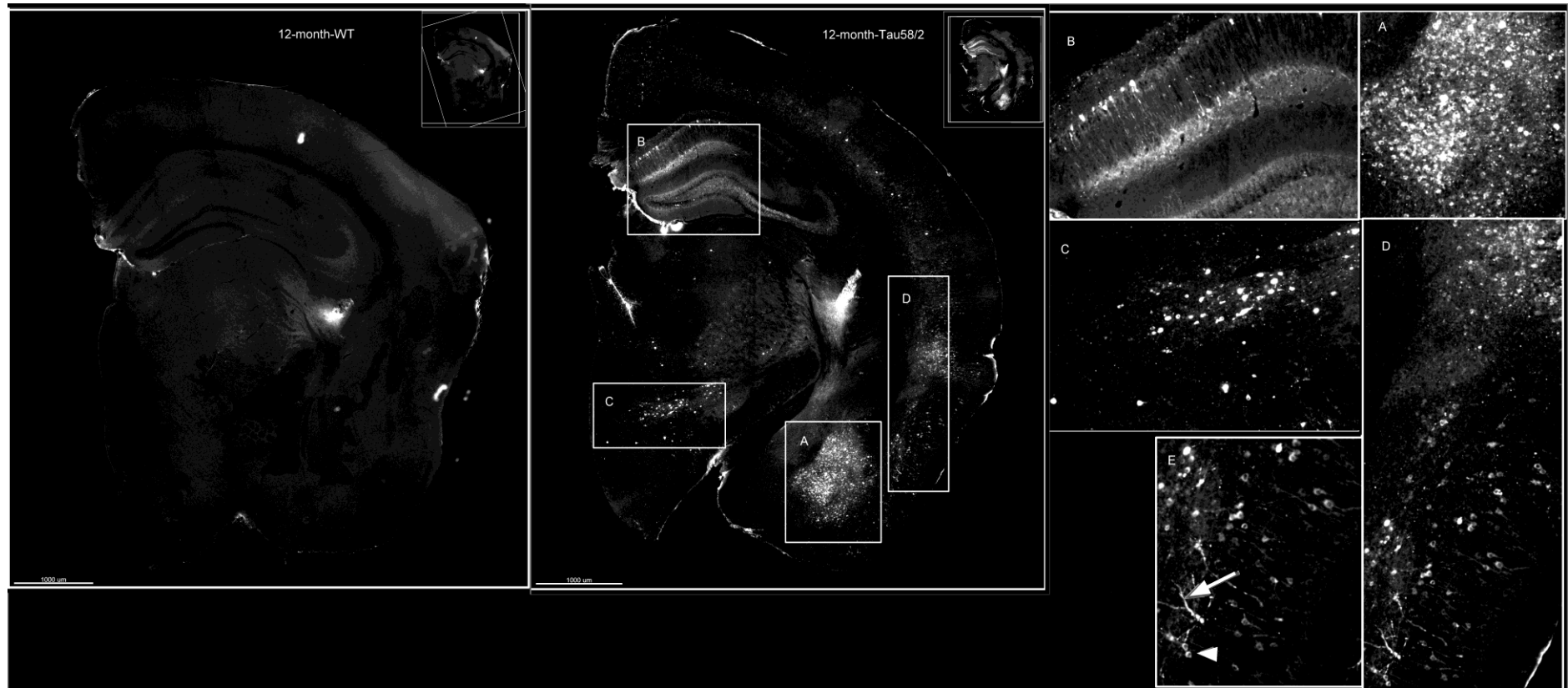


Figure 24. Tau phosphorylation at Ser202/Thr205 phosphorylation site marked by AT8 in 12-month-old TAU58/2 and WT mice. Selections A-D demonstrate various brain regions; A: amygdala, B: hippocampus, C: midbrain, D: cortex. Image E shows magnified Phospho-Tau in the forms of neuritic and puncta in magnified section of the cortex. A-D selected areas have been magnified three times and scale bar for brain section=1000 μ m. E image has been magnified five times.

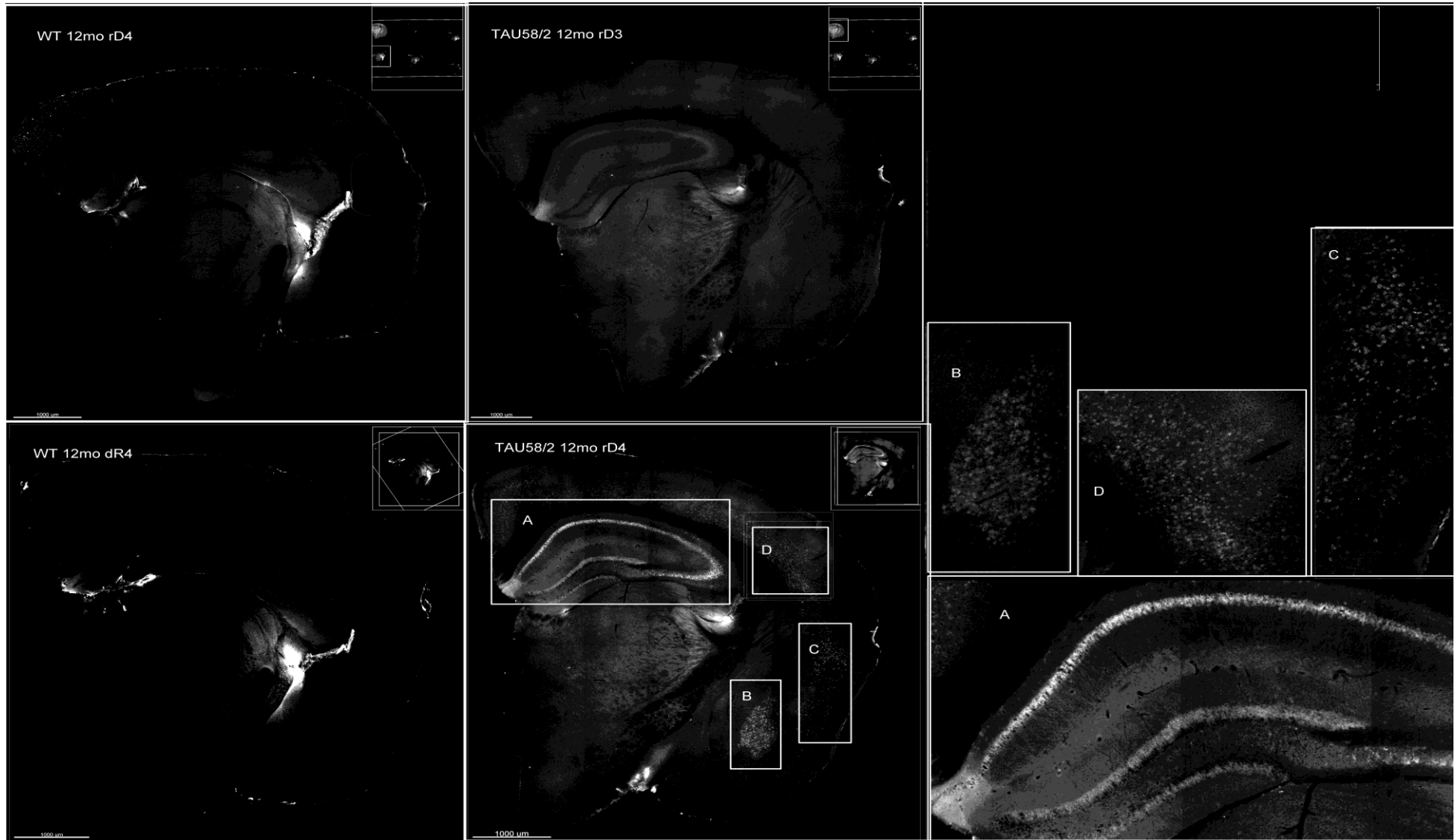


Figure 25. Tau isoforms rD3 and rD4 in 12-month-old TAU58/2 and WT mice. Selection A-D demonstrate hippocampus, amygdala, two regions in cortex. selected areas have been magnified three times and scale bar for brain section=1000µm.

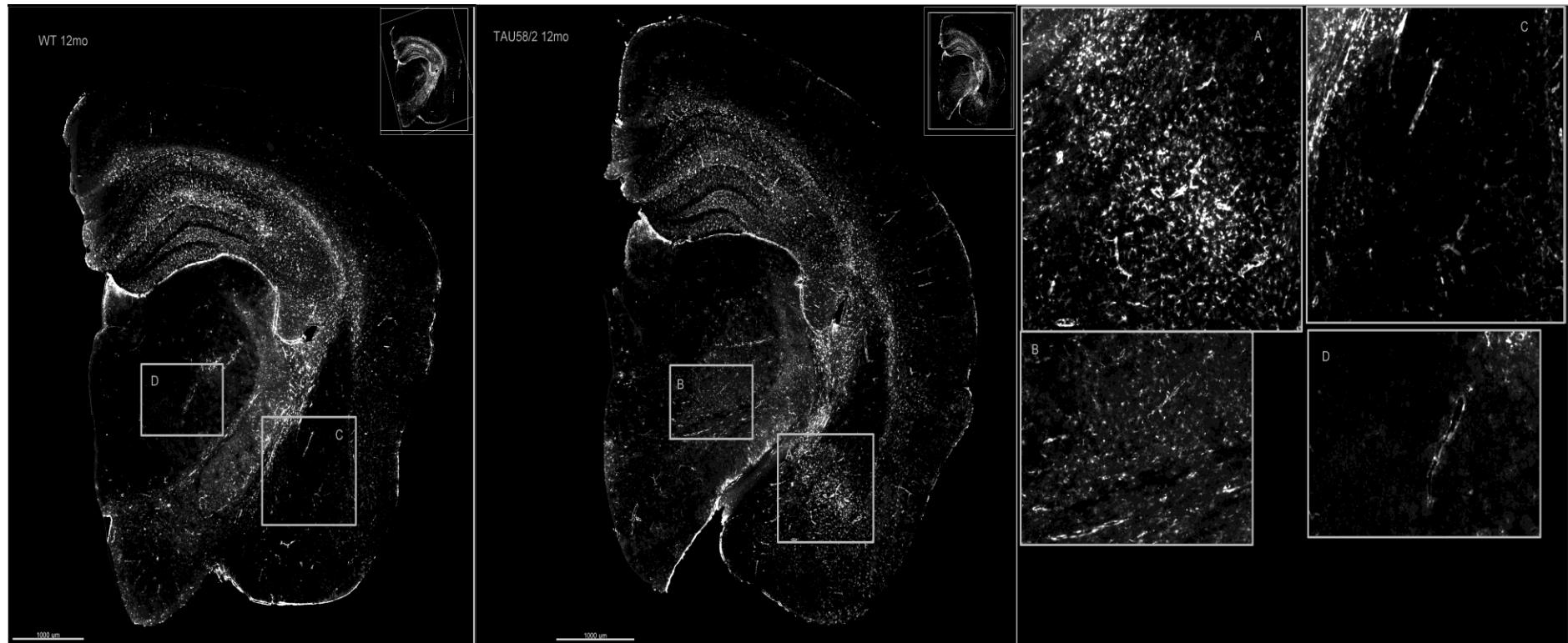


Figure 26. Astroglial staining detected by GFAP antibody in 12-month-old TAU58/2 and WT mice. Selections A and B magnify increase in Astrocytes number in amygdala and midbrain of TAU58/2 mice, in comparison with selections D and C from the same regions in WT mice. These selected areas have been magnified three times and scale bar for brain section=1000um.

3.5.3 Nissl staining and counter staining

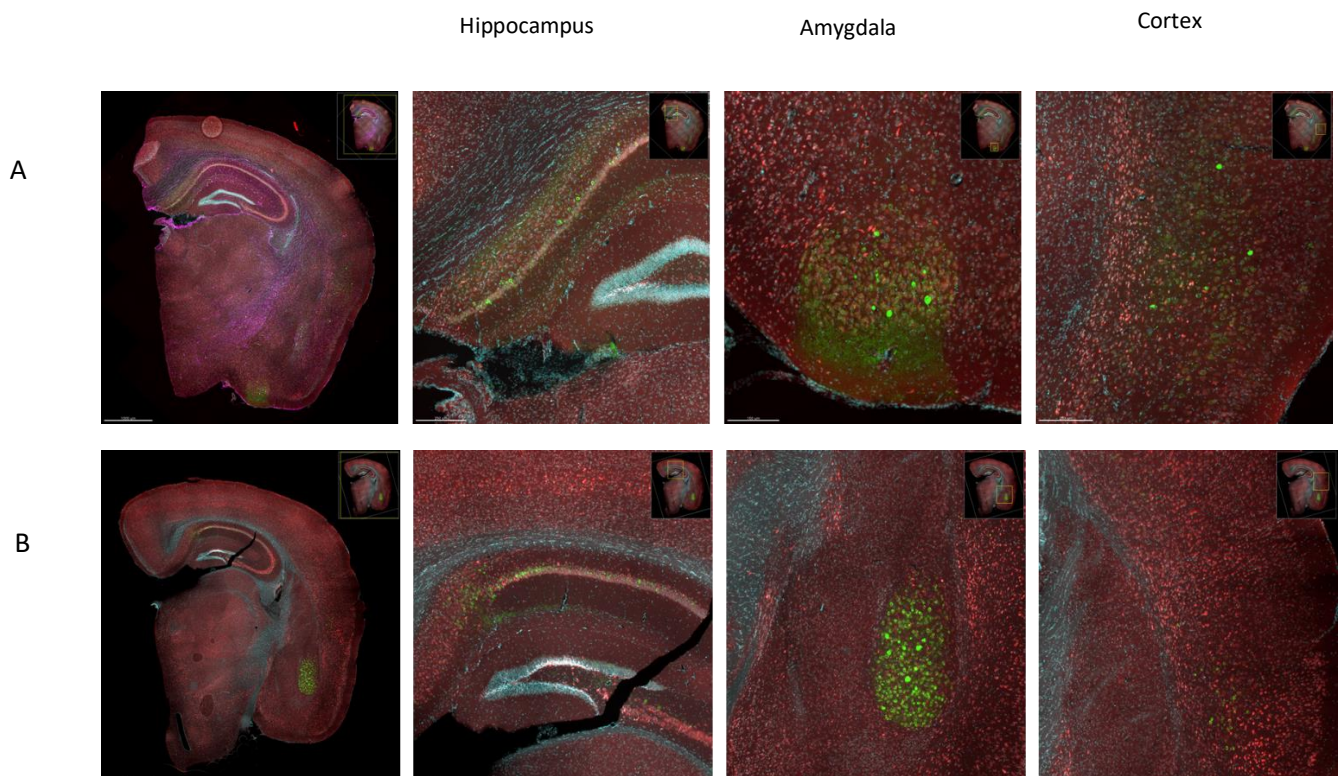
3.5.3.1 Nissl staining

Nissl staining has been used for years to visualise neurons through localizing cell bodies called Nissl bodies which can alter in pathological condition [121]. Neurotrace (Invitrogen, N21479 and N21482) was used as fluorescent Nissl stain and has been shown in following Figure 27 in red.

3.5.3.2 DRAQS

DRAQS is a popular nuclear counterstain for use in multicolour fluorescent techniques which stains nuclei specifically, as it is a DNA stain. 2.5 μ M DRAQS (Abcam, ab108410) was utilized for staining and has been shown in blue in the Figures 27.

Staining brain sections, on the one hand with Neurotrace which stains ribosomal RNA locating soma of neurons and on the other hand with DRAQ5 which stains nuclei, provided us with the image of stained neurons in which cell body and nuclei have been demonstrated in red and blue, respectively. Figure 27 depicts morphology of neurons and brain regions, and when combining with Tau Abs labelling, offers a comprehensive understanding of the location of phosphorylated Tau and NFT formation. Comparison between TAU58/2 sections with WT sections stained with Nissl staining and counterstaining, shows neuron population, apoptotic bodies, and cell deaths. Another important piece of information demonstrated here is formation of extra-NFTs and intra-NFTs based on their locations related to the identified neurons. Moreover, cell bodies can be distinguished from cell debris. To study neuronal loss and NFT stages, mentioned stains are demonstrated in Figure 23. Thus, we aimed to study these changes by conducting this part of the study, however, these two stains were not compatible as we anticipated. Therefore, we examined DAPI (another DNA bonding stain) instead of DRAQ5 and in combination with Neurotrace, and no interference was observed. Images of DAPI and Neurotrace in 12-month-old TAU58/2 brain sections and WT, combined with anti Tau antibody (rD4) have been illustrated in Figure 28.



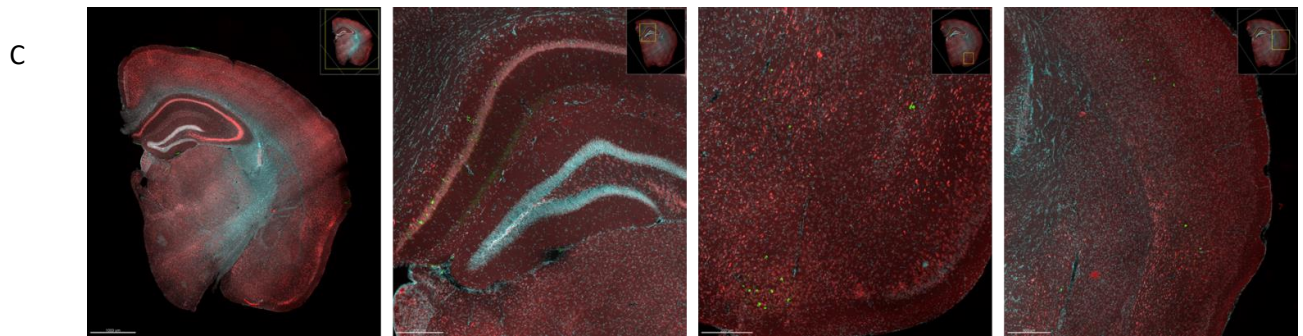


Figure 27. Nissl staining and counterstaining in addition to Tau protein expression in TAU58/2. A) Nissl staining, counterstaining, GFAP and AT8 in 12-month-old TAU58/2 brain sections marked with red, blue, violet, and green, respectively. B) Nissl staining, counterstaining, HT7 in 12-month-old TAU58/2 brain sections marked with red, blue, and green, respectively. C) Nissl staining, counterstaining, GFAP and HT7 in 3-month-old TAU58/2 brain sections stained in red, blue, violet, and green, respectively. In each row, first image on the left shows hemisected brain and three others at higher magnification show hippocampus, cortex and amygdala regions of the brain.

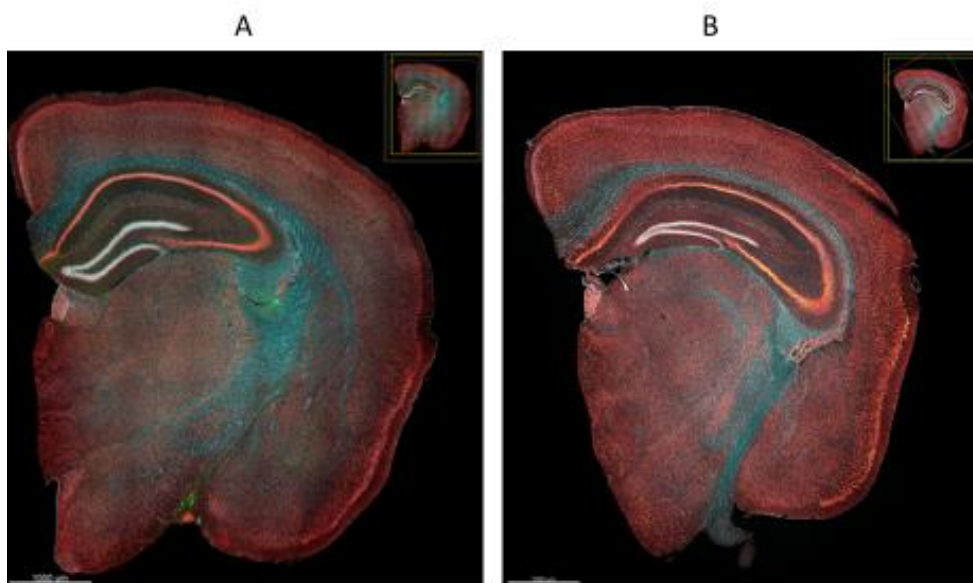


Figure 28. Staining with DAPI and Neurotrace in both TAU58/2 and WT mice at 12-month-old. A) 12-month-old TAU58/2 brain section labelled with anti Tau isoform rD4 in combination with DAPI and Neurotrace. B) 12-month-old wild type brain section labelled with anti Tau isoform rD4 in combination with DAPI and Neurotrace. In both images Neurotrace, DAPI and anti Tau isoform rD4 are marked with red, blue, and green, respectively. Comparison between two time points based on histology study.

3.5.4 IHC overview

Immunohistochemistry allows for confirmation and complete data collection to look at specific brain region changes. As tissue exploited for Western blot was only from hippocampal homogenates, in this approach I investigated location specific alterations. In addition, neuroinflammation and neuronal death have been studied in relation with Tau pathology in this mice model at different ages. Despite there being a similar increasing trend in Tau expression and phosphorylation detected by both methods, as we did not quantify IHC results, we cannot compare these results quantitatively between two methods and two agepoints. However, increase tauopathy as disease progresses can be seen by IHC. To confirm these results, we suggest quantification for IHC as well as performing Western blot for other regions of the brain, particularly regions in which these changes have reported in our IHC findings (cortex, amygdala, and midbrain).

Moreover, neuroinflammation may be studied further through investigating possible microgliosis in addition to Astrogliosis. This can be studied by staining sections with Iba1 antibody, which labels allograft inflammatory factor 1 (AIF1), also known as IBA1, that is an actin-binding protein and have a role in activation of microglia. Though I attempted to perform this analysis, the images produced were not optimal and staining microglia is needed to be repeated and therefore not included in this thesis.

Finally, assessing neuronal loss by counterstaining and Nissl staining determines whether any timepoint is late to be chosen as optimal time for therapeutic interventions regarding occurrence of neuronal death. Additionally, these further staining can offer more information like NFT stages and location, apoptotic cells and cell debris. These methods were performed as described earlier, however due to interaction between stains, images provided are not optimal. Thus, counterstaining and Nissl staining in TAU58/2 mouse model especially in older mice is recommended to be performed to study various aspects of tauopathy described earlier.

4

Discussion

4.1 Study background

This study aimed to assess the expression baseline for total and phosphorylated Tau protein in a transgenic mouse model (TAU58/2), to identify suitable ages for therapeutic treatment with siRNA that targets Tau expression. This transgenic mouse expresses a variant of human Tau (P301S), which is associated with FTLN [69], and commonly used in tauopathies studies refer to Alzheimer's disease (AD) or frontotemporal lobe degeneration (FTLD). This project studied 3-month-old and 12-month-old TAU58/2 mice and assessed the accumulation of both soluble and insoluble Tau, as well as different phosphorylated forms of Tau at both ages.

4.2 Results summary

The first objective of this study sought to determine changes in Tau protein levels both quantitatively and qualitatively in transgenic TAU58/2 in comparison with wild type littermates at two timepoints (3 months and 12 months) in hippocampus by Western blot. For this purpose, soluble and insoluble Tau protein was extracted from hippocampus region. Different pathological forms of Tau were investigated by using five different antibodies: two for labelling Ser202/Thr205 and Thr231 phosphorylation sites, two for recognizing Tau isoforms and one marking total Tau.

In three months, soluble Tau levels (Total Tau and Phospho-Tau and 4-repeat Tau isoform) were all increased in TAU58/2. However, there was no evidence of accumulation of insoluble Tau in 3-month-old TAU58/2 mice. Similarly, in 12-month-old cohort, data showed a significant increasing trend in total Tau protein level and phosphorylation at both sites; in addition, rD4 isoform expression was recorded in both soluble and insoluble Tau. Notably, all these changes were observed in both soluble and insoluble fractions (RAB and RIPA for soluble and FA for insoluble Tau) except for the phosphorylation at Thr231 site in which insoluble Tau formation was not significant. A possible explanation for this might be that according to literature, AT8 detects NFTs at all stages (pre-NFT, iNFT, eNFT) with higher percentage across all regions, in comparison with AT180 [54]. In addition, total Tau level was higher in aged mice, which is either due to the accumulation of total Tau over time or resulting from production of more Tau as a way of compensation for disturbed Tau function in pathologic condition.

In both timepoints, phosphorylation of Tau (soluble form) occurred at both Ser202/Thr205 and Thr231 phosphorylation sites, however less robustly expressed phosphorylation site amongst these two was T231, labeled by AT180 antibody. This rather contradictory result may be due to different Tau phosphorylation at two phosphorylation sites, as phosphorylation at various sites can occur at different stage of the disease and previous finding have suggested a sequential phosphorylation at different sites; therefore, it is likely to be the case here and such sequence exist between phosphorylation sites [47].

The Western blot data from Chapter 3.4.3 showed that phosphorylation of Thr231 was consistent at both agepoints; however, phosphorylation at Ser202/Thr205 was substantially elevated between 3- and 12- month old TAU58/2 mice. This data suggests that phosphorylation of Ser202/Thr205 is associated with insoluble Tau accumulation, and as published previously TAU58/2 mice show behaviour defects at 12 months (and not 3 months) [111], suggesting that phosphorylation of

Ser202/Thr205 may be important for causing disease phenotype. The observed changes in Tau that were detected by Western blot were confirmed by IHC. Therefore, within the hippocampus, significant increase in Tau (total Tau, Phospho-Tau and 4-repeat isoform) was identified in 12-month-old TAU58/2 mice versus 3-month-old TAU58/2 mice.

IHC was also performed in other regions of the brain including hippocampus, amygdala, cortex, and midbrain as well, and detected widespread Tau expression. In all regions, total Tau was stained more than phosphorylated Tau at both sites, and between two phosphorylation sites phosphorylated Tau labeled by AT8 showed more signals than phosphorylated Tau reported by AT180. These findings were similar in both age groups, whereas overall intensity of Tau overexpression either total Tau or phosphorylated Tau were more in 12-month-old TAU58/2. Tau insoluble formation and aggregation marked by dense puncta, were observed in both age cohorts, and as anticipated, more in number in 12-month-old TAU58/2. There were differences between brain regions regarding distribution in both ages. The most Tau expression was observed in amygdala, hippocampus, cortex, and midbrain, respectively. Accumulation of insoluble Tau were more in amygdala. Tau aggregation were seen in the form of puncta mainly in amygdala and midbrain, while in other regions cytoplasmic and axonal Tau was identified. Astrogliosis was reported near regions harbouring phosphorylated Tau such as amygdala and midbrain.

4.3 Limitations

The generalizability of these results is subject to several limitations. First, due to time constraints this study was limited by the lack of quantification of protein measurements by immunoblotting for other regions of the brain including cortex, amygdala, and midbrain. Another issue which is not addressed in this study was whether gliosis and neuronal loss occurred at these timepoints in TAU58/2, which could shed light on the severity of tauopathy. Gliosis was examined by labelling with Iba1 antibody but due to low quality of the antibody, efficient staining was not provided. Nissl staining by Neurotrace and counterstaining by DRAQ5 were chosen to stain soma and nuclei of the neurons to investigate morphology of neurons and brain regions, also location of phosphorylated and aggregated Tau when merged to Tau staining. In addition, neuronal death, and formation of extra-NFTs and intra-NFTs could be argued after this stage. Unfortunately, due to the fact that DRAQ5 interferes with Neurotrace, images provided were not optimal. Therefore, co-localization by DAPI and Neurotrace was tested and seems to be a better combination for further studies. Moreover, assessment of ubiquitin inclusions could suggest better understanding of NFT formation and Tau aggregations. Since the study was limited to interpretation of IHC result qualitatively and not quantitatively, it was not possible to draw a precise comparison between two time points regarding Tau phosphorylation, Tau aggregation and Astrogliosis observed in both age cohorts by immunostaining. Lastly, the major limitation of this study is that given the early-onset alterations by 3 months of age, more age cohorts would confirm optimum treatment option regarding this matter. Notwithstanding these limitations, the current study certainly adds to our understanding of tauopathy in TAU58/2 mice at different stages of the disease.

4.4 Future directions

This research has thrown up many questions in need of further investigation. Research in Tau protein expression and its quantification for cortex, midbrain and amygdala can offer a better understanding of Tau phosphorylation in other regions of the brain at different timepoints. More broadly, research is also needed to determine Tau protein phosphorylation at other phosphorylation sites (other than at Ser202/Thr205 and Thr231) in various brain regions, to shed light on targeting phosphorylation sites for evaluating treatments in the future. The issue of ubiquitin inclusions, gliosis and neuronal loss are intriguing ones, which would be usefully explored in further studies, and in combination with Tau alterations can determine that at these timepoints how much damage has already occurred regarding neuronal death and neuroinflammation. Consequently, depicted characteristics of TAU58/2 tauopathy

described by these complementary data, will give rise to choosing the best time to apply treatments to alleviate pathological condition in AD in TAU58/2 mice.

4.5 Conclusion

To choose the best treatment timepoint regarding our results, various characteristics of tauopathy should be considered such as Tau phosphorylation, Tau aggregation leading to formation of insoluble Tau, neuroinflammation and neuronal loss.

Based on different aspects of tauopathy reported in each age cohort, each timepoint can offer their contributions to future AD studies. 3-month-old TAU58/2 mice are excellent for investigating whether NP therapy can knock-down soluble Tau levels and alter specific phosphorylation sites (Ser202/Thr205 and Thr231). As soluble Phospho-Tau has been previously pointed out as an independent agent involved in pathology of the disease, targeting soluble fraction can be beneficial as well as insoluble fraction [24]. Advantages of utilizing this age would be quick studies with short breeding times.

12-month-old TAU58/2 mice is essential to assess whether NP therapy can alter insoluble Tau and more regions of the brain can be targeted. Regarding studying different phosphorylation sites, as Tau phosphorylation at Thr231 site seem to be revealed later than phosphorylation at Ser202/Thr205 site in TAU58/2 mice, if treatment aims to target this phosphorylation site, older cohort would be more suitable to be evaluated. Further investigations of neuron loss and neuroinflammation in this timepoint can add to its further applications. Disadvantage of devising old TAU58/2 mice is additional cost and time of maintaining the animals for a long duration.

In conclusion, TAU58/2 mice can be used as a reliable mouse model of tauopathy in AD as it demonstrates different aspects of AD pathology at different ages. However, findings for one timepoint cannot be extrapolated to all ages, and each stage of disease demonstrates its unique characteristics. Thus, optimum timing for therapeutic intervention entirely depends on which AD aspect will be therapeutically targeted in TAU58/2 mice.

A

A.1 Method

A.1.1 Mice tissue

Appendix

Hippocampus tissue dissected from harvested brain was weighed prior to protein extraction. Table A.1 demonstrates related weights in milligram recorded for TAU58/2 and WT mice for both age cohorts.

Table A.1. Mice hippocampus weight (mg)

3 months			
TAU58/2		WT	
Mouse no.	Weight (mg)	Mouse no.	Weight (mg)
570	10.8	571	21.5
578	0.9	576	15.1
564	20.8	577	13.5
12 months			
TAU58/2		WT	
Mouse no.	Weight (mg)	Mouse no.	Weight (mg)
420	23.2	415	19.6
426	17.5	421	17.5
433	18.2	425	20
414	15.6	432	15.7

A.1.2 Protein extraction

Sequential Extraction RAB/RIPA/Formic Acid protocol for mice has been attached.

Procedure:

- Turn on centrifuge, cool down to 4°C
- Weigh the tissue. Use this to calculate how much RAB to homogenise tissue in.
- Homogenise the tissue in 10uL/mg RAB (for hippocampus and amygdala) + protease inhibitor in an eppendorf tube using the plastic douncer, stamping tissue approximately 30 times. Use 20uL/mg and motorized homogenizer for cortex, cerebellum, midbrain.
- Pass the solution through a 29-gauge syringe ~10 times.

- Centrifuge samples at 50,000g for 20 min at 4°C
- Collect the supernatant as the RAB fraction, snap freeze.
- Resuspend the remaining pellet in RAB, pass through a syringe and spin as before (wash step), discard supernatant.
- Resuspend the remaining pellet in 7.5uL/mg of RIPA buffer (hippocampus and amygdala, 15uL/mg for cortex, cerebellum, midbrain), pass through a syringe as before.
- Centrifuge samples at 50,000g for 20 min at 4°C
- Collect the supernatant as the RIPA fraction, snap freeze.
- Resuspend the pellet with RIPA and spin as before (wash step), discard supernatant.
- Resuspend and sonicate final pellet in 7.5uL/mg 70% Formic acid (under hood!) = FA fraction for hippocampus and amygdala, 15uL/mg for cortex, cerebellum, midbrain. Samples need to be dialyzed prior to analysis by Western blot.

A.2 Results

A.2.1 Western blot

Two transfer buffers were tested (Bio-Rad and Invitrogen). Among these was chosen due to consistency between samples transference.

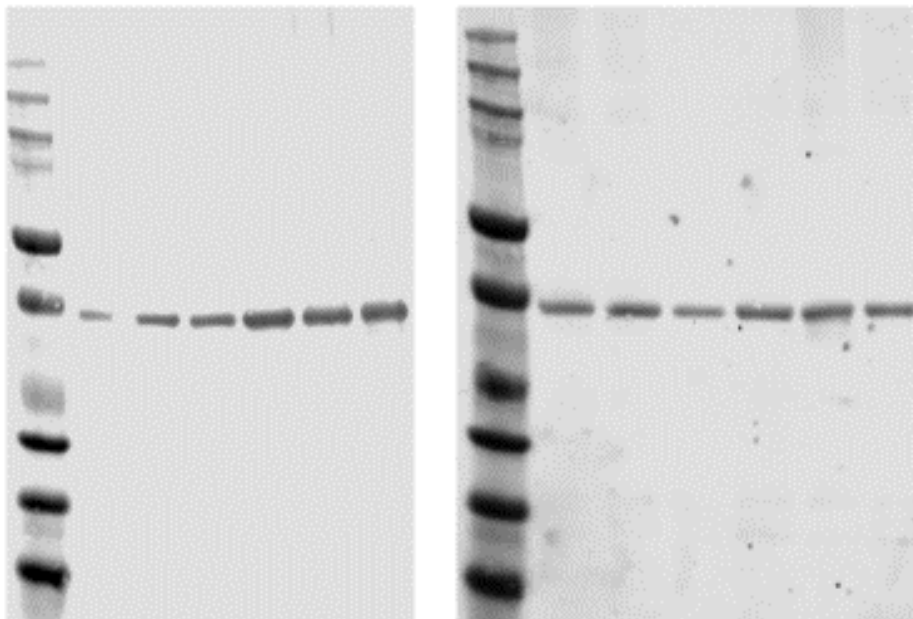


Figure A.1. Comparison between Bio-Rad and Invitrogen transfer buffers. Left blot demonstrates GAPDH bands after transfer step with Invitrogen, whereas right blot shows GAPDH bands after transferring with Bio-Rad.

A.2.2 Total protein

To check our transfer method, Total protein staining (Revert 700 Total Protein Stain) was used for imaging the blot. TAU58/2 mice hippocampus practice tissue were used for protein extraction and Western Blot.

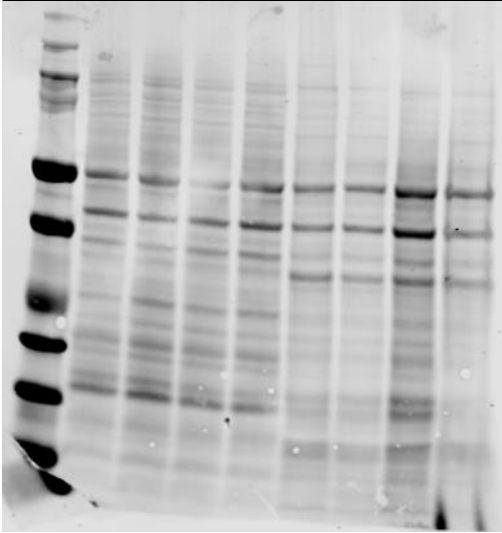


Figure.A.2. Total protein staining.

References

1. Livingston, G., et al., *Dementia prevention, intervention, and care*. The Lancet, 2017. **390**(10113): p. 2673-2734.
2. BROWN, L., E. HANSNATA, and H.A. LA, *Economic Cost of Dementia in Australia 2016-2056: Report prepared for Alzheimer's Australia*. 2017.
3. Alzheimer's, A., *2015 Alzheimer's disease facts and figures*. Alzheimer's & dementia: the journal of the Alzheimer's Association, 2015. **11**(3): p. 332.
4. Qiu, C., M. Kivipelto, and E. von Strauss, *Epidemiology of Alzheimer's disease: occurrence, determinants, and strategies toward intervention*. Dialogues in clinical neuroscience, 2009. **11**(2): p. 111.
5. Webster, L., et al., *Core outcome measures for interventions to prevent or slow the progress of dementia for people living with mild to moderate dementia: Systematic review and consensus recommendations*. PLoS One, 2017. **12**(6): p. e0179521.
6. Trinczek, B., et al., *Domains of tau protein, differential phosphorylation, and dynamic instability of microtubules*. Molecular biology of the cell, 1995. **6**(12): p. 1887-1902.
7. De Calignon, A., et al., *Propagation of tau pathology in a model of early Alzheimer's disease*. Neuron, 2012. **73**(4): p. 685-697.
8. Iqbal, K., F. Liu, and C.-X. Gong, *Tau and neurodegenerative disease: the story so far*. Nature Reviews Neurology, 2016. **12**(1): p. 15.
9. Yan, R. and R. Vassar, *Targeting the β secretase BACE1 for Alzheimer's disease therapy*. The Lancet Neurology, 2014. **13**(3): p. 319-329.
10. Karch, C.M. and A.M. Goate, *Alzheimer's disease risk genes and mechanisms of disease pathogenesis*. Biological Psychiatry. **77**(1): p. 43-51.
11. Haass, C., et al., *The Swedish mutation causes early-onset Alzheimer's disease by β -secretase cleavage within the secretory pathway*. Nature medicine, 1995. **1**(12): p. 1291.
12. Fish, P.V., et al., *New approaches for the treatment of Alzheimer's disease*. Bioorganic & medicinal chemistry letters, 2018.
13. Alafuzoff, I., et al., *Histopathological criteria for progressive dementia disorders: clinical-pathological correlation and classification by multivariate data analysis*. Acta neuropathologica, 1987. **74**(3): p. 209-225.
14. Grundke-Iqbal, I., et al., *Abnormal phosphorylation of the microtubule-associated protein tau (τ) in Alzheimer cytoskeletal pathology*. Proceedings of the National Academy of Sciences, 1986. **83**(13): p. 4913-4917.
15. Mandelkow, E., *Alzheimer's disease: the tangled tale of tau*. Nature, 1999. **402**(6762): p. 588.
16. Arendt, T., J.T. Stieler, and M. Holzer, *Tau and tauopathies*. Brain research bulletin, 2016. **126**: p. 238-292.
17. Andreadis, A., *Misregulation of tau alternative splicing in neurodegeneration and dementia, in Alternative Splicing and Disease*. 2006, Springer. p. 89-107.
18. Ishihara, T., et al., *Age-dependent emergence and progression of a tauopathy in transgenic mice overexpressing the shortest human tau isoform*. Neuron, 1999. **24**(3): p. 751-762.
19. Iseki, E., et al., *Familial frontotemporal dementia and parkinsonism with a novel N296H mutation in exon 10 of the tau gene and a widespread tau accumulation in the glial cells*. Acta neuropathologica, 2001. **102**(3): p. 285-292.

20. Alonso, A.d.C., et al., *Promotion of hyperphosphorylation by frontotemporal dementia tau mutations*. Journal of Biological Chemistry, 2004. **279**(33): p. 34873-34881.
21. Alonso, A.d.C., et al., *Interaction of tau isoforms with Alzheimer's disease abnormally hyperphosphorylated tau and in Vitro Phosphorylation into the disease-like protein*. Journal of Biological Chemistry, 2001. **276**(41): p. 37967-37973.
22. Holtzman, D.M., et al., *Tau: from research to clinical development*. Alzheimer's & Dementia, 2016. **12**(10): p. 1033-1039.
23. Querfurth, H.W. and F.M. LaFerla, *Mechanisms of disease*. N Engl J Med, 2010. **362**(4): p. 329-344.
24. Alonso, A.d.C., et al., *Role of abnormally phosphorylated tau in the breakdown of microtubules in Alzheimer disease*. Proceedings of the National Academy of Sciences, 1994. **91**(12): p. 5562-5566.
25. Iqbal, K., et al., *Defective brain microtubule assembly in Alzheimer's disease*. The Lancet, 1986. **328**(8504): p. 421-426.
26. Congdon, E.E. and E.M. Sigurdsson, *Tau-targeting therapies for Alzheimer disease*. Nature Reviews Neurology, 2018. **14**(7): p. 399-415.
27. Hasegawa, M., et al., *Protein sequence and mass spectrometric analyses of tau in the Alzheimer's disease brain*. Journal of Biological Chemistry, 1992. **267**(24): p. 17047-17054.
28. Eidenmüller, J., et al., *Phosphorylation-mimicking glutamate clusters in the proline-rich region are sufficient to simulate the functional deficiencies of hyperphosphorylated tau protein*. Biochemical Journal, 2001. **357**(3): p. 759-767.
29. Ksiazek-Reding, H., et al., *Akt/PKB kinase phosphorylates separately Thr212 and Ser214 of tau protein in vitro*. Biochimica et Biophysica Acta (BBA)-Molecular Basis of Disease, 2003. **1639**(3): p. 159-168.
30. Sengupta, A., et al., *Phosphorylation of tau at both Thr 231 and Ser 262 is required for maximal inhibition of its binding to microtubules*. Archives of biochemistry and biophysics, 1998. **357**(2): p. 299-309.
31. Khatoun, S., I. Grundke-Iqbal, and K. Iqbal, *Brain levels of microtubule-associated protein τ are elevated in Alzheimer's disease: A radioimmuno-slot-blot assay for nanograms of the protein*. Journal of neurochemistry, 1992. **59**(2): p. 750-753.
32. Poppek, D., et al., *Phosphorylation inhibits turnover of the tau protein by the proteasome: influence of RCAN1 and oxidative stress*. Biochemical Journal, 2006. **400**(3): p. 511-520.
33. Wang, J.-Z., et al., *Dephosphorylation of Alzheimer paired helical filaments by protein phosphatase-2A and- 2B*. Journal of Biological Chemistry, 1995. **270**(9): p. 4854-4860.
34. Wang, J.-Z., I. Grundke-Iqbal, and K. Iqbal, *Restoration of biological activity of Alzheimer abnormally phosphorylated τ by dephosphorylation with protein phosphatase-2A, - 2B and- 1*. Molecular brain research, 1996. **38**(2): p. 200-208.
35. Goedert, M., M. Masuda-Suzukake, and B. Falcon, *Like prions: the propagation of aggregated tau and α -synuclein in neurodegeneration*. Brain, 2016. **140**(2): p. 266-278.
36. Ayers, J.I., B.I. Giasson, and D.R. Borchelt, *Prion-like spreading in tauopathies*. Biological psychiatry, 2018. **83**(4): p. 337-346.
37. Clavaguera, F., et al., *Transmission and spreading of tauopathy in transgenic mouse brain*. Nature cell biology, 2009. **11**(7): p. 909.
38. Takeda, S., *Progression of Alzheimer's disease, tau propagation, and its modifiable risk factors*. Neuroscience Research, 2019. **141**: p. 36-42.
39. Yang, X., et al., *Increased Phosphorylation of Tau and Synaptic Protein Loss in the Aged Transgenic Mice Expressing Familiar Alzheimer's Disease-Linked Presenilin 1 Mutation*. Neurochemical Research, 2012. **37**(1): p. 15-22.
40. Pooler, A.M., et al., *Propagation of tau pathology in Alzheimer's disease: identification of novel therapeutic targets*. Alzheimer's Research & Therapy, 2013. **5**(5).
41. Takeda, S., et al., *Neuronal uptake and propagation of a rare phosphorylated high-molecular-weight tau derived from Alzheimer's disease brain*. Nature Communications, 2015.

42. Asai, H., et al., *Depletion of microglia and inhibition of exosome synthesis halt tau propagation.*(Report). Nature Neuroscience, 2015. **18**(11): p. 1584.
43. Wang, J., Y. Zheng, and M. Zhao, *Exosome-based cancer therapy: implication for targeting cancer stem cells.* Frontiers in pharmacology, 2017. **7**: p. 533.
44. Braak, H. and E. Braak, *Neuropathological staging of Alzheimer-related changes.* Acta neuropathologica, 1991. **82**(4): p. 239-259.
45. Bancher, C., et al., *Accumulation of abnormally phosphorylated τ precedes the formation of neurofibrillary tangles in Alzheimer's disease.* Brain research, 1989. **477**(1-2): p. 90-99.
46. Oddo, S., et al., *Reduction of soluble A β and tau, but not soluble A β alone, ameliorates cognitive decline in transgenic mice with plaques and tangles.* Journal of Biological Chemistry, 2006. **281**(51): p. 39413-39423.
47. Augustinack, J.C., et al., *Specific tau phosphorylation sites correlate with severity of neuronal cytopathology in Alzheimer's disease.* Acta neuropathologica, 2002. **103**(1): p. 26-35.
48. Morishima-Kawashima, M., et al., *Hyperphosphorylation of tau in PHF.* Neurobiology of aging, 1995. **16**(3): p. 365-371.
49. Mercken, M., et al., *Monoclonal antibodies with selective specificity for Alzheimer Tau are directed against phosphatase-sensitive epitopes.* Acta neuropathologica, 1992. **84**(3): p. 265-272.
50. Biernat, J., et al., *The switch of tau protein to an Alzheimer-like state includes the phosphorylation of two serine-proline motifs upstream of the microtubule binding region.* The EMBO journal, 1992. **11**(4): p. 1593-1597.
51. Goedert, M., R. Jakes, and E. Vanmechelen, *Monoclonal antibody AT8 recognises tau protein phosphorylated at both serine 202 and threonine 205.* Neuroscience letters, 1995. **189**(3): p. 167-170.
52. Kimura, T., et al., *Sequential changes of tau-site-specific phosphorylation during development of paired helical filaments.* Dementia and Geriatric Cognitive Disorders, 1996. **7**(4): p. 177-181.
53. Jicha, G.A., et al., *A conformation- and phosphorylation-dependent antibody recognizing the paired helical filaments of Alzheimer's disease.* Journal of neurochemistry, 1997. **69**(5): p. 2087-2095.
54. SHIMAZAKI, M., H. NAKANO, and K. Kobayashi, *Correlation between tau phosphorylation sites and tangle morphology in Alzheimer's disease.* Psychogeriatrics, 2005. **5**(2): p. 22-35.
55. Vandebroek, T., et al., *Identification and isolation of a hyperphosphorylated, conformationally changed intermediate of human protein tau expressed in yeast.* Biochemistry, 2005. **44**(34): p. 11466-11475.
56. Wittmann, C.W., et al., *Tauopathy in Drosophila: neurodegeneration without neurofibrillary tangles.* Science, 2001. **293**(5530): p. 711-714.
57. Santacruz, K., et al., *Tau suppression in a neurodegenerative mouse model improves memory function.* Science, 2005. **309**(5733): p. 476-481.
58. Lin, W.-L., et al., *Ultrastructural neuronal pathology in transgenic mice expressing mutant (P301L) human tau.* Journal of neurocytology, 2003. **32**(9): p. 1091-1105.
59. Gray, E., M. Paula-Barbosa, and A. Roher, *Alzheimer's disease: paired helical filaments and cytomembranes.* Neuropathology and applied neurobiology, 1987. **13**(2): p. 91-110.
60. Wang, J.-Z., I. Grundke-Iqbal, and K. Iqbal, *Glycosylation of microtubule-associated protein tau: An abnormal posttranslational modification in Alzheimer's disease.* Nature medicine, 1996. **2**(8): p. 871-875.
61. Liazoghli, D., et al., *Fragmentation of the Golgi apparatus induced by the overexpression of wild-type and mutant human tau forms in neurons.* The American journal of pathology, 2005. **166**(5): p. 1499-1514.
62. Yoshiyama, Y., et al., *Synapse loss and microglial activation precede tangles in a P301S tauopathy mouse model.* Neuron, 2007. **53**(3): p. 337-351.
63. Kim, I., W. Xu, and J.C. Reed, *Cell death and endoplasmic reticulum stress: disease relevance and therapeutic opportunities.* Nature reviews Drug discovery, 2008. **7**(12): p. 1013-1030.

64. McGeer, P.L., et al., *Reactive microglia in patients with senile dementia of the Alzheimer type are positive for the histocompatibility glycoprotein HLA-DR*. *Neuroscience letters*, 1987. **79**(1-2): p. 195-200.
65. Heneka, M.T., et al., *Neuroinflammation in Alzheimer's disease*. *The Lancet Neurology*, 2015. **14**(4): p. 388-405.
66. Puzzo, D., et al., *Effect of phosphodiesterase-5 inhibition on apoptosis and beta amyloid load in aged mice*. *Neurobiology of aging*, 2014. **35**(3): p. 520-531.
67. Sasaguri, H., et al., *APP mouse models for Alzheimer's disease preclinical studies*. *The EMBO journal*, 2017. **36**(17): p. 2473-2487.
68. Mullane, K. and M. Williams, *Preclinical Models of Alzheimer's Disease: Relevance and Translational Validity*. *Current protocols in pharmacology*, 2019. **84**(1): p. e57.
69. Poorkaj, P., et al., *Tau is a candidate gene for chromosome 17 frontotemporal dementia*. *Annals of neurology*, 1998. **43**(6): p. 815-825.
70. Hutton, M., et al., *Association of missense and 5'-splice-site mutations in tau with the inherited dementia FTDP-17*. *Nature*, 1998. **393**(6686): p. 702-705.
71. Spillantini, M.G., et al., *Mutation in the tau gene in familial multiple system tauopathy with presenile dementia*. *Proceedings of the National Academy of Sciences*, 1998. **95**(13): p. 7737-7741.
72. Eersel, J., et al., *Early-onset axonal pathology in a novel P301S-Tau transgenic mouse model of frontotemporal lobar degeneration*. *Neuropathology and Applied Neurobiology*, 2015. **41**(7): p. 906-925.
73. Burnett, J.C. and J.J. Rossi, *RNA-based therapeutics: current progress and future prospects*. *Chemistry & biology*, 2012. **19**(1): p. 60-71.
74. Kole, R., A.R. Krainer, and S. Altman, *RNA therapeutics: beyond RNA interference and antisense oligonucleotides*. *Nature reviews Drug discovery*, 2012. **11**(2): p. 125-140.
75. Southwell, A.L., et al., *Antisense oligonucleotide therapeutics for inherited neurodegenerative diseases*. *Trends in molecular medicine*, 2012. **18**(11): p. 634-643.
76. Carthew, R.W. and E.J. Sontheimer, *Origins and mechanisms of miRNAs and siRNAs*. *Cell*, 2009. **136**(4): p. 642-655.
77. Kim, D.H. and J.J. Rossi, *Strategies for silencing human disease using RNA interference*. *Nature Reviews Genetics*, 2007. **8**(3): p. 173-184.
78. Xu, H., et al., *Tau silencing by siRNA in the P301S mouse model of tauopathy*. *Current gene therapy*, 2014. **14**(5): p. 343-351.
79. Hosokawa, M., et al., *Methylene blue reduced abnormal tau accumulation in P301L tau transgenic mice*. *PloS one*, 2012. **7**(12).
80. Min, S.-W., et al., *Critical role of acetylation in tau-mediated neurodegeneration and cognitive deficits*. *Nature medicine*, 2015. **21**(10): p. 1154.
81. Myeku, N., et al., *Tau-driven 26S proteasome impairment and cognitive dysfunction can be prevented early in disease by activating cAMP-PKA signaling*. *Nature medicine*, 2016. **22**(1): p. 46.
82. Asuni, A.A., et al., *Immunotherapy targeting pathological tau conformers in a tangle mouse model reduces brain pathology with associated functional improvements*. *Journal of Neuroscience*, 2007. **27**(34): p. 9115-9129.
83. Boutajangout, A., et al., *Passive immunization targeting pathological phospho-tau protein in a mouse model reduces functional decline and clears tau aggregates from the brain*. *Journal of neurochemistry*, 2011. **118**(4): p. 658-667.
84. Asuni, A.A., D. Quartermain, and E.M. Sigurdsson, *O2-05-04: Tau-based immunotherapy for dementia*. *Alzheimer's & Dementia: The Journal of the Alzheimer's Association*, 2006. **2**(3): p. S40-S41.
85. Boutajangout, A., et al., *Passive tau immunotherapy diminishes functional decline and clears tau aggregates in a mouse model of tauopathy*. *Alzheimer's & Dementia: The Journal of the Alzheimer's Association*, 2010. **6**(4): p. S578.

86. Wischik, C.M., et al., *O3-04-07: Tau aggregation inhibitor (TAI) therapy with rember™ arrests disease progression in mild and moderate Alzheimer's disease over 50 weeks*. *Alzheimer's & Dementia: The Journal of the Alzheimer's Association*, 2008. **4**(4): p. T167.
87. Harrington, C., et al. *Methylthioninium chloride (MTC) acts as a tau aggregation inhibitor in a cellular model and reverses tau pathology in transgenic mice models of Alzheimer's disease*. in *International Conference on Alzheimer's Disease Abstracts*. 2008.
88. Winblad, B., et al., *Defeating Alzheimer's disease and other dementias: a priority for European science and society*. *The Lancet Neurology*, 2016. **15**(5): p. 455-532.
89. Ankarcona, M., et al., *Current and future treatment of amyloid diseases*. *Journal of internal medicine*, 2016. **280**(2): p. 177-202.
90. Piazza, F. and B. Winblad, *Amyloid-Related Imaging Abnormalities (ARIA) in immunotherapy trials for alzheimer's disease: need for prognostic biomarkers?* *Journal of Alzheimer's Disease*, 2016. **52**(2): p. 417-420.
91. Hong, C., et al., *Herpes simplex virus RNAi and neprilysin gene transfer vectors reduce accumulation of Alzheimer's disease-related amyloid- β peptide in vivo*. *Gene therapy*, 2006. **13**(14): p. 1068.
92. Fol, R., et al., *Viral gene transfer of APPs α rescues synaptic failure in an Alzheimer's disease mouse model*. *Acta neuropathologica*, 2016. **131**(2): p. 247-266.
93. Zheng, H., et al., *β -Amyloid precursor protein-deficient mice show reactive gliosis and decreased locomotor activity*. *Cell*, 1995. **81**(4): p. 525-531.
94. Senechal, Y., et al., *Amyloid precursor protein knockdown by siRNA impairs spontaneous alternation in adult mice*. *Journal of neurochemistry*, 2007. **102**(6): p. 1928-1940.
95. Hu, X., et al., *BACE1 deficiency causes altered neuronal activity and neurodegeneration*. *Journal of Neuroscience*, 2010. **30**(26): p. 8819-8829.
96. Alvarez-Erviti, L., et al., *Delivery of siRNA to the mouse brain by systemic injection of targeted exosomes*. *Nature biotechnology*, 2011. **29**(4): p. 341.
97. Chauhan, N.B. and G.J. Siegel, *Antisense inhibition at the β -secretase-site of β -amyloid precursor protein reduces cerebral amyloid and acetyl cholinesterase activity in Tg2576*. *Neuroscience*, 2007. **146**(1): p. 143-151.
98. McGowan, E., J. Eriksen, and M. Hutton, *A decade of modeling Alzheimer's disease in transgenic mice*. *Trends in genetics*, 2006. **22**(5): p. 281-289.
99. Elbashir, S.M., et al., *Duplexes of 21-nucleotide RNAs mediate RNA interference in cultured mammalian cells*. *nature*, 2001. **411**(6836): p. 494.
100. Gregori, M., M. Masserini, and S. Mancini, *Nanomedicine for the treatment of Alzheimer's disease*. *Nanomedicine*, 2015. **10**(7): p. 1203-1218.
101. Singer, O., et al., *Targeting BACE1 with siRNAs ameliorates Alzheimer disease neuropathology in a transgenic model*. *Nature neuroscience*, 2005. **8**(10): p. 1343.
102. Zhang, T.-T., et al.
103. Thomas, C.E., A. Ehrhardt, and M.A. Kay, *Progress and problems with the use of viral vectors for gene therapy*. *Nature Reviews Genetics*, 2003. **4**(5): p. 346.
104. Coelho, T., et al., *Safety and efficacy of RNAi therapy for transthyretin amyloidosis*. *New England Journal of Medicine*, 2013. **369**(9): p. 819-829.
105. Yin, H., et al., *Non-viral vectors for gene-based therapy*. *Nature Reviews Genetics*, 2014. **15**(8): p. 541.
106. Zheng, M., et al., *Nanotechnology-based strategies for siRNA brain delivery for disease therapy*. *Trends in biotechnology*, 2018. **36**(5): p. 562-575.
107. Banks, W.A., *From blood-brain barrier to blood-brain interface: new opportunities for CNS drug delivery*. *Nature reviews Drug discovery*, 2016. **15**(4): p. 275.
108. Anraku, Y., et al., *Glycaemic control boosts glucosylated nanocarrier crossing the BBB into the brain*. *Nature communications*, 2017. **8**(1): p. 1001.
109. Abramowski, D., et al., *Transgenic expression of intraneuronal A β 42 but not A β 40 leads to cellular A β lesions, degeneration, and functional impairment without typical Alzheimer's disease pathology*. *Journal of Neuroscience*, 2012. **32**(4): p. 1273-1283.

110. Liu, Q., et al., *Neurofilamentopathy in neurodegenerative diseases*. The open neurology journal, 2011. **5**: p. 58.
111. Ittner, L., et al., *Early-onset axonal pathology in a novel P301S-Tau transgenic mouse model of frontotemporal lobar degeneration*. 2015.
112. Ke, Y.D., et al., *CNS cell type-specific gene profiling of P301S tau transgenic mice identifies genes dysregulated by progressive tau accumulation*. Journal of Biological Chemistry, 2019. **294**(38): p. 14149-14162.
113. Yin, Z., et al., *Progressive motor deficit is mediated by the denervation of neuromuscular junctions and axonal degeneration in transgenic mice expressing mutant (P301S) tau protein*. Journal of Alzheimer's Disease, 2017. **60**(s1): p. S41-S57.
114. Przybyla, M., et al., *Disinhibition-like behavior in a P301S mutant tau transgenic mouse model of frontotemporal dementia*. Neuroscience letters, 2016. **631**: p. 24-29.
115. Van der Jeugd, A., et al., *Impulsivity, decreased social exploration, and executive dysfunction in a mouse model of frontotemporal dementia*. Neurobiology of learning and memory, 2016. **130**: p. 34-43.
116. van Erssel, J., et al., *Early-onset Axonal Pathology in a Novel P301S-Tau Transgenic Mouse Model of Frontotemporal Dementia*. Neuropathology Appl Neurobiol., 2015.
117. Probst, A., et al., *Axonopathy and amyotrophy in mice transgenic for human four-repeat tau protein*. Acta neuropathologica, 2000. **99**(5): p. 469-481.
118. Ngwenya, L.B., A. Peters, and D.L. Rosene, *Light and electron microscopic immunohistochemical detection of bromodeoxyuridine-labeled cells in the brain: different fixation and processing protocols*. Journal of Histochemistry & Cytochemistry, 2005. **53**(7): p. 821-832.
119. Lu, Q.L. and T.A. Partridge, *A new blocking method for application of murine monoclonal antibody to mouse tissue sections*. Journal of Histochemistry & Cytochemistry, 1998. **46**(8): p. 977-983.
120. Akiyama, H., et al., *Inflammation and Alzheimer's disease*. Neurobiology of aging, 2000. **21**(3): p. 383-421.
121. Byrne, J.H., R. Heidelberger, and M.N. Waxham, *From molecules to networks: an introduction to cellular and molecular neuroscience*. 2014: Academic Press.